sid.inpe.br/mtc-m21c/2020/05.27.18.15-TDI

A SPATIO-TEMPORAL BAYESIAN NETWORK MODEL: A CASE STUDY IN BRAZILIAN AMAZON DEFORESTATION PREDICTION

Alexsandro Cândido de Oliveira Silva

Doctorate Thesis of the Graduate Course in Applied Computing, guided by Dra. Leila Maria Garcia Fonseca, approved in May 4, 2020.

URL of the original document:
<http://urlib.net/8JMKD3MGP3W34R/42J382B>

INPE
São José dos Campos
2020

PUBLISHED BY:

Instituto Nacional de Pesquisas Espaciais - INPE
Gabinete do Diretor (GBDIR)
Serviço de Informação e Documentação (SESID)
CEP 12.227-010
São José dos Campos - SP - Brasil
Tel.:(012) 3208-6923/7348
E-mail: pubtc@inpe.br

sid.inpe.br/mtc-m21c/2020/05.27.18.15-TDI

A SPATIO-TEMPORAL BAYESIAN NETWORK MODEL: A CASE STUDY IN BRAZILIAN AMAZON DEFORESTATION PREDICTION

Alexsandro Cândido de Oliveira Silva

Doctorate Thesis of the Graduate Course in Applied Computing, guided by Dra. Leila Maria Garcia Fonseca, approved in May 4, 2020.

URL of the original document:
<http://urlib.net/8JMKD3MGP3W34R/42J382B>

INPE
São José dos Campos
2020

Cataloging in Publication Data

Silva, Alexsandro Cândido de Oliveira.

Si38s A spatio-temporal bayesian network model: a case study in brazilian Amazon deforestation prediction / Alexsandro Cândido de Oliveira Silva. – São José dos Campos : INPE, 2020.

xxi + 100 p. ; (sid.inpe.br/mtc-m21c/2020/05.27.18.15-TDI)

Thesis (Doctorate in Applied Computing) – Instituto Nacional de Pesquisas Espaciais, São José dos Campos, 2020.

Guiding : Dra. Leila Maria Garcia Fonseca.

1. Bayesian networks. 2. Spatio-temporal bayesian networks. 3. Spatio-temporal modeling. 4. Land-use and land-cover changes. 5. Deforestation. I.Title.

CDU 528.8:504.122

MINISTÉRIO DA CIÊNCIA, TECNOLOGIA E INOVAÇÕES
INSTITUTO NACIONAL DE PESQUISAS ESPACIAIS

FOLHA DE APROVAÇÃO

A FOLHA DE APROVAÇÃO SERÁ INCLUIDA APÓS RESTABELECIMENTO DAS ATIVIDADES PRESENCIAIS.

Por conta da Pandemia do COVID-19, as defesas de Teses e Dissertações são realizadas por vídeo conferência, o que vem acarretando um atraso no recebimento nas folhas de aprovação.

Este trabalho foi aprovado pela Banca e possui as declarações dos orientadores (confirmando as inclusões sugeridas pela Banca) e da Biblioteca (confirmando as correções de normalização).

Assim que a Biblioteca receber a Folha de aprovação assinada, esta folha será substituída.

Qualquer dúvida, entrar em contato pelo email: pubtc@inpe.br.

Divisão de Biblioteca (DIBIB).

To my parents, to my sister
and to the love of my life.

ACKNOWLEDGMENTS

First of all, I would like to express my gratitude to my advisor Dr[a] Leila Maria Garcia Fonseca for the dedication, encouragement, and friendship with which she accompanied me throughout my postgraduate course.

To Dr. Thales Sehn Korting for all his support and friendship. To the researches Dr. Sidnei Sant'Anna, Dr. Solon Carvalho, Dr. Carlos Renato Francês, and Dr. Raul Feitosa for accepting the invitation to participate and contribute to this work.

To the researches, colleagues, and employees of the National Institute for Space Research who directly or indirectly contributed to the completion of this work and my personal and professional growth. To the CAPES for funding this research.

To my parents Ailton and Rosana, and to my sister Gabriella for all their support and unconditional love.

To my longtime friends.

To the love of my life.

ABSTRACT

The key tool for dealing with probabilities in AI is the Bayesian Network (BN). A BN provides a coherent framework for representing and reasoning under uncertainties, which are estimated based on probability theory. However, BNs present some limitations as they do not explicitly model spatial and temporal relationships between variables. Some extensions of BNs have been used to overcome those BN's weaknesses, such as the Spatial BN that integrates GIS and BN and confers to the BN a spatially explicitly strategy, and the Dynamic BN that extends the concept of BNs by relating variables across time. BN approaches have already been proposed to predict LULCC such as deforestation processes. However, deforestation has been considered as a static process when modeled by BNs. In this context, the main goal of this work is to build Spatio-Temporal BN (STBN) models to incorporate both spatial and temporal information in the deforestation risk prediction. For this, we also implemented a package for the *R* programming language, which enables the development of STBN-based LULCC models for other earth observation applications besides the deforestation process. The STBN models proposed in this thesis are used as a LULCC model for predicting deforestation risk in three priority areas of the Brazilian Legal Amazon: (i) in the southwest of Amazonas State; (ii) in the northwesters of Mato Grosso State; and (iii) surrounding the BR-163 highway in the southwest of Pará State. Among the variables selected to compose the STBN models, the distance from hotspots fires variable stood out as one of the most important for deforestation risk prediction, while protected areas variable was important as a deforestation risk mitigator. The proposed STBN models presented a strong performance with a great agreement between deforestation events and predictions over the years. STBN models' results also showed that there was an increase in uncertainty in predictions over time, indicating that more long-term the prediction is, the less accurate it will be. With this, we can state that STBN-based LULCC models are recommended for short-term prediction of deforestation risk.

Keywords: Bayesian Networks; Spatio-Temporal Bayesian Networks; Spatio-Temporal Modeling; Land-use and Land-cover Changes; Deforestation.

UM MODELO DE REDE BAYESIANA ESPAÇO-TEMPORAL: UM ESTUDO DE CASO NA PREDIÇÃO DO DESMATAMENTO DA AMAZÔNIA BRASILEIRA

RESUMO

A principal ferramenta para lidar com probabilidades na IA é a Rede Bayesiana (RB). Uma RB fornece uma estrutura coerente para representar e raciocinar sob incertezas, as quais são estimadas com base na teoria da probabilidade. No entanto, os RBs apresentam algumas limitações uma vez que não modelam explicitamente as relações espaciais e temporais entre as variáveis. Algumas variações das RBs têm sido utilizadas para superar tais fraqueza, como a RB espacial que integra GIS e RB e confere à RB uma estratégia espacialmente explícita, além da RB dinâmica que estende o conceito de RBs, relacionando suas variáveis ao longo do tempo. Algumas abordagens de RB já foram propostas para prever as mudanças de uso e cobertura da terra (LULCC), como processos de desmatamento. No entanto, o desmatamento tem sido considerado como um processo estático quando modelado por RBs. Nesse contexto, o principal objetivo deste trabalho é construir modelos de RBs espaço-temporais (STBN) para incorporar informações espaciais e temporais na previsão de risco de desmatamento. Para isso, também foi implementado um pacote para a linguagem de programação *R*, que permite o desenvolvimento de modelos LULCC baseados em STBN para outras aplicações de observação da terra além do desmatamento. Os modelos STBN propostos nesta tese são utilizados como modelo LULCC para prever o risco de desmatamento em três áreas prioritárias da Amazônia Legal Brasileira: (i) no sudoeste do estado do Amazonas; (ii) no noroeste do estado de Mato Grosso; e (iii) ao redor da rodovia BR-163, no sudoeste do estado do Pará. Entre as variáveis selecionadas para compor os modelos STBN, a variável distância dos focos de incêndio se destacou como uma das mais importantes na previsão de risco de desmatamento, enquanto a variável áreas protegidas foi importante como mitigadora de risco de desmatamento. Os modelos STBN propostos apresentaram um ótimo desempenho com uma grande concordância entre eventos e previsões de desmatamento ao longo dos anos. Os resultados dos modelos STBN também mostraram que houve um aumento na incerteza nas previsões ao longo do tempo, indicando que, quanto mais longa for a previsão, menos precisa ela será. Com isso, pode-se afirmar que os modelos LULCC baseados no STBN são recomendados para a previsão a curto prazo do risco de desmatamento.

Palavras-chave: Redes Bayesianas; Redes Bayesianas Espaço-Temporais; Modelagem Espaço-Temporal; Mudanças do Uso e Cobertura da Terra; Desmatamento.

LIST OF FIGURES

LIST OF TABLES

LIST OF ABBREVIATIONS

AB	–	Agent-based
AI		Artificial Intelligence
ANN	–	Artificial Neural Network
AUC-ROC	–	Area Under the Receiver Operating Characteristic curve
AWIFS	–	Advanced Wide Field Sensor
BLA	–	Brazilian Legal Amazon
BN	–	Bayesian Network
CA	–	Cellular Automata
CBERS	–	China-Brazil Earth-Resources Satellite
CPT	–	Conditional Probability Table
CRAN	–	Comprehensive R Archive Network
DBN	–	Dynamic Bayesian Network
DETER	–	Near Real-Time Deforestation Detection System
DT	–	Decision Tree
EB	–	Economic-base
EBF	–	Evidential Belief Function
FR	–	Frequency Ratio
GAM	–	Generalized Additive Model
GIS	–	Geographic Information System
INPE	–	National Institute for Space Research
LAI	–	Leaf Area Index
LR	–	Logistic Regression
LULCC	–	Land Use Land Cover Change
MC	–	Markov Chain
ML	–	Machine Learning
MODIS	–	Moderate-Resolution Imaging Spectroradiometer
PPCDAm	–	Action Plan to Prevent and Control Deforestation in Amazon
PRODES	–	Brazilian Amazon forest monitoring by satellite
RF	–	Random Forest
ROC	–	Receiver Operating Characteristic
ROI	–	Region of Interest
SB	–	Statistical-based
SBN	–	Spatial Bayesian Network
STBN	–	Spatio-Temporal Bayesian Network
SVM	–	Support Vector Machine
WFI	–	Wide Field Imager
WoE	–	Weights of Evidence

CONTENTS

1. INTRODUCTION

Artificial Intelligence (AI) systems should be able to reason probabilistically to cope with uncertainties that may affect the results of any modeling. The probability theory is a suitable foundation for representing the strengths of beliefs and summarize uncertainties that may come from various sources. The key tool for dealing with probabilities in AI is the Bayesian Network (BN), which is a type of probabilistic graphical model capable of representing the dependency relationship among variables with an explicit treatment of uncertainty by means of probabilities. This makes the BNs a suitable approach for probabilistic reasoning of multiple areas.

BNs are acknowledged for their unique probabilistic modeling approach and their high model transparency (LANDUYT et al., 2013). They provide an intuitive graphical representation of the variables conditional dependencies via a directed acyclic graph. Since variables' relationships are graphically represented, the BN's semantic facilitates the understanding and the decision-making process for the users (DE SANTANA et al., 2007). A BN also provides an inference mechanism, which is possible thanks to conditional probability distributions that quantify the causal relationships between the network variables. The usefulness of BNs lies in the fact that by using Bayes' theorem, one can proceed not only from causes to consequences but also deduce the probabilities of different causes given the consequences (UUSITALO, 2007).

Additionally, BNs can model complex systems with a large number of variables, besides to handle small and incomplete data sets and perform proper predictions. In case of a lack of sufficient empirical data, expert and stakeholder knowledge can be incorporated via a participatory modeling procedure (AGUILERA et al., 2011; LANDUYT et al., 2013). Notwithstanding such advantages, BNs present some limitations. BNs do not explicitly model the spatial domain. However, the states of a phenomenon in the field of Earth observation, for example, may have some spatial variability. To represent changes in space statically, the solution is straightforward so that BN and Geographic Information System (GIS) are integrated to overcome BN's weakness in representing spatially distributed variables. This approach, known as Spatial BN (SBN), confers to the BN a spatially explicit strategy, but it only permits to reproduce static changes through space (SPEROTTO et al., 2017).

A BN also does not explicitly model temporal relationships between variables. The probabilistic reasoning is carried out at a particular point in time and, therefore, a BN is actually a static model. The only way to relate a variable with its past or future is by replicating it for each time-step and assigning a time index to it. Consequently, we have to work with a given discrete time scale to adapt the BN as a Markovian process. A Markov process is any stochastic process that satisfies the Markov property that the current state depends on only a finite fixed number of previous states. The simplest one is a first-order Markov process, in which the current state depends only on the previous state and not on any earlier state (RUSSELL; NORVING, 2010). One way of extending Markov models is to allow higher-order interactions between variables.

Even with the Markov property, there is a classical problem when working with BNs in the temporal domain: do we need to specify a different conditional probability distribution for each time-step? To avoid this problem, we assume that changes in the world state are caused by a stationary process, i.e., a process of change that is driven by laws that do not themselves change over time (DE SANTANA et al., 2007; RUSSELL; NORVING, 2010). A BN replicated over time that satisfies the Markov property and is stationary is know as a Dynamic Bayesian Network (DBN). Hence, DBNs extend the concept of BNs by relating variables across time.

Therefore, the SBN and DBN overcome BN's weaknesses of not explicitly model spatial and temporal relationships between variables, respectively. However, space and time play a crucial role in monitoring and managing environmental systems and, thus, should not be considered separately. To that end, a Spatio-Temporal Bayesian Network (STBN) seems to be an appropriate approach to combine the spatial and temporal variability of a spatio-temporal process, such as deforestation, into the BN modeling.

SBNs have been employed in the land-use and land-cover changes (LULCC) modeling (CELIO; KOELLNER; GRÊT-REGAMEY, 2014), as well as to predict deforestation risk (DLAMINI, 2016; KRÜGER; LAKES, 2015; MAYFIELD et al., 2017). However, in these studies, deforestation has been considered as a static process, in which the temporal domain is not taken into account. An attempt to fill this gap was made by Silva et al. (2020), in which the authors presented a stepwise application of an SBN approach over time, which can be seen as a snapshot model for each moment. In this way, the temporal dynamics of deforestation processes was not directly incorporated into the modeling. In fact, static SBN modeling was carried out in each step.

In this context, the main goal of this work is to build STBN models to predict deforestation risk areas. To accomplish that, we assume the hypothesis that STBN-based LULCC models are able to represent and capture the variables' spatio-temporal relationships to appropriately predict deforestation risk. The STBN models developed in this work ware tested to predict deforestation risk in three deforestation frontiers in the Amazon forest: (i) in the southwestern of Amazon state, (ii) in the northwestern of Mato Grosso state, and (iii) in the southwestern of Pará state. Within the context of this study, we define Amazon deforestation as the total removal of primary forests (clear cut).

In order to develop the STBN-based LULCC models, we implemented in the context of this thesis the package named *stbnR* (**S**patio-**T**emporal **B**ayesian **N**etwork for **R**), which enables the development of STBN-based LULCC models within the *R* environment. The *stbnR* package was developed in *R* because it is a constantly evolving open-source programming language. This allows anyone to test and contribute to improvements to the *stbnR* package. Furthermore, *R* is a powerful language for statistical computing and analysis and has available a massive collection of packages to support the development of new ones.

Therefore, this thesis presents mainly three contributions. First, we encompass the temporal domain into the LULCC modeling, specifically in the prediction of deforestation risk. Second, we implemented the *stbnR* package, which enables the development of STBN-based LULCC models within the *R* environment for other earth observation applications besides the deforestation process. And third, we proposed a new approach for predicting deforestation risk areas based on the Spatio-Temporal Bayesian Network (STBN).

This thesis is organized as follows. This first chapter provides the context, contribution, hypothesis, and objective of the work. Chapter 2 presents an overview of the Brazilian Amazon environmental governance as well as a taxonomy of LULCC models and BN approaches. Chapter 3 provides a detailed description of the *stbnR* package functions, while Chapter 4 describes the case studies in addition to the dataset used and pre-processings carried out. Chapter 5 presents the results of each case study. Finally, Chapter 6 concludes this thesis with an overview of the work.

2. LITERATURE REVIEW

2.1 Amazon forest environmental governance

Amazon Biome encompasses an area of about 6.7 million km^2 shared by nine countries: Brazil, Bolivia, Peru, Ecuador, Colombia, Venezuela, Guyana, Suriname, and French Guiana, with the majority area inside Brazilian boundaries. The Amazon rainforest covers most of the Amazon Biome, being the most extensive continuous remaining tropical forest in the globe. Much attention has been given to this region since it provides unique environmental services, houses at least one in ten of the world's known biodiversity, and plays a critical role in maintaining climate functions regionally and globally (ALVES et al., 2017; NOBRE; BORMA, 2009; WWF, 2019).

In Brazil, an anthropization process started in the 1960s in response to the government policies to integrate the Amazon region with the rest of the country (SHIMABUKURO et al., 2012). In 1966, the government instituted the Brazilian Legal Amazon[1] (BLA), which corresponds to more than 60% of the Brazilian territory, encompassing the states of Acre, Amapá, Amazonas, Mato Grosso, Pará, Rondônia, Tocantins, and the western part of Maranhão state (BRASIL, 2007), hence, including the Brazilian Amazon biome and part of the Cerrado and Pantanal Biomes. BLA's territorial boundaries have a sociopolitical rather than geographical bias as it was established as a way to plan and promote the social and economic development of the region (IBGE, 2014).

Such integration process was carried out mainly through the construction of a massive highway network, and migration incentive policies such as the National Development Plans (SIMMONS, 2002). Consequently, this shifted the agricultural frontier towards the Amazon region, creating the so-called arc of deforestation (SHIMABUKURO et al., 2012). At the time, cattle ranching became a great investment choice, given the plentiful and inexpensive lands, besides high world beef prices (SIMMONS, 2002). Afterward, development policies in the Amazon region shifted toward mineral extraction, and during the Brazilian government transition from a military regime to democracy in the 1980s,

[1] The term "Legal Amazon" was only incorporated in recent legislations and is not explicitly stated in the laws that defined the Brazilian Amazon area for public policy purposes in previous decades. The use of the adjective "legal" is due to the need to differentiate the Amazon basin, Amazon Biome, as well as the International Amazon (IBGE, 2014).

concerns about forest loss increased as the incentive to economic development also presented several environmental damages (ARIMA et al., 2014; SIMMONS, 2002).

In the late 1980s, indigenous rights got much attention, which resulted in a significant number of indigenous reserves along with some conservation units (SIMMONS, 2002). Additionally, the National Institute for Space Research (INPE) started to monitor the BLA with satellite images, reporting yearly deforestation rates, which the Brazilian government has been using as an indicator for proposing environmental public policies and for evaluating their effectiveness (INPE, 2019c). The Brazilian Forest Code was a significant restriction on deforestation on private lands that established a minimum portion of each property (20 to 50%) that should be kept as a forest reserve (NEPSTAD et al., 2014). Nevertheless, in 1995, INPE announced the largest deforestation rate in history (INPE, 2019a). The president at the time increased forest reserves portion in the properties to 80%, making compliance practically unattainable and reducing the law's credibility (NEPSTAD et al., 2014). Although rates declined in the following years, Amazon deforestation became far more sensitive to commodity market conditions, and technological advances favored the large-scale expansion of mechanizes crops, mainly soybean, whose prices spiked in the early 2000s, so did deforestation rates, which returned to the high levels in 2004 (ARIMA et al., 2014; NEPSTAD et al., 2014).

After deforestation rates in the BLA sharply increased in 2004, the Brazilian government implemented the Action Plan to Prevent and Control Deforestation in Amazon (PPCDAm-I) (BRASIL, 2004). Deforestation rates declined in the following years, but this trend reversed in 2008 (INPE, 2019a), and the government instituted the PPCDAm-II (BRASIL, 2009). Deforestation reduction became the central issue in the government climate change agenda, and the implemented environmental public policies produced significant externalities such as the restructuring of Brazil's environmental enforcement agency (IBAMA) and the expansion of the protected areas network and indigenous lands (ARIMA et al., 2014; MELLO; ARTAXO, 2017).

Along with these government actions, other factors also influenced deforestation reduction. In 2004, law enforcement capacity increased with the release of a real-time deforestation detection system (DETER) by INPE (SHIMABUKURO et al., 2012). In 2005, the profitability of soybean production plummeted (NEPSTAD et al., 2014), as well as the cattle ranching (ARIMA et al., 2014). In the next year, the Soy Moratorium was established (GIBBS et al., 2015), and the Term of Adjustment of Conduct for

meatpacking companies was signed in 2009 (CARVALHO et al., 2019). Both were agreements to block the commercialization of soybean and cattle, respectively, from deforested areas. As a result of all those factors, deforestation in BLA reached the lowest rate in 2012 (INPE, 2019a), as shown in Figure 2.1. Brazil's success in reducing deforestation has made it a global leader in climate change mitigation (ARTAXO, 2019).

Figure 2.1 - Deforestation rates in Brazilian Legal Amazon over the years.

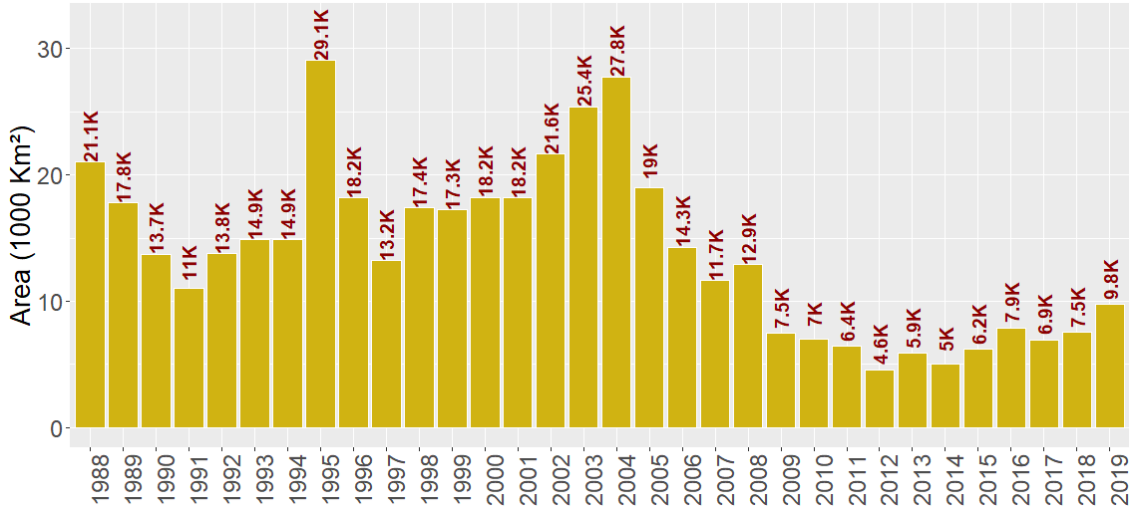

Source: INPE (2019a).

However, Brazil's environmental governance had always been a target of the agribusiness and mining parliamentary front. In 2012, this coalition took advantage of deforestation rates drop to propose controversial revisions to the Forest Code, which drastically reduced environmental protections, besides to soften legislation regulating land use and management on private property, and grant amnesty for owners of areas illegally deforested in the past (SOARES-FILHO et al., 2014). The approval of the new Brazilian Forest Code (BRASIL, 2012) became a turning point in the downward trend of deforestation rates that subsequently crept back up (INPE, 2019a). Additionally, the rising demand for hydropower and mining resources was pushing harder the protected areas network. The same coalition presented legislative proposals to open strictly protected areas for mining concessions, besides prohibiting new protected areas in regions of high mineral or hydropower potential (FERREIRA et al., 2014).

INPE has continually monitoring deforestation in the BLA since the 1980s. The Amazon Deforestation Satellite Monitoring Project (PRODES) (SHIMABUKURO et al., 2012) is

an internationally recognized INPE's monitoring systems that map the clear-cutting deforestation (when there is the complete removal of the forest cover) to compute the official yearly deforestation rates. Despite that, PRODES methodology (CÂMARA et al., 2013) requires time to produce such data, which rule out the rapid intervention from government and environmental control agencies to stop illegal deforestation activities.

To get around this, INPE created the Near Real-Time Deforestation Detection System (DETER) to exploit the high temporal resolution of nearly daily coverage of the MODIS sensor at $250\ m$ spatial resolution (SHIMABUKURO et al., 2012). The DETER system was designed to be an early warning system to support surveillance and control of deforestation, mapping the occurrence of forest degradation and clear-cutting areas greater than 25 ha (DINIZ et al., 2015). However, the reduction in the average size of deforested areas over the years became a major limitation for MODIS-based methodology. Because of that, DETER system started using AWIFIS and WFI sensors imageries at $56\ m$ and $64\ m$ spatial resolutaion, respectively, both with 5 days temporal resolution, to adapt to the changes in deforestation process (DINIZ et al., 2015).

Additionally, INPE maintains the TerraClass Project, which represents a concerted effort to monitor LULCC in the BLA. The database used in this project comprises deforested areas mapped under the PRODES Project, as well as LANDSAT5/TM images and MODIS time-series. Based on information about deforestation dynamics, remote sensing, and geoprocessing techniques, systemic maps of the use and coverage of deforested lands in the BLA have been produced (ALMEIDA et al., 2016). INPE also supports the Wildfire System that detects vegetation fires from different polar-orbiting and geostationary satellites operationally processed in near-real-time (INPE, 2008, 2019b; SETZER et al., 2012).

Given the overview in this chapter, one can be seen that the Amazon rainforest has been under constant pressure despite numerous efforts to monitor it and mitigate deforestation. As stated by Rochedo et al. (2018), "deforestation control is a result of forces arising from institutional arrangements such as enforcing the rule of law and sending signals that may […] incentivize economic agents to decide whether or not to deforest illegally." In summary, environmental governance in Brazil can be separated into three majors periods: before 2004, a period with weak governance and high deforestation rates; between 2005–2012, when there were improvements in environmental governance with effective results

in reducing deforestation; and the period after 2013 when governance has been gradually deteriorating (ROCHEDO et al., 2018).

2.2 Land use and land cover change models

Understanding LULCC is essential for effective natural resource management. Usually, involved parties employ models to explore LULCC dynamics and driving factors, and to support causes and consequences analysis of these changes in order to formulate proper environmental policies. In addition to that, analyses of past LULCC provide necessary information that may assist in comprehend current changes and can be used as parameters to draft alternative scenarios of future LULCC.

LULCC modeling is a complex domain. As stated by Noszczyk (2018), it requires interdisciplinary knowledge, familiarity with statistical and spatial data, and skill in analyses and statistical methods. The selection of the appropriate approach depends on various factors, such as research aims and problems, spatial and temporal scale, and data availability (DANG; KAWASAKI, 2016; NOSZCZYK, 2018). Given the various modeling approaches, choosing the appropriate one can be complicated. Hence, the arrangement of models into similar conceptual approaches allows for a better understanding of their advantages and limitations (CHANG-MARTÍNEZ et al., 2015).

Indeed, LULCC models can be classified in different ways. For instance, as spatial or non-spatial models, which attempt to, respectively, explore the spatial distribution and patterns of change (land allocation), or estimate the rates or quantity of change (land demand) (DALLA-NORA et al., 2014; MAS et al., 2014). LULCC models can also be arranged as static or dynamic. A static model is time-invariant, meaning that it considers the modeled system in equilibrium (steady-state). In turn, a dynamic model is time-dependent, accounting for changes in the system's state over time (WAGNER et al., 2019).

LULCC models can yet be classified as deterministic or stochastic. In deterministic models, there is no randomness associated with it. The output is fully determined by model parameters values and a given set of initial conditions. Therefore, the same model run several times will always produce the same result (possibly repeated over time and spatial units). Conversely, stochastic models, also known as probabilistic models, have inherent randomness. Inputs are described by probability distributions as a way to incorporate uncertainty into the model calculations, and the same parameter values and

initial conditions may lead to different outputs (ABIDEN et al., 2013; ROSA; AHMED; EWERS, 2014; UUSITALO et al., 2015).

Several review studies have previously been produced to create LULCC model taxonomies (VERBURG et al., 2004; HEISTERMANN; MÜLLER; RONNEBERGER, 2006; KOOMEN; RIETVELD; DE NIJS, 2008). More recently, Brown et al. (2012) and Chang-Martínez et al. (2015) described LULCC models into two categories: according to whether the approach is data-driven or theory-driven. The first category includes inductive models, which are consistent in reproducing LULCC patterns, but weak in explaining correlations (KOOMEN; BEURDEN, 2011). These models are empirically fitted (training) from LULCC pattern data over space and time. The variable to be predicted represents the LULCC, whereas predictor variables are factors or indicators that may be related to the changes, such as accessibility (e.g., distance to roads), terrain suitability (e.g., slope), public policies (e.g., protected areas), besides non-spatial data like census data. The data-driven model's output is a map of potential changes, and the model's evaluation is usually centered on the spatial comparison between observed and simulation maps (BROWN et al., 2012; CHANG-MARTÍNEZ et al., 2015).

In turn, the theory-driven approach includes deductive models that are consistent in explaining how and why LULCC will happen, but weak in the spatial allocation of the change (KOOMEN; BEURDEN, 2011). Usually, theory-driven models rest on expert knowledge and information about decision-making that leads to LULCC (process-based). These models seek to represent the essential interactions between agents and their environment, which means the model's calibration consists of determining the agent's behavior rules. Simulation is fundamental to the theory-driven models. Having prospective LULCC maps as output, theory-driven models can be evaluated by the same methods as data-driven models do, but as the primary goal of these models is modeling the change processes, their evaluation centers on agent's rules for decision-making (BROWN et al., 2012; CHANG-MARTÍNEZ et al., 2015).

In addition to those two categories, a hybrid modeling approach could also be defined, representing a compromise between data-driven and theory-driven models. Indeed, there are overlaps among modeling approaches, which complicates their exact classification into one of those two categories. In this context and based on the reviews presented by Brown et al. (2014), Dang and Kawasaki (2016), Michetti and Zampieri (2014), and Noszczyk (2018), seven types of LULCC modeling approaches could be identified: (i)

machine learning; (ii) statistical-based; (iii) Markov chains; (iv) cellular automata; (v) economic-based; (vi) agent-based; and (vii) hybrid approach. It is worthy of mentioning that these approaches are not the only ones to cover the full range of LULCC modeling approaches, but can be considered the key ones.

2.2.1 Machine learning

Machine learning (ML) models are powerful techniques for simulating and predicting LULCC. They are computer algorithms developed to learn from data on how to carry out a particular task automatically (ABURAS; AHAMAD; OMAR, 2019). Hence, ML models are useful for situations where patterns data are available, and theory about processes is scant (BROWN et al., 2014). In LULCC modeling, the learning is commonly supervised and, consequently, both input (change-related variables) and output (change) data must be provided to the ML model to build a functional relationship between these data, capturing LULCC patterns. Unsupervised ML models are less common in LULCC modeling (OMRANI et al., 2015).

As ML models are data-driven, there is a risk of overfitting. This happens when the model fits too well to details of input data (training data) in a way that it fails in generalization (BROWN et al., 2014). Even though, ML models are useful for extrapolations of the functional relationship among variables under the strong assumption of a stationary LULCC process, in which change patterns stay the same as in the precedent time (i.e., business-as-usual scenario). In this sense, the stationarity assumption turns to be a limitation to ML models. New predictor variables might arise over time, and this cannot be accounted for in the predictions. Moreover, calculated transitions rules cannot be changed and be uninterpretable to the users as in an Artificial Neural Network (ANN), which is known as a "black-box" model (DANG; KAWASAKI, 2016; NOSZCZYK, 2018).

ANNs plays a central role in the ML approaches (ABURAS; AHAMAD; OMAR, 2019), but several ML techniques, such as Support Vector Machine (SVM), Decision Trees (DT) (SAMARDŽIĆ-PETROVIĆ et al., 2017), Randon Forest (RF) (KAMUSOKO; GAMBA, 2015), ensemble approaches (BRADLEY et al., 2017), and even deep learning approaches (CAO; DRAGIĆEVIĆ; LI, 2019; HELBER et al., 2018; ZHANG et al., 2019) are also employed for LULCC modeling. ML models are commonly integrated with process-based models, such as Cellular Automata (CA), to improve overall simulation capabilities (BASSE et al., 2014; MUSTAFA et al., 2018).

2.2.2 Statistical-based

Statistical-based (SB) models are also dependent on data to delineate a relationship between LULCC and predictor variables. Such a relationship is generally obtained through linear or logistic regression, binomial or multinomial logit methods, among others (DANG; KAWASAKI, 2016; NOSZCZYK, 2018). SB models assume a fixed mathematical equation whose coefficients are estimated by a statistical process to produce an optimal fit. That is, coefficients are estimated in order to a regression curve fits as closely as possible to the data. Hence, coefficients indicate the influence of independent variables regarding the dependent variable. SB models also provide a confidence degree concerning the contribution of independent variables (BROWN et al., 2014; DANG; KAWASAKI, 2016)

Some limitations might compromise the SB model's usefulness (BROWN et al., 2012). Like ML models, SB models are built based on historical data, and they also assume a stationary LULCC process to extrapolate the mathematical equation to the future. However, SB models are limited in the ability to make out-of-sample predictions and are not suitable for long-term and divergent scenarios. Also, spatial and temporal dependence of data affects SB models (DANG; KAWASAKI, 2016; NOSZCZYK, 2018). SB models are generally used to address linear problems (ABURAS; AHAMAD; OMAR, 2019), and assumptions such as a log-linear relationship between independent and dependent variables are required, which might be a limitation in modeling (BROWN et al., 2012). Even though Logistic Regression (LR) is a widely used SB model in LULCC modeling (ABURAS; AHAMAD; OMAR, 2019). Other SB models such as Frequency Ratio (FR), Weights of Evidence (WoE), Evidential Belief Function (EBF) (AL-SHARIF; PRADHAN, 2016; DING; CHEN; HONG, 2016; SOMA; KUBOTA; ADITIAN, 2019), and non-linear methods, as Generalized Additive Model (GAM) (FENG; TONG, 2017; SUN; ROBINSON, 2018) have also been employed to model LULCC.

2.2.3 Markov chains

Markov chain (MC) models provide a straightforward methodology by which a dynamic system can be analyzed (KUMAR; RADHAKRISHNAN; MATHEW, 2014). MC models are probably the most well-known approach for LULCC models rest on the continuation of historical trends (BROWN et al., 2014), which means that these models also work under the stationarity assumption. In a Markov process, the future system’s state can be simulated purely based on the immediately preceding state. Hence, MC

models describe LULCC from one period to another and apply it to predict future changes (KUMAR; RADHAKRISHNAN; MATHEW, 2014). To do so, these models employ a stochastic transition matrix to represent all possible changes among LULCC classes. For instance, three classes of LULCC result in a matrix M_{3X3} with nine possible changes. Transition matrix defines the probabilities of shifting from one LULCC category to another. It can be obtained by comparing two maps of LULCC classes over time or by expert knowledge (DANG; KAWASAKI, 2016; MAS et al., 2014).

Due to its simplicity, the MC model was a common approach in the early phase of LULCC modeling (BROWN et al., 2014). However, a drawback of MC models is the disregard of the LULCC spatial aspect, i.e., the assumption of spatial independence (NOSZCZYK, 2018). Only cell states are considered, and the influence of neighboring cells is not considered (DANG; KAWASAKI, 2016). To overcome this limitation, MC models have been combined with GIS systems to spatialize the LULCC probabilities, and several hybrid approaches have been proposed by merging MC models with other approaches that simulate the spatial pattern of change, such as Cellular Automata (KUMAR; RADHAKRISHNAN; MATHEW, 2014; LOSIRI et al., 2016; NASIRI et al., 2018).

2.2.4 Cellular automata

Cellular automata (CA) models rest on a mathematical theory of self-reproduction in automata and stochasticity within a two-dimension cellular-grid environment, which is discrete in terms of time and space (DANG; KAWASAKI, 2016; NOSZCZYK, 2018). A CA model consists of five elements: cell space, cell states, neighborhood, transition rules, and time steps. The CA's basic unit of simulation is the cell, and the set of cells make up the cell space. In remote sensing and GIS fields, cells are usually concerned with pixels or any other land unit. All the possible states that can be assigned to the cells correspond to the cell states. Neighborhood defines which adjacent cells to a given cell will be considered during the simulation. In turn, transition rules specify which new state will be assigned to a given cell, taking into account neighboring cells states. Lastly, time step concerns to a time interval between changes in the course of the simulation.

Underlying assumptions of CA models are the continuation of historical trends and patterns, and allocation based on land suitability and neighborhood interaction (BROWN et al., 2014). CA's core principle is that the state of a given cell at time $t + 1$ can be

determined by its state and neighboring cells states at time t (NOSZCZYK, 2018). Changes in each cell are simulated either rest on transition rules or some algorithm. Transition rules can be derived from expert knowledge or statistical analysis. Unlike ANNs, transition rules in CA models are clearly defined. In turn, an algorithm can be employed to update cell states, representing decision-making. This algorithm is applied synchronously to all cell space, and its output stems solely from the cell's attributes (BROWN et al., 2014; NOSZCZYK, 2018).

As CA are spatial models, they are compatible with most spatial data, easily integrated with GIS, and allows to represent straightforward LULCC processes. On the other hand, CA models are entirely reliant on the spatial unit, which means modeling results may change with the variation of cell size and neighborhood configuration (NOSZCZYK, 2018). Nevertheless, CA models are widely used for LULCC modeling (ABURAS; AHAMAD; OMAR, 2019). They are often combined with other modeling approaches (MUSTAFA et al., 2017; RIMAL et al., 2018) besides being part of GIS software (MAS et al., 2014; SOARES-FILHO; RODRIGUES; FOLLADOR, 2013).

2.2.5 Economic-based

Economic-based (EB) models stem from traditional economic theories and aim at explaining changes in land-use patterns with economic-related variables, such as production, consumption, prices, access to markets (MICHETTI; ZAMPIERI, 2014). Hence, these models rest on the assumption that economics is the primary driver of LULCC, and they do not usually take the climate and biophysical drivers into account. Moreover, EB models consider that landowners will use the land to maximize the land's usefulness and expected profits (BROWN et al., 2014; NOSZCZYK, 2018). These models also assume the equilibrium theory to estimate land changes considering the demand-supply relationship (DANG; KAWASAKI, 2016; MICHETTI; ZAMPIERI, 2014). Some EB models can be distinguished by the scope of the economic system they represent. A general equilibrium model represents the global economy, while partial equilibrium models consider detailed descriptions of specific sectors, such as agriculture or forestry production (BROWN et al., 2014; REN et al., 2019).

EB models can describe and quantify the influence of LULCC drivers on land demand. Besides that, they provide the means for exploring the interactions within the human-environment system, as well as for accessing the consequences of policies and decisions

made regarding land uses and their probable effects (CHANG-MARTÍNEZ et al., 2015; MICHETTI; ZAMPIERI, 2014). EB models' parameters are often estimated using econometric methods. In other cases, parameters may be guided by either theory taken from previous studies or a range of values to explore the model's sensitivity (BROWN et al., 2014). A drawback of EB models is that they do not take into full account the geographical location of change (NOSZCZYK, 2018), as these models assume economics as the primary driver of LULCC.

2.2.6 Agent-based

Agent-based (AB) models, often called as multi-agent systems, describe intelligent agents, their environment, and possible interactions. Agents are discrete entities characterized by their attributes and their behaviors. They can interact with each other and with the environment to collect information or carry out actions that modify their context. Regarding the LULCC, agents could be landowners, households, farmers, policy-making bodies, or any actors that make decisions or take actions that affect the LULCC patterns (BROWN et al., 2014). AB models allow modelers to capture the stakeholder's specialized knowledge and perform scenario analysis (DANG; KAWASAKI, 2016). Hence, an AB model for LULCC consists of a map of the area of interest and a model with agents representing human decision-making in a very flexible and context-dependent way (GROENEVELD et al., 2017; NOSZCZYK, 2018).

As stated by Groeneveld et al. (2017), the majority of human decisions AB models for LULCC are not explicitly based on theory, and the flexibility of these models comes along with ad hoc assumptions of the decision process. AB models facilitate modeling of feedback loops between human and environmental systems. Any interaction in AB models is based on prescribed rules whose descriptions can be difficult and controversial. For instance, agent preferences may be determined by expert judgment with questionnaire surveys. Apart from expert knowledge, AB models facilitate the integration of other data sources, such as current trends and existing models (NOSZCZYK, 2018). However, these models tend to concentrate on the most readily apparent and quantifiable aspects of LULCC and do not account for factors such as outmigration, changes in techniques and input use, and the influence of regional and global economic variables (DANG; KAWASAKI, 2016).

2.2.7 Hybrid approaches

No single model can take all LULCC characteristics into account owing to the complex nature of it. In light of this, a hybrid approach, i.e., a merger of two or more individuals models, is employed to represent the various aspect of LULCC patterns and processes (BROWN et al., 2014; NOSZCZYK, 2018). Hybrid approaches take advantage of the strengths of individual ones in order to reduce some of their inherent limitations, allowing better representation of the LULCC (BROWN et al., 2014). As stated by Dang and Kawasaki (2016), combining the best aspect of different approaches helps to cover several disciplines, mutual relationships, and link social science with spatial data to represent the LULCC process.

Broad diversity of hybrid approaches have evolved over the years. Figure 2.2 tries to summarize the development of hybrid approaches for LULCC modeling with a relative timing. The arrows indicate the approximate moment when two or more different approaches were ensemble and employed in LULCC modeling, according to Dang and Kawasaki (2016). Additionally, Figure 2.2 presents a rough arrangement of LULCC models in terms of their emphasis on data-driven (blue zone) or theory-driven (green zone).

Some hybrid approach achievements include solving problems of temporal and spatial scale and covering multi-discipline and multi-scale approach (DANG; KAWASAKI, 2016). For example, an SB model like spatial regression can be used to solve spatial mismatches between the imposition of regular boundaries on grid cells of a CA model. On the other hand, an EB model is used to estimate land demand, while an ML model like ANN is used to explain land allocation (DALLA-NORA et al., 2014; DANG; KAWASAKI, 2016).

Figure 2.2 - LULCC models classification according to whether the approach is data-driven or theory-driven. The development of hybrid approaches over time is presented.

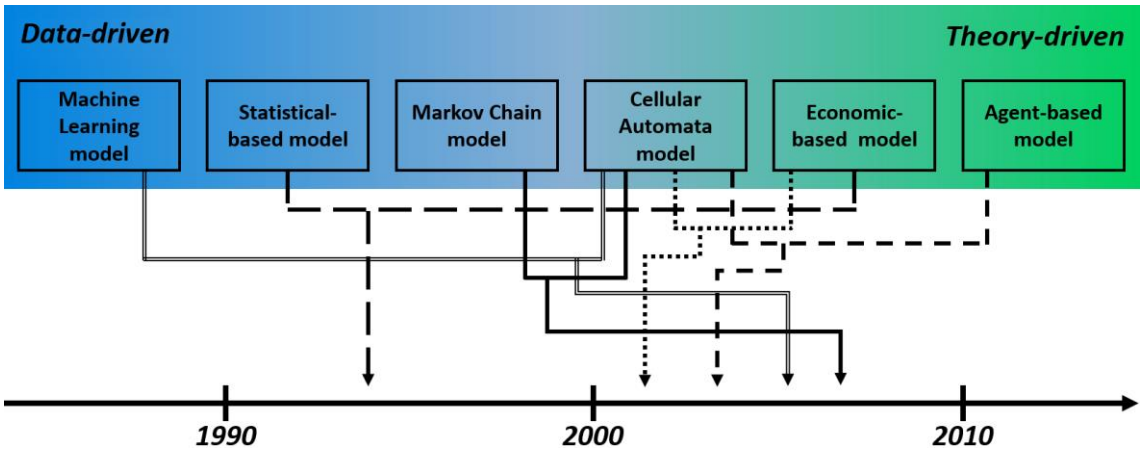

Source: Adapted from Dang and Kawasaki (2016).

However, the combination of different methods/techniques also has some drawbacks. It requires a vast knowledge of appropriate tools and leads to an increased modeling complexity, which might reduce the interpretation of simulated LULCC. Models calibration and validation can be challenging (BROWN et al., 2014). Feedback loops and cross-scale interactions is a time-consuming task. A higher level of methodological integration requires more data. Besides that, data integration process can be laborious when data sources, units of analysis, spatial or time resolutions do not coincide (DANG; KAWASAKI, 2016).

Although the review studies aforementioned do not explicitly bring up Bayesian Network (BN) as an example of a LULCC model, it can be defined as a hybrid approach, comprising a linkage between data-driven and theory-driven approaches. BN models stand out among other approaches because the definition of their structure and parameters can rest on different sources of information, such as empirical data, expert knowledge, or a combination of both (JOHNSON; LOW-CHOY; MENGERSEN, 2012; LANDUYT et al., 2013; POLLINO; HENDERSON, 2010). In this context, a BN model can be defined as a supervised ML approach since its parameters can directly be computed from the dataset. Besides that, BN models rest on a robust statistical framework for uncertainties analysis (PUGA; KRZYWINSKI; ALTMAN, 2015) that allows classifying them also as an SB approach. On the other hand, when data learning cannot be applied because of data scarcity, experts and stakeholders' elicitations can be employed (SPEROTTO et al., 2017), and a BN model turns to be a more theory-driven related model.

2.3 Bayesian networks

Bayesian Networks (BNs), also known as Bayesian Belief Networks, are probabilistic graphical models based on qualitative and quantitative components (AGUILERA et al., 2011; NEAPOLITAN, 2004). The qualitative component $\boldsymbol{G} = (\boldsymbol{V}, \boldsymbol{A})$ is a direct acyclic graph (DAG) that comprises a set of n nodes $\boldsymbol{V} = \{V_1, V_2, \dots, V_n\}$, representing n variables in the model; and also a set of directed arcs $\boldsymbol{A} \subseteq \boldsymbol{V} \times \boldsymbol{V}$, indicating the existence of statistical dependence among the variables (AGUILERA et al., 2011). Thereby, an arc $V_i \rightarrow V_j$ indicates that V_i (parent node) has an effect on V_j (child node).

The quantitative component refers to a set of conditional probability distributions. Considering that variables in a BN modeling are discrete or continuously discretized, parent and child variable relationships can be computed through discrete conditional probability distributions, which is represented by a conditional probability table (CPT) in the form $P\big(V_i|pa(V_i)\big)$, i.e., the probability of the node V_i takes on a specific state given the states of its parents $pa(V_i)$. For parentless node, $P\big(V_i|pa(V_i)\big)$ simplify to $P(V_i)$ (LANDUYT; BROEKX; GOETHALS, 2016). A conditional probability distribution is attached to each node, quantitatively describing the dependencies on its parents.

Figure 2.3 illustrates an example of a BN made up by a set of four nodes $\boldsymbol{V} = \{A, B, C, D\}$. Each node has two mutually exclusive states: $True$ and $False$. In turn, the BN's arcs are defined by $\boldsymbol{A} = \big\{\{A, C\}, \{B, C\}, \{C, D\}\big\}$, which means that A and B are parent nodes of C, while C is the parent of node D. The CPT attached to each node is presented through the bar-plot in Figure 2.3. For instance, for the parentless node A, the probability of this node to take on the state $True$ equals to 0.8, i.e., $P(A = True) = 0.8$, while the probability of it to take on the state $False$ must be complementary and, therefore, equals 0.2, i.e., $P(A = False) = 0.2$. These values are represented by the black and gray stacked bars for node A. Regarding node C that has two parent nodes, its probability is conditionally dependent on A and B. Thus, considering that both nodes A and B takes on $True$ state (two black dots above the bars), we have $P(C = True \mid A = True,\ B = True) = 0.9$ and $P(C = False \mid A = True,\ B = True) = 0.1$. On the other hand, if A and B takes on $False$ state (two gray dots above the bars), $P(C = True \mid A = False,\ B = False) = 0.05$ and $P(C = False \mid A = False,\ B = False) = 0.95$.

Figure 2.3 - Example of a BN model with four variables $\mathbf{V} = \{\mathrm{A}, \mathrm{B}, \mathrm{C}, \mathrm{D}\}$ (on the left). Grey colored node indicates an evidence presence by selecting a state ($\mathrm{C} = \mathrm{true}$). Values in other nodes are the posterior probabilities given such evidence. Bar plot (on the right) illustrates the probability distributions attached to each variable. Conditional probabilities for variables C and D describe dependencies on their parents.

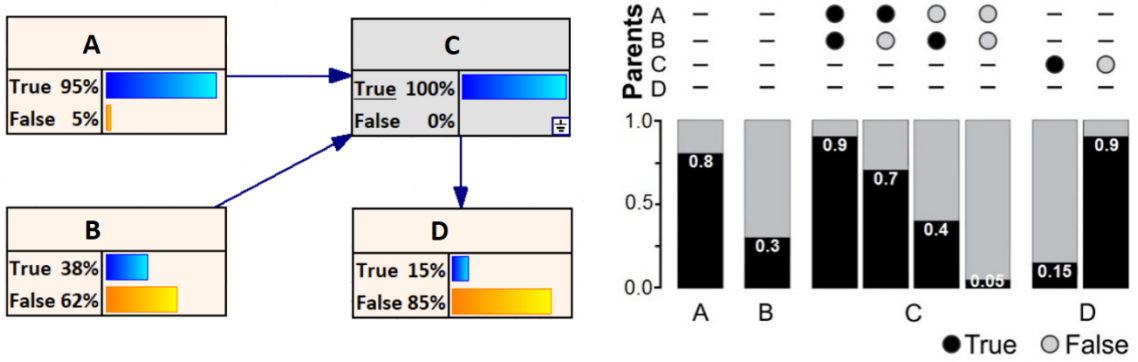

Source: author's production.

An important quantity in a BN is the joint probability distribution (Equation 2.1), which is obtained by multiplying all conditional probability distributions (NEAPOLITAN, 2004). It corresponds to the probability of a specific scenario occurring, which means each node in the model takes on a state. In the example BN (Figure 2.3), the joint probability is calculated by $P(A, B, C, D) = P(A)P(B)P(C|A, B)P(D|C)$.

$$P(V_1, \ldots, V_n) = \prod_{i=1}^{n} P\big(V_i \mid pa(V_i)\big). \tag{2.1}$$

The fundamental assignment of the BNs is to compute the probability of an event occurring in the light of new evidence. As each node in the BN has a set of mutually exclusive states, the evidence is entered into the network by the instantiation (i.e., the observation) of a state in one or more nodes (CHEN; POLLINO, 2012). The reasoning to update the probabilities of the other variables lies in the Bayes' theorem (NEAPOLITAN, 2004):

$$P(V_i = v_i \mid e) = \frac{P(e \mid V_i = v_i)P(V_i = v_i)}{P(e)}. \tag{2.2}$$

The term $P(V_i = v_i \mid e)$ is the posteriori probability of the event $V_i = v_i$ (variable V_i takes on the state v_i) conditioned upon some evidence e; $P(e \mid V_i = v_i)$ is the likelihood of e given $V_i = v_i$. The term $P(V_i = v_i)$ is the prior or marginal probability of the event $V_i = v_i$ and $P(e)$ is a normalizing constant. Through the Bayes' theorem, it is possible to consistently propagate the impact of the evidence throughout the network, updating the

priori probabilities of the other variables. For instance, taking into account the BN in Figure 2.3, estimations about the variable A can be refined by observing the state of the variable C. Thus, the prior knowledge $P(A = true) = 80\%$ (illustrated in the bar plot) is updated to $P(A = true \mid C = true) = 95\%$. Therefore, having information about C increases the beliefs about A. This ability to compute posterior probabilities given new evidence is called inference.

2.4 Spatial bayesian networks

BNs have limitations in representing spatial variability. A Spatial BN (SBN) can be a BN designed to model the spatial variability through its structure (i.e., DAG). It is assumed that the value of a variable in any location depends only on the variables at adjacent locations (POLLINO; HENDERSON, 2010). Hence, two SBN approaches can be designed: (i) each spatial unit (region, cell or pixel) is represented by one network's node (Figure 2.4-a) that can be linked to neighboring nodes (DAS et al., 2017); and (ii) each spatial unit is represented by one instance of the network (Figure 2.4-b), in which output nodes are linked to input nodes of adjacent networks (GIRETTI; CARBONARI; NATICCHI, 2012). Nonetheless, for modeling in high spatial resolution (i.e., small spatial units), or a study area encompassing a large territorial extension, a huge number of nodes and causal links would be required to incorporate spatial variability into the model, regardless of the employed approach. Besides that, feedback loops cannot occur due to the acyclic nature of BN's structure, unless the model also incorporates temporal variability, which will further increase the BN's structure complexity (GIRETTI; CARBONARI; NATICCHI, 2012; POLLINO; HENDERSON, 2010).

Figure 2.4 - Example of SBN approaches. Spatial units represented by network's nodes (a); spatial units represented by instances of the network (b); and network with spatial node (c).

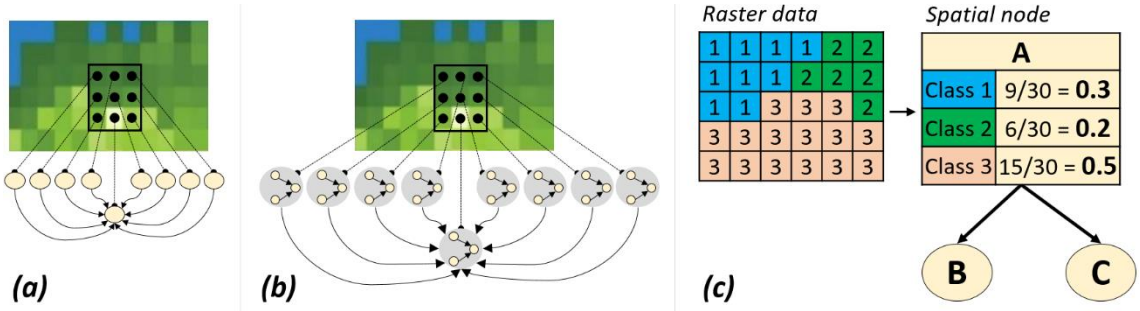

Source: author's production.

As any LULCC has a spatial dimension of interest, it should be considered in the modeling. Thus, another approach to overcome BN's weakness in representing geographic information is by using spatial nodes (Figure 2.4-c). This type of node is spatially described (JOHNSON; LOW-CHOY; MENGERSEN, 2012), and it summarizes the spatial distribution of the variable through the probability distribution. This approach confers to the BN a spatially explicit strategy, but it only permits to reproduce static changes through space (SPEROTTO et al., 2017), representing the system and variables relationships at a particular point in time (CHEN et al., 2019). In general, the LULCC analysis relies on the use of static data from two points in time corresponding to the begin and end of the time frame (WAGNER et al., 2019)

For each spatial node in the SBN, a raster layer from a GIS tool must be available. Hence, it is useful to consider the integration of BNs with GIS. BN-GIS integration has gained considerable interest over the years as the potential way to include spatial information into the modeling (CHEN; POLLINO, 2012; LANDUYT et al., 2013). The connection between BNs and GIS can be accomplished in different ways (JOHNSON; LOW-CHOY; MENGERSEN, 2012), but it is predominantly used to map BN's outputs based on the georeferenced inputs (LANDUYT et al., 2013). That means a GIS tool stores the raster data needed to parametrize the BN, whose output is then computed for each location (region/cell/pixel as inputted from GIS) to represent the outcomes in spatially explicit maps. Therefore, BN-GIS integration allows for quantifying and visualizing the uncertainties associated with the spatial system (LANDUYT et al., 2015).

Among the several BN software and packages available (KORB; NICHOLSON, 2010), *Netica* and *Hugin* are commonly used in BN-GIS integration. The reviews presented by Aguilera et al. (2011), Landuyt et al. (2013), and Pérez-Miñana (2016) demonstrate the scientific community preference for the software *Netica*, followed by *Hugin*. For instance, Grêt-Regamey and Straub (2006) embedded a BN from the *Hugin* software into the *ArcGIS* to accesses the uncertainties involved in the avalanche run-out zones as well as estimating the damage potential. Aitkenhead and Aalders (2009) applied an evolutionary process to a BN developed from *Netica* with spatial input data extracted from *ArcGIS* to predict LULCC. Stelzenmüller et al. (2010) used the *Netica* software to develop a BN-GIS framework that supports marine spatial planning and evaluate the impact of human activities on marine habitats.

To enhance the interaction between BN models and spatial data, Landuyt et al. (2015) developed a plug-in that couples *Netica* and *QGIS* software to model spatial processes and associated uncertainties. Balbi et al. (2016) proposed a BN-GIS framework combining the software *GeNIe* and *QGIS* to assess the benefits of early warning for urban flood risk to people. Likewise, Abebe, Kabir, and Tesfamariam (2018) embedded spatial information from *ArcGIS* into the BN constructed from *Netica* to model the urban areas' flood vulnerability. In turn, Sahin et al. (2019) presented an integrated approach combining BNs developed on *Netica*, with input data extracted from *ArcGIS* spatial layers to predict coastal erosion induced by sea-level rise.

Therefore, SBNs may integrate two tools: one to build the BN and another to deal with spatial data. Those commonly used BNs software aforementioned (*Netica* and *Hugin*) provide efficient Bayesian inference algorithms with a comprehensible user-friendly interface. However, they are expensive when compared to open source software (LANDUYT et al., 2015). Besides that, there are packages and libraries from specific programming languages like *R* (R CORE TEAM, 2019) capable of dealing with both BNs and spatial data in the same programming environment.

In this context, studies have employed *R*'s packages to create SBN methods for different purposes. For instance, Mello et al. (2013) developed a method able to incorporate expert's knowledge and tested it on a case study for soybean crop mapping. This method has been improved by Silva, Fonseca, and Körting, (2017) and applied it as a prediction tool for identifying potential areas for sugarcane expansion. Gonzalez-Redin et al. (2016) proposed a tool also developed with *R*'s packages to evaluate trade-offs between forest production and conservation measures to preserve biodiversity in forested habitats. In turn, Wijesiri et al. (2018) presented a spatial BN method to model urban water quality and identify environmental and anthropogenic factors that pose risks to human health. All these studies are pixel-based, which means the outputs of the proposed method are raster layers, where pixels values correspond to occurrence probabilities of the studied phenomenon.

2.5 Dynamic bayesian networks

In addition to spatial variability, it is also essential to model how the world changes over time. However, BNs also have limitations in representing dynamic systems (POLLINO; HENDERSON, 2010; UUSITALO, 2007). Due to the acyclic characteristics of its structure (i.e., DAG), a BN is unable to represent feedback loops and systems that change

over time (CHEN; POLLINO, 2012; LANDUYT et al., 2013), which means BNs are static, modeling a system at a specific moment. Thus, a "dynamic" approach of BNs could depict more realistic modeling.

Dynamic Bayesian Networks[2] (DBNs) extend the concept of BNs by relating variables across time (MALDONADO et al., 2019). In DBN modeling, the timeline is always broken into a finite number of intervals called time-slices (SPEROTTO et al., 2017), and a BN is replicated for each time-slice (SHIHAB, 2008). In this context, a DBN can be seen as a sequence of snapshots of the system (KHAKZAD, 2019), each one represented by one BN at a given time (HU et al., 2015). These BNs are sequentially chained so that network nodes from a previous time-slice are linked to network nodes from the next time-slice (LANDUYT et al., 2013). Figure 2.5 presents an example of a DBN model. Figure 2.5-a shows an unconventional graphical notation, which is used to represent a collapsed DBN model with feedback loops (MALDONADO et al., 2019). The same DBN is presented in Figure 2.5-b, but propagated for three time-slices thereby the arcs became acyclic.

Figure 2.5 - Example of a Dynamic Bayesian Network (DBN). A collapsed DBN (a); and an unrolled DBN in three time-slices (b). Full-filled black arrows indicate non-temporal arcs, while the red dashed arrows are temporal arcs.

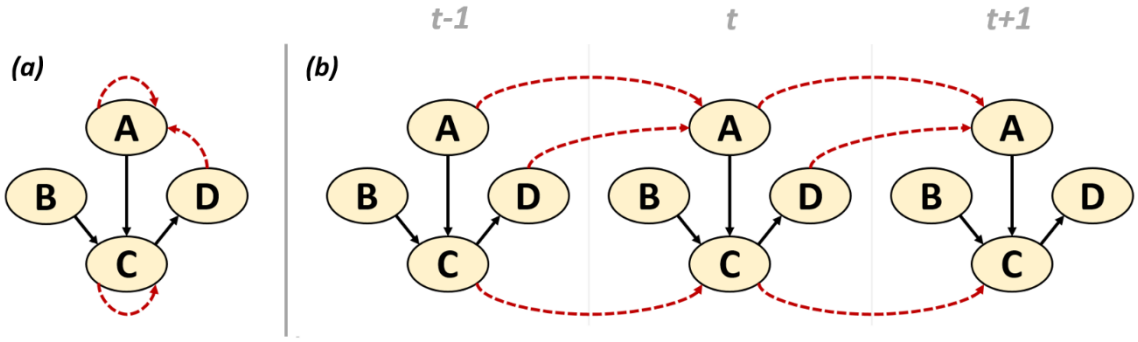

Source: author's production.

Let's consider a set of nodes $\boldsymbol{V} = \{V_1, V_2, \ldots, V_n\}$ that represents variables of the system to be modeled. When constructing a DBN, one node V_i and for each time-slice t must be included in the network. Hence, the system at the time t is represented by the set of nodes

[2] Also called as Dynamic Belief Networks, Probabilistic Temporal Networks or Temporal Bayesian Networks (KHAKZAD; KHAN; AMYOTTE, 2013; KORB; NICHOLSON, 2010; MARCOT; PENMAN, 2019).

$\boldsymbol{V^t} = \{V_1^t, V_2^t, \ldots, V_n^t\}$. As variables can be related to each other at the same time-slice as well as at successive time-slice, a DBN can present arcs connecting (i) different nodes at the same time-slice, $V_i^t \rightarrow V_j^t$; (ii) the same node over time, $V_i^t \rightarrow V_i^{t+1}$; and (ii) different nodes over time, $V_i^t \rightarrow V_j^{t+1}$ (KORB; NICHOLSON, 2010).

Temporal variables that change over time and have effects on other variables in the future are represented by temporal nodes in the DBN. These nodes are linked by temporal arcs (i.e., arcs linking nodes from different time-slices). In turn, those static variables that do not change over time and are related to others only in the current time-slice, are represented by static nodes. In Figure 2.5, just B is a static node, while A, C, and D are temporal nodes. One can observe that a DBN does not have backward links between successive time-slices. Only forward temporal arcs are allowed, reflecting the causal flow of time (HU et al., 2015; MURPHY, 2002)

Normally, it is assumed that the structure of the replicated BN is the same, regardless of the time-slice (RUSSELL; NORVING, 2010). Furthermore, the assumption of a steady process is taken (GIRETTI; CARBONARI; NATICCHI, 2012) and, therefore, temporal arcs are also the same for any transition $t \rightarrow t + 1$. In this context, a DBN is a time-invariant model (MALDONADO et al., 2019). Note that the term "dynamic" means that the system's development is modeled over time and not that the model structure and its parameters change over time (MOLINA et al., 2013; MURPHY, 2002).

In the case of systems with multiple variables, the number of nodes and arcs in a DBN can increase very quickly in a few time-slices, especially if the interval between time-slices is too short. Moreover, considering that the system's state at time t may depend on its states at previous k time-slices, with $1 \leq k < t - k$ (MOLINA et al., 2013), establish dependence relationships among nodes can become cumbersome, requiring more time and computational power to run the DBN (POLLINO; HENDERSON, 2010). To work around this issue, the system is considered to be a first-order Markov process, so that:

$$P(\boldsymbol{V^t} \mid \boldsymbol{V^{0:t-1}}) = P(\boldsymbol{V^t} \mid \boldsymbol{V^{t-1}}). \quad (2.3)$$

This assumption takes that the system's state depends only on the immediately preceding state ($k = 1$) and not on any earlier ones. In other words, the current state provides enough information to make the future conditionally independent of the past (MOLINA et al., 2013; RUSSELL; NORVING, 2010). However, there is no fundamental reason why a system cannot be depended on its earlier states, and even though the first-order Markov

property is quite restrictive, it is assumed to simplify the DBN modeling (MOLINA et al., 2013; MURPHY, 2002; POLLINO; HENDERSON, 2010).

A DBN under the first-order Markov property is often defined as a pair $(\boldsymbol{G_1}, \boldsymbol{G_{\rightarrow}})$, in which $\boldsymbol{G_1}$ represents the initial BN with the prior distributions $P(\boldsymbol{V^1})$, and $\boldsymbol{G_{\rightarrow}}$ is a two-slice temporal BN (2TBN) that defines the transition distributions $P(\boldsymbol{V^{t-1} \mid V^t})$ (MOLINA et al., 2013; MURPHY, 2002). As with BNs, the relationships among variables are quantified by conditional probability distributions represented by conditional probability tables (CPTs) associated with each DBN's node, as follows $P(V_i^t \mid pa(V_i^t))$, in which V_i^t is the i's node at the time t, and $pa(V_i^t)$ represents all parent nodes of V_i^t in the graph (MURPHY, 2002; NEAPOLITAN, 2004). Note that $pa(V_i^t)$ may include nodes from the previous as well as from the current time-slices.

Taking into account all the assumptions aforementioned, DBN's specification must include: (i) nodes and their names; (ii) non-temporal arcs; (iii) temporal arcs; (iv) CPTs for the BN in the time-slice $t-1$ (when there are no parent nodes from a previous time); and (v) CPTs for the BN in the time-slice t (when parent nodes may be from $t-1$ or t time-slices) (KORB; NICHOLSON, 2010). It is worthy to mention that this specification encompasses other models such as Hidden Markov Models (HMMs) and Kalman Filter Models (KFMs), which can be generalized by DBNs (BARBER; CEMGIL, 2010; MURPHY, 2002).

According to the survey carried out by Korb and Nicholson (2010), among the various BN software and packages available, only a few have support for DBN modelings, such as *GeNIe*, *BNT-Matlab*, *Hugin*, and *Netica*. Carmona, Castillo, and Millán (2008) developed DBNs through *GeNIe* software to model and evaluate students' learning styles. Mcnaught and Zagorecki (2009) used the same software to design a DBN to the prognostic modeling of equipment in order to better inform maintenance decision-making. More recently, Petousis et al. (2016) proposed a set of DBNs also developed thought the *GeNIe* software to identify high-risk lung cancer; the DBNs demonstrated high discrimination and predictive power. In turn, Chhabra, Krishna, and Verma (2019) used *GeNIe* to design a DBN that considers driver, vehicle, and environment information for driver behavior classification to support an intelligent transportation system.

Other software and packages have also been used for DBN modeling in diverse areas. For instance, Ghanmi, Awal, and Kooli (2017) developed through the *BNT-Matlab* toolbox a

DBN approach to recognize Arabic handwritten words; while Uusitalo et al. (2018) and Maldonado et al. (2019) developed a series of DBNs to assess and analyze structural changes in a marine ecosystem. Also using the *BNT* toolbox, Kourou (2020) developed a DBN model for cancer classification based on genetic information. Cai, Liu, and Xie (2016) developed a DBN through *Netica* software to model the dynamic degradation process of electronic systems for fault diagnosis. In turn, Cuaya et al. (2013) employed the *Hugin* software to develop DBN models to predict the individual's risk of fall based on pathological gait data, whereas Kozlow, Abid, and Yanushkevish (2018) focused on utilizing biometrics characteristics to identify abnormalities on individual's gait.

2.6 Spatio-temporal bayesian networks

As presented in the previous sections, BNs are limited to dealing with systems that may change over space and time. Thus, SBN and DBN are necessary to incorporate spatial and temporal domains into the modeling. However, space and time should not be considered separately, since both are inherent to an environmental system's evolution and, therefore, play a crucial role in monitoring and managing of spatio-temporal processes, such as LULCC. In this context, a Spatio-Temporal Bayesian Network (STBN) is appropriate to combine the spatial and temporal variability of a system into the BN modeling.

An STBN may represent the spatial and temporal variability through its structure. Similarly to SBN, two approaches can be designed: (i) each spatial unit is represented by one network's node (Figure 2.6-a) that is linked to the neighboring nodes in the current and next time-slice (DAS; GHOSH, 2019); and (ii) each spatial unit is represented by one instance of the network (Figure 2.6-b), so that, output nodes are linked to input nodes of networks in adjacent spatial units and in the next time-slice (GIRETTI; CARBONARI; NATICCHI, 2012). Nonetheless, these approaches can quickly become unwieldy and impracticable since an enormous number of nodes and causal connections are required to represent both spatial and temporal variability in a few time-slices forward.

STBN modeling has been employed for diverse purposes. For instance, Giretti, Carbonari, and Naticchi (2012) presented an STBN model as a decision support system for risk management of forest fires. The proposed approach refers to that one presented in Figure 2.6-b, in which instances of the same network are used to represent each spatial unit. Employing a similar approach, Wilkinson et al. (2013) and Chee et al. (2016) presented an STBN model that uses object-oriented techniques and state-and-transition

models to manage both woody shrubs unwanted expansions and eucalyptus woodland restoration. Also using that approach, Das and Ghosh (2019) proposed an STBN model to capture the temporal dynamics of spatial dependency among variables. They carried out a case study of predicting Normalized Difference Vegetation Index (NDVI) imagery.

On the other hand, an STBN can also be designed by incorporating spatial nodes into DBNs (Figure 2.6-c). As previously mentioned, this type of node summarizes the spatial distribution of the variable through the conditional probability table (CPT) attached to the node. This approach requires a GIS-tool integration to confers to the DBN a spatially explicit strategy (MARCOT; PENMAN, 2019). A spatial node must be replicated for each time-slice of the DBN (i.e., spatio-temporal nodes) if the spatial variable it represents changes over time. Figure 2.6-c shows an example in which the spatial variable changes between $t-1$ and t time-slices, as can be seen in the raster data. The CPT attached to the spatio-temporal node A^t represents the transitions among the variable's classes from previous to current time-slice. Therefore, for any spatio-temporal variable included in the STBN modeling, a raster data time series must be provided as input to compute CPTs that indicate changes over time (SILVA et al., 2020).

Figure 2.6 - Example of STBN approaches. Spatial units represented by network's node (a); spatial units represented by instances of networks (b); and spatio-temporal node (c).

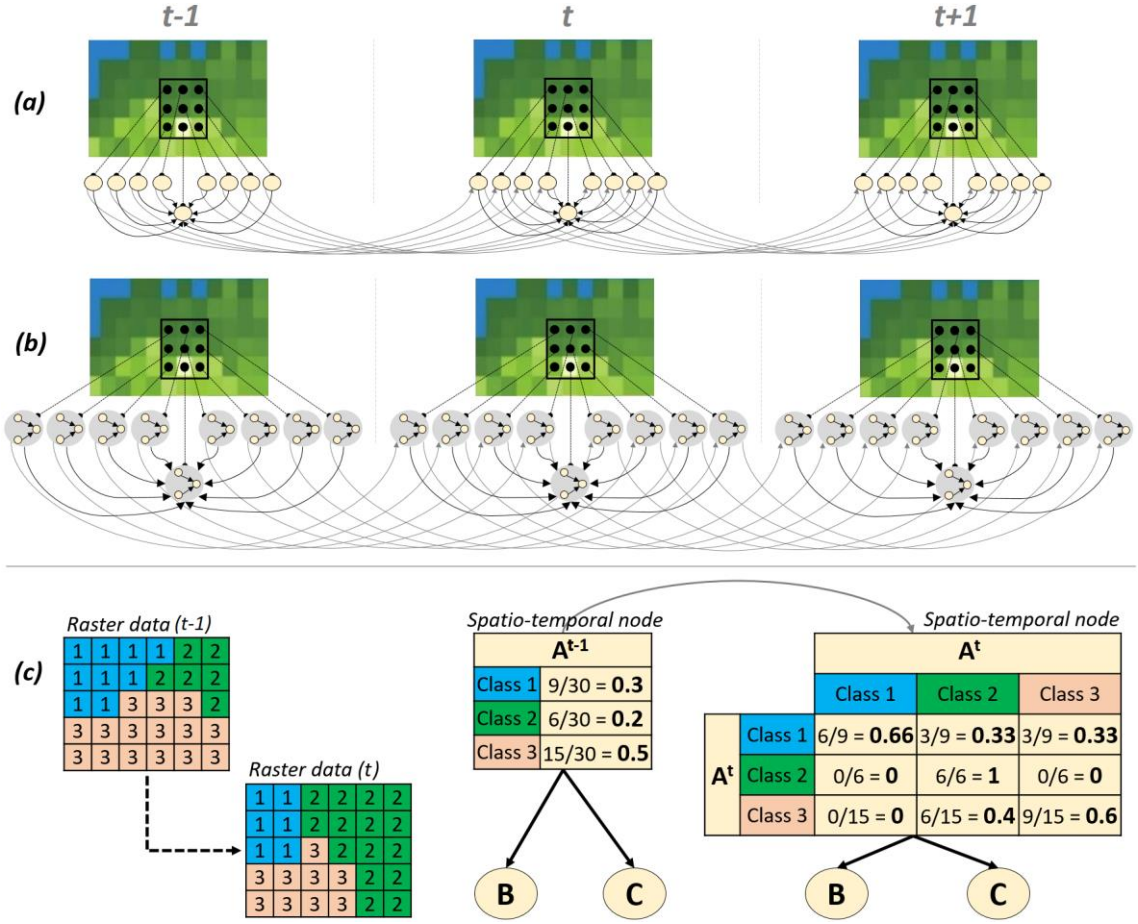

Source: author's production.

STBN approaches derived from the use of spatial nodes into DBNs, as in Figure 2.6-c, are also widely used. Qu, Zhang and Wang (2012), and Zhang et al. (2012) presented an STBN model to improve the estimation of leaf area index (LAI) time series by using remotely sensed data, ground meteorological station data, and crop growth information. Trifonova et al. (2015, 2017) used STBNs to model the marine species dynamics as well as their interactions with external stressors. Hasan and Haddawy (2016), and Haddawy et al. (2018) demonstrated the potential of an STBN model as a system to support targeted interventions by predicting the weekly occurrence of malaria at local levels. In turn, Silva et al. (2020) presented an approach that refers to a stepwise application of an SBN model over time, as an alternative to estimate deforestation risk in an expansion frontier with the Brazilian Amazon region.

In general, the aforementioned studies show that modeling the current state or the evolution of systems that may change over space and time is a tough task given the

various uncertainties involved. As an STBN model can perform probabilistic reasonings considering both the spatial and temporal domains, it seems to be an appropriate approach to estimate LULCC, particularly deforestation risk. Apply BNs to predict deforestation risk is not unprecedented (DLAMINI, 2016; KRÜGER; LAKES, 2015; MAYFIELD et al., 2017). However, deforestation has been considered as a static process when modeled by BNs, which means no time information has been incorporated into the modeling. In this context, the STBN models developed in this thesis can be readily used to predict deforestation risk taking into account both space and time information.

3. SPATIO-TEMPORAL BAYESIAN NETWORK FOR R (*stbnR*)

Including spatio-temporal information into the BN model presents some challenges. Several works that employ Spatial BNs (SBNs) or Spatio-Temporal BN (STBNs) use at least two different tools to perform the complete analysis: a BN software to build the network structure and carry out Bayesian analysis, in addition to GIS that provides necessary functions for spatial data collection, management, and storage (STEINIGER; HAY, 2009). Although efforts have already been made to BN-GIS integration (LANDUYT et al., 2015), the use of two different tools can bring up challenges such as the integration, transfer, and conversion of data from one tool to another.

Therefore, a framework capable of integrating all the steps to perform STBN modeling into a single environment seems to be a great demand. In this context, the contribution of this thesis is the implementation of a package for *R* programming language named *stbnR* (**S**patio-**T**emporal **B**ayesian **N**etwork for **R**), which enables complete STBN modeling within the *R* environment. This package integrates other ones already available for *R* language that specifically deal with either spatial and spatio-temporal data manipulation or BN analysis and inference. Hence, the *stbnR* package enables the development of STBN-based models for any phenomenon that has some spatio-temporal variation and/or is influenced by some spatio-temporal variable.

R is free software and programming language (R CORE TEAM, 2019) that provides a consistent working environment for statistical computing and analysis. Packages are fundamental units of reproducible *R* code that increase the power of *R* by improving existing base *R* functionalities or by adding new ones. For instance, the *raster* package (HIJMANS et al., 2019) is for gridded spatial data manipulation and analysis, while the *gRain* package (HØJSGAARD, 2012, 2019) handles with analysis and inference of categorical BNs. Both *raster* and *gRain* packages were the basis for the *stbnR* package development.

In addition to those, special attention should be given to the *bnspatial* package (MASANTE, 2019) as it is directly related to the work developed in this thesis. This package also integrates functions from both *raster* and *gRain* packages to enable the development of SBN models, employing the spatial node concept (as represented in Figure 2.3-c). Hence, the *bnspatial* package provides the necessary functions for a complete SBN modeling in *R*. On the other hand, there seem to be no available options for STBN modeling.

Figure 3.1 shows a general workflow with the *stbnR* package. In short, input raster data of the variables model are required as well as a settings file. Based on this file, the raster data are converted to a formatted table, which is used to build and parameterize the STBN. An external BN model can optionally be used to build it. With the STBN trained, the next step is to compute the occurrence probability of the studied phenomenon in the future for the entire region of interest.

Figure 3.1 - General workflow of the stbnR package. Blue boxes represent procedures, while yellow boxes represent input/outputs.

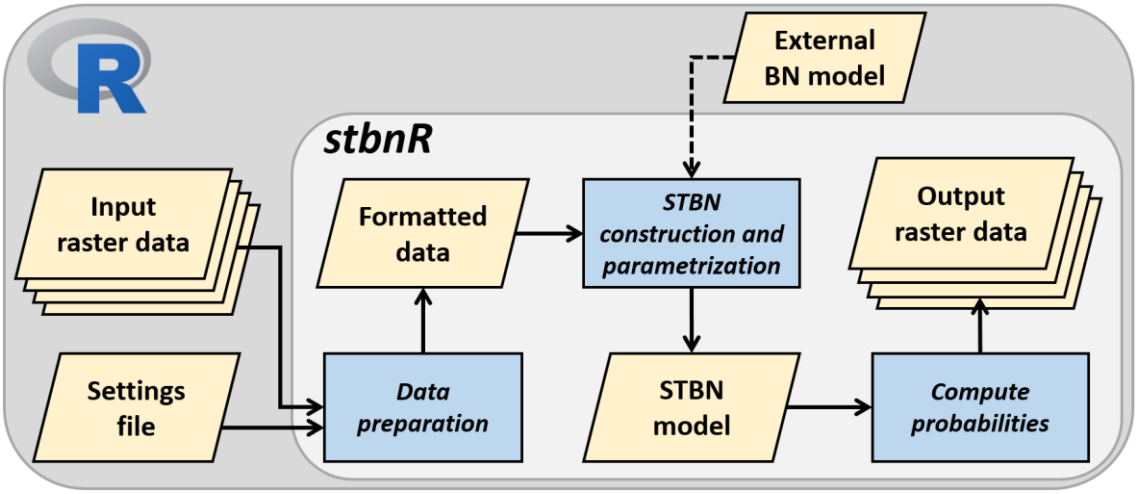

Source: author's production.

Some requirements must be pre-established before starting the modeling with the stbnR package, such as (i) the variables to be included in the model; (ii) the relationship among these variables; (iii) the thresholds to discretize continuous variables; (iv) the analysis period; and (v) the interval Δt between time-slices. Variables selection can be carried out through feature selection methods (CHANDRASHEKAR; SAHIN, 2014; VERGARA; ESTÉVEZ, 2014), along with the support of experts and stakeholders. Their knowledge can also be used as a source of information to define the model's structure and parameters (AGUILERA et al., 2011; LANDUYT et al., 2013; PÉREZ-MIÑANA, 2016). As the *stbnR* package deals with only discrete variables, continuous ones are discretized according to the thresholds defined by the user. Regarding the modeling period, it establishes the amount of data needed to enter into the STBN as observed evidence. The interval Δt is mainly defined by the frequency at which data are available. For instance, if data availability is daily, the interval Δt may be one day, so the time-slice $t-1$

represents how the system was yesterday, while the time-slice t represents how the system is today. The analogy is the same for availability of weekly, monthly, or annual data.

An example of an STBN-based LULCC model is presented for a better understanding of the *stbnR* package functions. Let us consider that the requirements aforementioned have already been established and we obtained the STBN model presented in Figure 3.2. It shows the variables that make up the model and how they are related to each other in the same time-slice and between time-slices. The example STBN model is composed of four variables represented by nodes A, B, C, and D in two different time-slices. At least two time-slices are mandatory to build an STBN model using the *stbnR* package. The first one corresponding to how the system was in the past, while the second time-slice corresponds to the variables changes after a time interval Δt.

Figure 3.2 - The example STBN model. It is composed of A, B, C, and D nodes in two different time-slices. Full-filled black arrows indicate non-temporal arcs, while the red dashed arrows are temporal arcs.

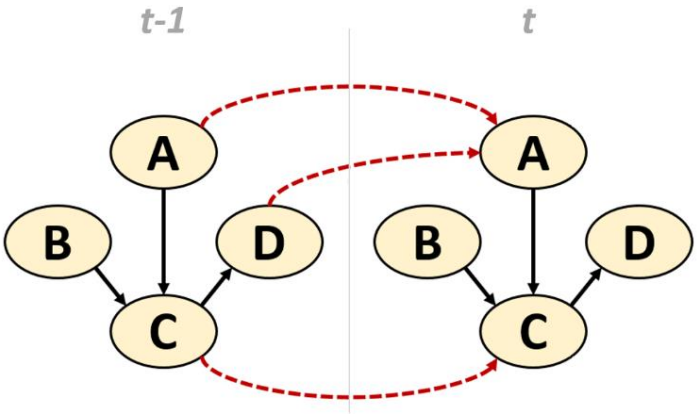

Source: author's production.

3.1 Input raster data

From the STBN model (Figure 3.2), one can note that A, C, and D are temporal nodes, as they have effects on other variables in the future, and B is a static node since it has effects on other nodes only within the time-slice. With that in mind, let us assume that all network nodes are spatial, i.e., they represent spatially distributed variables. Consequently, A, C, and D are spatio-temporal nodes, while B is a static spatial node. Moreover, let us also consider that node B represents a continuous variable, which will be discretized later, while the other nodes represent discrete variables. Taking into account all these

assumptions, the raster data of the variables included in the example STBN are presented in Figure 3.3.

The *stbnR* package integrates the *raster* package (HIJMANS et al., 2019) to deal with raster data. All input raster data must be provided in the *GeoTiff* format (OGC, 2019), which is a widely accepted format and supported by the *raster* package. This package also defines the *RasterLayer* and *RasterStack* classes. A *RasterLayer* class object is a single raster layer, while a *RasterStack* class object constitutes a collection of *RasterLayer* objects with the same extent, spatial resolution, and coordinate reference system (HIJMANS et al., 2019). A *RasterStack* object can be useful when dealing with multiple layers, as in the case of spatio-temporal variables in the STBN modeling.

Figure 3.3 - Raster data of the variables included in the example STBN model. On the left – A, C, and D are discrete spatio-temporal variables. The first column shows how these variables were spatially distributed at time-slice $t-1$. The second column shows how these variables were spatially distributed in the next time-slice t. On the right – B is a continuous static spatial variable. The mask defines the region of interest (ROI).

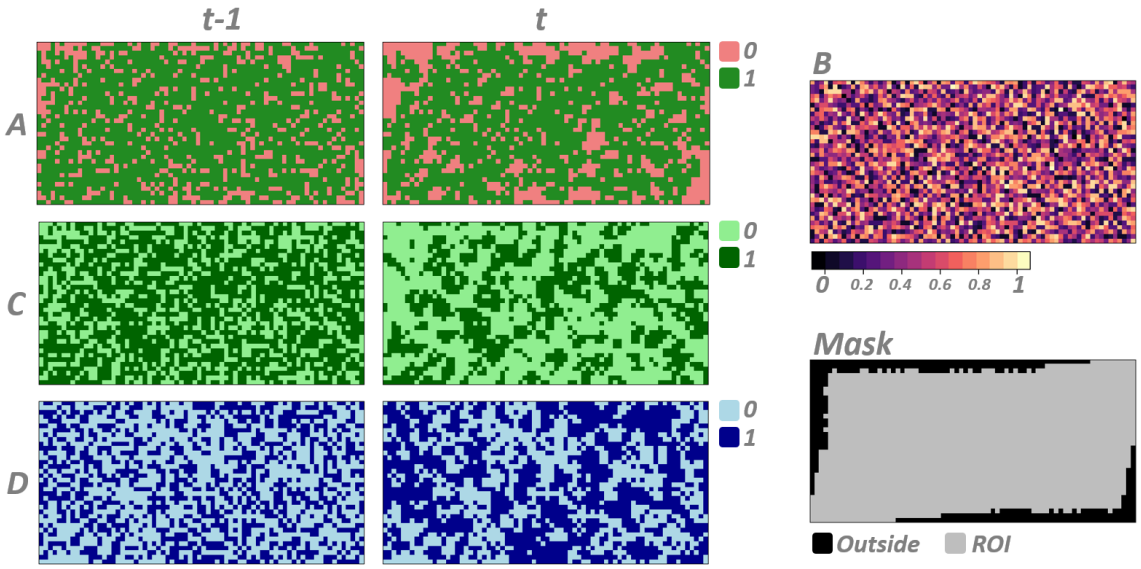

Source: author's production.

The *stbnR* package loads spatio-temporal variables as *RasterStack* objects. Each *RasterStack* layer is assumed to represent the same variable but in different time-slices. Each layer is associated with the node in its respective time-slice. Therefore, all spatio-temporal variables must be compatible in terms of the number of layers. (Figure 3.3). Concerning to static spatial variables, *stbnR* package loads them as *RasterLayer* objects. Hence, each static spatial variable must have only one raster layer, which will be

replicated to all time-slices. It is important to mention that the *stbnR* package distinguishes the variables between temporal or static according to the number of layers. Therefore, spatio-temporal variables must have two or more raster layers, while static spatial variables must have only one.

As not all pixels in the entire geographic area may be of interest, the user can provide a mask as an input raster layer to specify the region of interest (ROI), as presented in Figure 3.3. Only pixels within the ROI will be considered in the analysis, and results will be calculated only for these pixels. This can bring a significant gain in processing time. Additionally, the coordinates of the pixels within the ROI will be used as a reference to observe/collect the values from the other input raster data. Because of this, input raster data with different spatial resolutions are allowed, saving some data pre-processing time. The proposal of using a mask to define the ROI is based on the *bnspatial* package (MASANTE, 2019). In Figure 3.3, the gray region in the mask represents the ROI, while the black region represents the area of no interest.

If a mask is provided, its bounding box and spatial resolution will be inherited by the output raster data. However, if the user does not provide a mask, output raster data inherit the finest resolution of the input raster data and the maximum extent that encloses all of them. Besides that, results are calculated for all pixels within the outlined bounding box. Therefore, it is strongly recommended to provide a mask, otherwise, huge output raster data can be created, once the *stbnR* package allows input raster data to have different extents and spatial resolutions. The only requirement is all of them have the same coordinate reference system.

3.2 Settings file

Once defined the variables to be included in the model, the user must prepare the settings file, which is used to format a table according to the *Raster**[3] objects. The settings file is a text file (*.txt*) and must contain some specifications for those nodes that will be associated with a *Raster** objects. The text has to be formatted as follows: (i) the first line specifies the node name, (ii) the second line lists the node states, and (iii) the third line enumerates the values from the *Raster** object to be associated to the node states; such values will be integers for discrete data or thresholds of each interval to discretize

[3] *Raster** refers to *RasterLayer* or *RasterStack*.

continuous data. Specifications of the next node start in the subsequent line following the same pattern. Since all nodes from the example STBN will be associated with a *Raster** object, the setting file contents would be as shown in Figure 3.4.

Figure 3.4 - Settings file. Specifications for each node in the example STBN model.

```
A
TRUE, FALSE
1, 0
B
TRUE, FALSE
-Inf, 0.3, Inf
C
TRUE, FALSE
1, 0
D
TRUE, FALSE
1, 0
```

Source: author's production.

Node A specifications (i.e., the first three lines in the setting file) show that this node will have two states named $TRUE$ and $FALSE$, and values 1 and 0 from the *RasterStack* object will be related to these states respectively. Since A is a spatio-temporal node that will be associated with a *RasterStack* object, its specifications are equally applied for all time-slices and/or *RasterStack* layers. The process is similar for nodes C and D taking into account their specifications.

Node B specifications show that this node will also have two states named $TRUE$ and $FALSE$. However, unlike previous nodes whose states will be related to integer values, node B states will be related to intervals of values. The *RasterLayer* object, to which the node will be associated with, has continuous values that will be discretized according to the thresholds provided in the setting file. Consequently, values from the interval $(-Inf, 0.3)$ will be related to the $TRUE$ state, while values from the interval $[0.3, Inf)$ will be related to the $FALSE$ state. Values $-Inf$ and Inf guarantee the entire range of values from the *RasterLayer* object will be included in the discretization process.

3.3 Formatted data

With both input raster data and settings file properly prepared, the user can proceed to the next step, which is building the formatted data frame. To perform this step, the *stbnR*

package provides the *BuildDataFrame* function. The purpose of this function is to build a data frame of discrete observations from the input raster data and according to the specifications described in the settings file. The function header and description of its arguments are presented in Table 3.1.

The *BuildDataFrame* function result is a formatted data frame. A data frame is a two-dimensional data structure in *R* commonly used to store data as tables. Actually, it is a special case of vectors list with the same number of observations, i.e., equal length. Each vector corresponds to one column, while each observation corresponds to one row of the data frame (R CORE TEAM, 2019). Considering the input raster data of the example STBN (Figure 3.3), and the setting file with their specifications (Figure 3.4), *BuildDataFrame* function result would be as shown in Table 3.2.

Table 3.1 - *BuildDataFrame* function.

```
BuildDataFrame(setting, spatialData, mask = NULL, sampling = TRUE,
               size = 0.7, debug = TRUE)
```

Arguments	**Description**
`setting`	Character. The path to the formatted text file.
`spatialData`	Either vector or list. A vector of characters with the paths to the *GeoTiff* files or a list of *Raster** objects. If paths to the *GeoTiff* files are provided, these files are then loaded as *Raster** objects. All *Raster** object must be in the same Coordinate Reference System.
`mask`	Either character or *RasterLayer* object. The path to the *GeoTiff* file or the mask *RasterLayer* object. The raster layer passed to `mask` is used as a reference to define the ROI. Pixels with *NA* values are ignored, i.e., they are considered outside the ROI. The default is `mask = NULL`. In this case, the ROI is defined by the union of the *Raster** objects passed to the `spatialData` argument.
`sampling`	Logical. If *TRUE*, pixels from the ROI are randomly sampled to build the data frame. If *FALSE*, all pixels within the ROI are considered The default is `sampling = TRUE`.
`size`	Numeric. A number greater than 0 and less than 1, corresponding to the percentage of pixels to be randomly sampled. This argument is used only if `sampling = TRUE`. The default is `size = 0.7`. In this case, 70% of the pixels from the ROI are selected.
`debug`	Logical. If *TRUE*, some debugging is printed. Otherwise, the function is silent. The default is `debug = TRUE`.

Table 3.2 - *BuildDataFrame* function result for the example data.

A.1	A.2	B	C.1	C.2	D.1	D.2
$TRUE$	$TRUE$	$FALSE$	$FALSE$	$FALSE$	$FALSE$	$FALSE$
$TRUE$	$TRUE$	$TRUE$	$FALSE$	$FALSE$	$TRUE$	$TRUE$
$TRUE$	$TRUE$	$TRUE$	$TRUE$	$FALSE$	$FALSE$	$FALSE$
...	...	...	...	...	...	...
$TRUE$	$TRUE$	$FALSE$	$FALSE$	$FALSE$	$TRUE$	$TRUE$
$TRUE$	$TRUE$	$TRUE$	$TRUE$	$TRUE$	$FALSE$	$FALSE$
$TRUE$	$TRUE$	$TRUE$	$TRUE$	$TRUE$	$FALSE$	$FALSE$

The user must pay attention to the order in which both *Raster** objects and settings file specifications are provided. The *BuildDataFrame* function assigns the first specification from the settings file (i.e., the first three lines of the file) to the first *Raster** object. The second specification to the second *Raster** object and so on.

As shown in Table 3.2, spatio-temporal variables (A, C, and D) will appear more than once in the data frame followed by an index. This is a time index to reference which STBN time-slice the column will be associated with. Hence, column $A.1$ will be associated with the node A at time-slice $t-1$, while column $A.2$ will be associated with the same node but at time-slice t. Static spatial variables like B will appear only once. The total number of columns in the data frame is given by $(T * STV) + SSV$, where T is the number of time-slices, STV is the number of spatio-temporal variables, and SSV is the number of static spatial variables.

The number of rows in the formatted data frame is equal to the number of pixels within the ROI as defined by the mask (Figure 3.3). In this case, the `sampling` argument has been set to $FALSE$ and, consequently, the `size` argument is ignored. *Raster** object values are read from right to left and from top to bottom. Therefore, each line of the table corresponds to the observed values in each *Raster** object for the same pixel. These observed values are converted to classes according to the setting file specifications.

3.4 STBN model training

The *stbnR* package provides the *BuildSTBN* function to design the STBN model network. This function provides a graphical interface through which the user can easily insert his/her knowledge in defining all nodes' relationships. Thereafter, the function will

compute the conditional probability table (CPT) of each model node based on the defined relationships and observed values from the formatted data frame. STBN building and parameterizing refer to its training. The function header and description of its arguments are presented in Table 3.3.

Table 3.3 - *BuildSTBN* function.

```
BuildSTBN(markov = 1, net = NULL, data, debug = TRUE)
```

Arguments	**Description**
`markov`	Integer. The Markov order. The default is `markov = 1`, which means the first-order Markov property.
`net`	*StandardBN* object. The Bayesian Network that will be replicated to create the STBN. The default is `net = NULL`. In this case, the STBN is created from the data frame passed to the `data` argument.
`data`	Data Frame. A formatted data frame as returned by the `BuildDataFrame` function. This data frame is used to create STBN.
`debug`	Logical. If $TRUE$, some debugging is printed. Otherwise, the function is silent. The default is `debug = TRUE`.

3.4.1 STBN graphical model definition

Once the *BuildSTBN* function is run, graphical point-and-click interfaces (Figure 3.5) are made available, where the user can easily add and/or remove arcs between a pair of nodes. Two interfaces may pop up on the user's screen. The first one for the BN definition (Figure 3.5-a), and the second one for the STBN definition (Figure 3.5-b). These graphical interfaces are very intuitive. With the *Add* option enabled, the user must first click on the origin node and then click on the destination node. Thus, an arc will be created between these nodes. When all the nodes' relationships are defined, the user must click on the *Stop* option.

Figure 3.5 - Graphical point-and-click interfaces for the user interact with to define nodes' relationships. The example STBN model as illustrated in Figure 3.2 is designed. The graphical interface to define non-temporal arcs (a), and the graphical interface to define temporal arcs (b). In (b) time-slices are differentiated by colors.

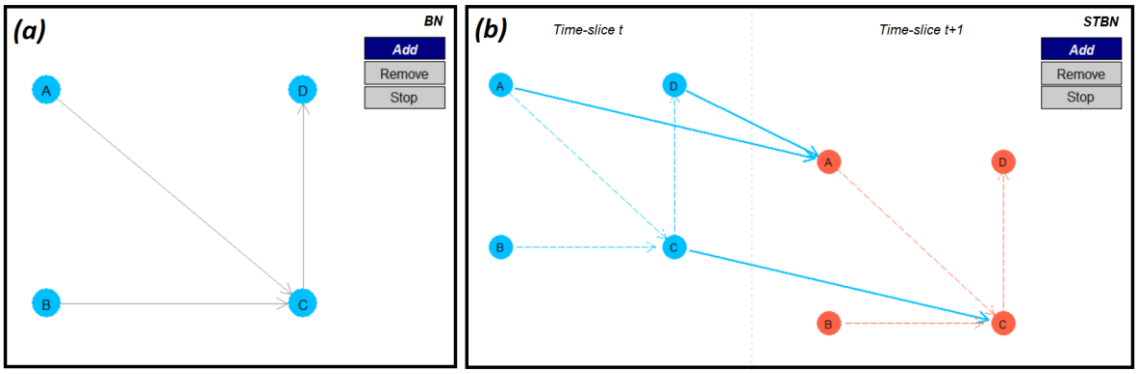

Source: *stbnR* package.

STBN models developed from the stbnR package are considered to be Markov processes, whose order is defined by the `markov` argument. With the default `markov = 1`, the STBN is assumed to represent a first-order Markov process, in which the current system state depends only on its immediately previous state and not on any earlier ones. In this case, the STBN will have two time-slices representing the system at time $t-1$ and t. Since there is no fundamental reason why a system cannot be depended on its earlier states (MOLINA et al., 2013; MURPHY, 2002), higher Markov orders are allowed.

The user can provide an external BN model for the *BuildSTBN* function through the `net` argument. The user can load a BN model that has been built beforehand either in *R* with the *gRain* (HØJSGAARD, 2012, 2019) and *bnlearn* (SCUTARI, 2009, 2019) packages or via external software such as *Hugin* (HUGINEXPERT, 2019) or *GeNIe* (BAYESFUSION, 2019). An external BN model makes it possible to employ nodes that are not related to spatial variables but represent, for example, socio-economic and political variables, among others.

Therefore, if an external BN model is provided, there is no needs to make the first interface available to the user, since the BN model has been already defined. Thus, this external BN model is replicated for each time-slice as defined by the `markov` argument. In sequence, the second interface (Figure 3.5-b) appears for the user to define the STBN temporal arcs.

The user also has the option to build the STBN model from scratch from the formatted data frame provided through the `data` argument. The *BuildSTBN* function will identify the unique nodes from the data frame columns. Thereafter, the first interface (Figure 3.5-a) will pop up on the screen, and the user has to define the directed acyclic graph (DAG) of the BN model. This first interface helps the user not to make mistakes like creating a cycle in the graph. Whenever an arc closes a cycle, it is promptly ignored.

After finishing the DAG editing, the second interface automatically appears (Figure 3.5-b), and the user has to define the STBN temporal arcs. Only forward arcs between pairs of temporal nodes are allowed. This second interface does not allow the user to create backward temporal arcs, temporal arcs between static nodes, or to edit non-temporal arcs. Figure 3.5 shows the graphical interfaces to create the example STBN.

3.4.2 Conditional probability tables computation

Once the STNB graphical model is defined, the *BuildSTBN* function will automatically compute the CPTs of all network nodes using the observed values in the formatted data frame. A CPT is calculated from the frequency table, which contains the number of occurrences of specific observations within a dataset. Probabilities are then calculated from the ratio between each frequency table entry by the total number of observations.

Let us consider the observed values for the node D^{t-1} (i.e., node D in the time-slice $t-1$ of the example STBN model). Figure 3.6-a shows that among all observations of this node, approximately 42% belong to the $TRUE$ state and, therefore, 58% belong to the $FALSE$ state. These values represent what would be the prior probability of the node D^{t-1}, that is $P(D^{t-1} = TRUE) = 0.42$ and $P(D^{t-1} = FALSE) = 0.58$.

Figure 3.6 - Prior probability distribution of node D^{t-1} (a), and the conditional probability of node. D^{t-1} given the node C^{t-1}(b).

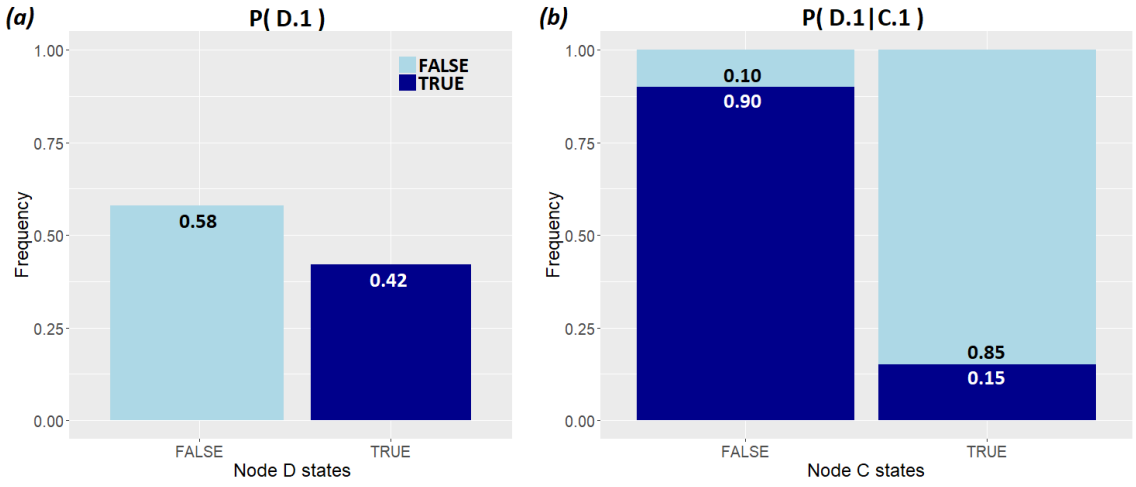

Source: author's production.

However, node D^{t-1} is statistically dependent on the node C^{t-1}, as shown in the STBN graphical model (Figures 3.2 and 3.5). This means that selecting any state of D^{t-1} depends on the states of C^{t-1}. Figure 3.6-b shows that the probability of randomly selecting the $TRUE$ state for D^{t-1} is higher when considering only those observations that are also $FALSE$ for C^{t-1}. In other words, knowing that C^{t-1} is $FALSE$ increases the beliefs about D^{t-1} be equals to $TRUE$, – $P(D^t = TRUE|C^t = FALSE) = 0.90$. On the other hand, these beliefs sharply reduce when if we previously know that C^{t-1} is $TRUE$ – $P(D^t = TRUE|C^t = TRUE) = 0.15$. Thus, Figure 3.6-b graphically illustrates how the CPT of node D^{t-1} would be.

Therefore, whenever a node is a descendent (child node) of other nodes (parent nodes), the child node CPT is dependent not only on its states but also on its parent nodes' states. This implies that the greater the number of parent nodes and/or the number of nodes states, the bigger the child node CPT. Figure 3.7 shows the CPT attached to each node in the example STBN model. One can note that the biggest CPT belongs to the node C^t, which is the node with the highest number of parent nodes.

The *BuildSTBN* function automatically computes the CPT of each node given its relationship with other network nodes and the observed values from the formatted data frame. However, in case the user does not agree with the calculated probability values, for instance, as they diverge from the expert's knowledge or do not represent reality properly, these probability values can be manually changed.

Figure 3.7 - Conditional probability tables attached to nodes of the example STBN model.

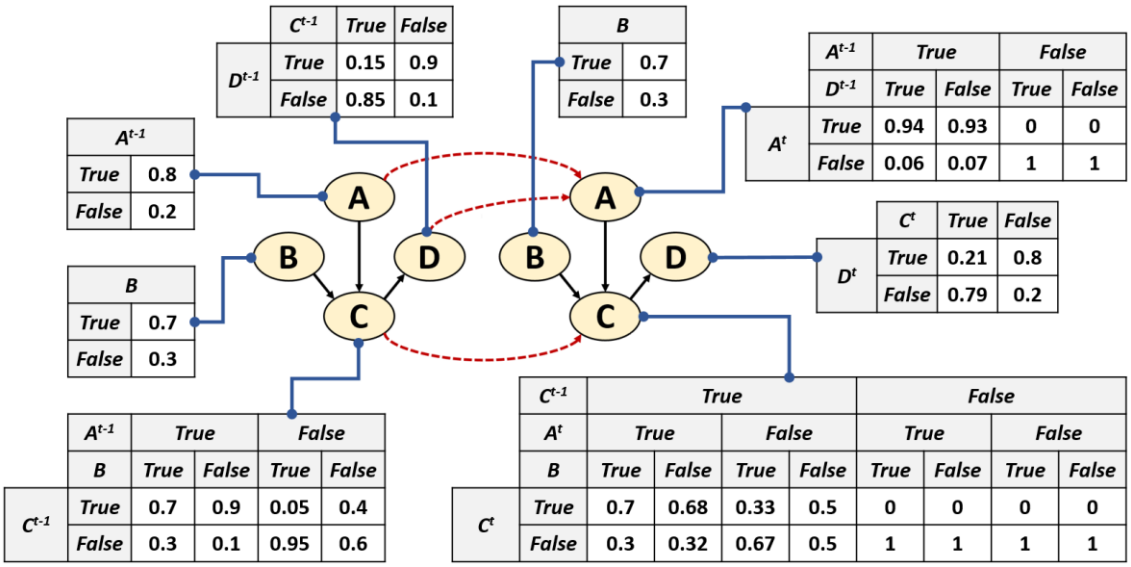

Source: author's production.

3.5 STBN query

After defining both the STBN structure and parameters, the next step is to calculate the occurrence probability of the studied phenomenon. This means calculating the posterior probabilities given the observed evidence. For this, the *stbnR* package provides the *QuerySTBN* function. The function header and description of its arguments are presented in Table 3.4.

Evidence is the observed value for a node. As each node from the STBN model has a set of mutually exclusive states, evidences are entered into the network by instantiating a specific state for one or more nodes. The evidence is always assigned to the nodes from the first time-slice $t-1$. By setting this evidence, the CPTs of all non-evidenced nodes, including those nodes from the next time-slice t, are updated using Bayes' theorem. With the updated probabilities, it is possible to query the STBN to answer the following question: "what is the probability of target occurrence in the future given this observed evidence at the present?" The *stbnR* package queries are supported by the *gRain* package (HØJSGAARD, 2012, 2019).

For instance, assuming node A as the target, the evidence will be given by observations for the nodes B, C^{t-1}, and D^{t-1}. Once the evidence $\boldsymbol{E^{t-1}}$ is set into the STBN model, the CPTs are updated and the posterior probability $P(A^t|\boldsymbol{E^{t-1}})$ can be calculated. That means

to calculate the target occurrence probability in the next time-slice, given the evidence from the previous time-slice.

Table 3.4 - *QuerySTBN* function.

```
QuerySTBN(stbn, target, evidence, nodes = NULL, nodesStates = NULL,
          toSave = FALSE, toContinue = FALSE, inParallel = FALSE,
          debug = TRUE)
```

Arguments	**Description**
`stbn`	*SpTmpBN* object. The STBN as returned by the *BuildSTBN* function.
`target`	Character. The node's name, which represents the studied phenomenon.
`evidence`	Data Frame. A formatted data frame as returned by the `BuildDataFrame` function.
`nodes`	Vector. A character vector with the names of non-spatial nodes to which specific evidence will be assigned to. The default is `nodes = NULL`.
`nodesStates`	Vector. A character vector with evidence (i.e. observed values) of non-spatial nodes provided in `nodes` argument. The default is `nodesStates = NULL`.
`toSave`	Logical. If $TRUE$, the updated STBN is saved into a *STBNinfo.RData* file for future queries. The default is `toSave = FALSE`.
`toContinue`	Logical. If $TRUE$, the STBN saved in the *STBNinfo.RData* file is loaded. Otherwise, new modeling is started. The default is `toContinue = FALSE`.
`inParallel`	Either integer or logical. The number of cores to be used in parallel processing. If $TRUE$, the maximum number of available cores minus one is set. The default is `inParallel = FALSE`.
`debug`	Logical. If $TRUE$, some debugging is printed. Otherwise, the function is silent. The default is `debug = TRUE`.

The formatted data frame rows represent scenarios, in which each spatial node at time-slice $t-1$ takes on a specific state (SILVA et al., 2020). Normally, the same scenario occurs several times, that is, the same values can be observed in different positions (data frame rows). In these cases, it would be redundant to query the STBN model repeatedly, since the same result would always be obtained. Therefore, queries are scenario-based in the *stbnR* package. That means the STBN model is queried only once for a specific scenario, and the computed probability is assigned to all positions in which this scenario occurs.

However, each scenario will produce a different update for the CPT of non-evidenced nodes. Because of that, a copy of the original STBN is made for each scenario. Thus, each STBN can be rolled up individually. The rolling up process (KORB; NICHOLSON, 2010; POPESCU et al., 2015) is based on the first-order Markov property, in which the current system state depends only on its immediately previous state and not on any earlier ones. In this context, the information from the past (time-slice $t-1$) is stored in the present through the update of nodes' CPTs in time-slice t after the evidence set in the nodes from the time-slice $t-1$. Thus, time-slice $t-1$ can be dropped and a new time-slice $t+1$ added in front of the STBN. As the STBN is assumed to be steady, the nodes' relationship in time-slice $t+1$ is the same as in other time-slices. Moreover, its nodes' CPTs are equal as in time-slice t before the updating. The rolling up process as described is applied simultaneously to all STBNs. Figure 3.8 illustrates the rolling up process of an STBN for two time-slices forward.

Figure 3.8 - The rolling up process for an STBN. For each iteration, a new time-slice is added in front of the STBN, while the last one is removed (gray time-slices).

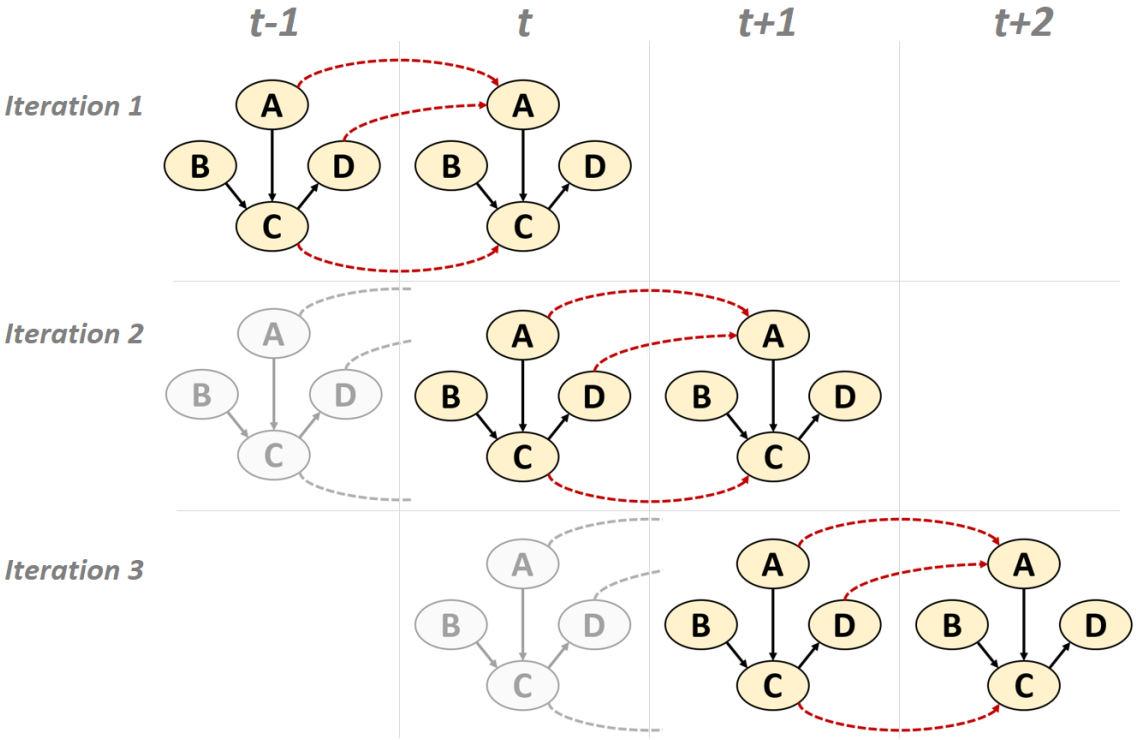

Source: author's production.

The above procedures described so far detail what would be one iteration of the *QuerySTBN* function. In the next iteration, new evidence $\boldsymbol{E^t}$ is set into the updated STBNs

to calculate the $P(A^{t+1}|\boldsymbol{E^t})$. The *QuerySTBN* function will return a list of matrices. The length of this list is given by the number of iterations of the model (i.e., one matrix for each time-slice forward). These matrices stores the occurrence probability values of the target node in one time-slice. Each matrix will have a (n, m)-dimension, where n is the number of rows corresponding to the number of pixels within the ROI, and m is the number of columns, which correspond to the number of target node states. Thus, each position (i, j) stores the occurrence probability of the state j in the pixel i within the ROI.

If the user sets `toSave = TRUE`, the set of updated STBNs is saved into a file named *STBNinfo.RData* at the end of the rolling up process. As new raster data for the model variables may become available in the future, the saved STBNs can be queried in the light of these new observed values, i.e., evidence. For that, the saved STBNs has to be loaded by setting `toContinue = TRUE`. Hence, the modeling can continue exactly where it left off, without the need to train an original STBN again. Besides that, with the `nodes` and `nodesStates` arguments, the *QuerySTBN* function allows the user to assign evidence to non-spatial nodes, i.e., nodes that represent, for example, socio-economic, political variables. Moreover, STBNs queries and updating can be performed in parallel by setting `inParallel = TRUE`.

3.6 STBN model outputs

After calculating the probabilities, the final step is to generate the STBN model outputs raster data. For this, the *stbnR* package provides the *TargetMapping* function, which creates a time series of probability images, each one corresponding to the target probability occurrence in each predicted time-slice. *TargetMapping* function is supported by the *bnspatial* package (MASANTE, 2019). The function header and description of its arguments are presented in Table 3.5.

Table 3.5 - *TargetMapping* function.

```
TargetMapping(target, probs, what = "probability", mask,
              toExport = FALSE, path, debug = TRUE)
```

Arguments	**Description**
`target`	Character. The node's name, which represents the studied phenomenon.
`probs`	List. A list of matrixes as returned by the `QuerySTBN` function.
`what`	Vector. A character vector specifying the required output. The options are (i) *class*, which returns the most likely state; (ii) *entropy*, which returns the Shannon entropy; and (iii) *probability*. The default is `what = "probability"`.
`mask`	Either character or *RasterLayer* object. The path to the *GeoTiff* file or the mask *RasterLayer* object. The raster layer passed to `mask` is used as a reference to define the ROI. Pixels with *NA* values are ignored, i.e., they are considered outside the ROI.
`toExport`	Logical. If $TRUE$ output raster data are saved as *GeoTiff* files. The default is `toExport = FALSE`.
`debug`	Logical. If $TRUE$, some debugging is printed. Otherwise, the function is silent. The default is `debug = TRUE`.

The *TargetMapping* function will return a raster layer for each time-slice rolled up forward. The results of this function can be changed according to `what` argument. For instance, if `what = class`, the value of each pixel within the ROI will refer to the most likely target state to occur. With `what = entropy`, pixel values will refer to the calculation of Shannon's entropy, which evaluates the uncertainties of each prediction (HAMMER et al., 2000). In turn, if `what = probability`, pixels values will be the probability values. In this case, a probability image will be generated for each target node state.

The target node must be the same as the one defined for the *QuerySTBN* function. The mask to be provided for the *TargetMapping* function must be the same as that provided for the *BuildDataFrame* function. As mentioned previously, this mask is used as a reference, its extension and spatial resolution will be inherent by the output raster data. Finally, the user can save all output raster data as *GeoTiff* files if `toExport = TRUE`.

4 STBN MODELS FOR DEFORESTATION RISK PREDICTION

This chapter aims to present the application of the STBN models proposed in this work to predict deforestation risk in some regions of the Brazilian Legal Amazon (BLA). Although employing BNs as an approach to predict deforestation risk had been proposed before (DLAMINI, 2016; KRÜGER; LAKES, 2015; MAYFIELD et al., 2017), the temporal domain has not been considered until then. Therefore deforestation has been considered as a static process when modeled by BN approaches. In this context, the STBN models developed from the *stbnR* package aim to meet this demand, since they enable incorporating spatial and temporal information into the modeling. Furthermore, with the case studies presented in this work, we can evaluate the potential of the STBN as a LULCC model.

4.1 Case study regions

To evaluate the STBN model to predict deforestation risk, three regions of interest (ROIs) were selected (Figure 4.1) with expert support to encompass different deforestation frontiers within the BLA. The selected regions are located in the Amazonas, Mato Grosso, and Pará states. These last two states accumulate more than 60% ($480728\ km^2$) of the entire deforested area in the BLA ($788352.9\ km^2$) until 2018 (INPE, 2019a). Hence, Pará and Mato Grosso are respectively the first and second states with the largest deforested areas. Although Amazonas state occupies the fifth position in this rank, there is a great concern due to the emergence of a new deforestation expansion frontier. Figure 4.1 also shows deforested areas until 2018 (red-colored) as well as forest areas (green-colored) within each region (INPE, 2019a). Following, we describe each of these regions.

Figure 4.1 - Regions of interest located in the Brazilian Legal Amazon. Amazonas state (a); Mato Grosso state (b); and Pará state (c). Red-colored regions correspond to deforested areas until 2018. Green-colored regions are forest areas. Yellow-colored regions represent non-forest areas.

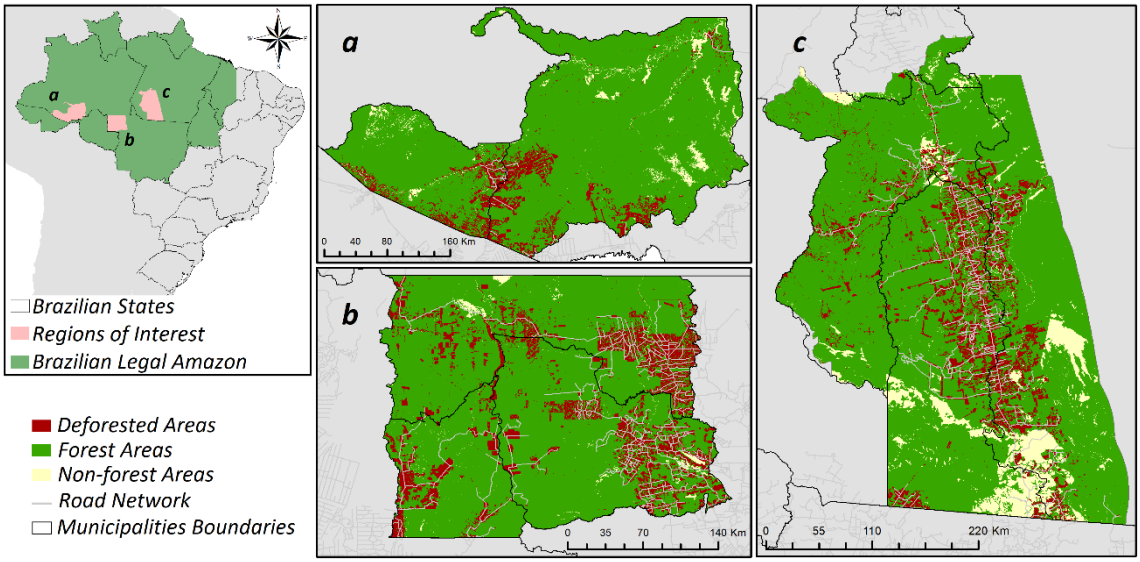

Source: author's production.

4.1.1 Amazonas case study

The Amazonas study case region is presented in Figure 4.1-a and has approximately 90341 km^2. It is located in the Amazonas state southwestern, encompassing the Boca do Acre municipality on the west and Lábrea municipalities on the east. Deforested areas are mainly concentrated in the central region, where are the municipalities' boundaries, as well as in the southern neighboring Acre and Rondônia states. This region has become a new front line against illegal deforestation. The huge amount of hotspot fires in the last years caused by cattle-ranching expansion has boosted deforestation rates (VASCONCELOS et al., 2013a, 2013b). Lábrea was the municipality of the Amazonas state with the largest deforested area until 2018, with approximately 4785 km^2, while Boca do Acre occupied the third position with 2619 km^2 (INPE, 2019a)

4.1.2 Mato Grosso case study

The Mato Grosso study case region is presented in Figure 4.1-b. With approximately 68541 km^2, it is located in the Mato Grosso state northwestern and encompasses Colniza, Aripuanã, and Rondolândia municipalities on the north, west, and east of the region, respectively. Illegal logging and cattle-ranching are the predominant activities in the region (DAVENPORT et al., 2016; SOUSA, 2016) and, therefore, the main

deforestation drivers. Deforested areas can be found throughout the case study region, but mainly concentrated in the eastern portion. Colniza, Aripuanã, and Rondolândia municipalities showed the largest deforestation increases in the Mato Grosso state between 2017-2018. Until this year, deforested areas in Colniza, Aripuanã, and Rondolândia was $4970\ km^2$, $4319\ km^2$, and $2031\ km^2$, respectively (INPE, 2019a).

4.1.3 Pará case study

The Pará study case region corresponds to a buffer around the BR-163 highway and has approximately $117138\ km^2$. The construction of this highway and more recent improvements in transportation infrastructure have intensified deforestation along its route over the years (FEARNSIDE, 2007; PINHEIRO et al., 2016), which has created an expansion deforestation corridor (SILVA et al., 2020), as can be seen in Figure 3.9-c. Extensive and traditional cattle farming is the main land use in this region (MÜLLER et al., 2016). The case study region encompasses the Novo Progresso municipality as well as the southern part of the Altamira and Itaituba municipalities. Until 2018, these municipalities were among those with the largest extension of deforested areas in the entire BLA. Novo Progresso municipality, which is completely within the case study region, had approximately $6289\ km^2$ of deforested area (INPE, 2019a).

4.2 Dataset and pre-processings

The variables chosen to compose the modeling as well as their pre-processing are detailed below. All procedures were carried out through the *R* software (R CORE TEAM, 2019). The same set of variables was used in three case studies. Therefore, all the procedures described here were equally applied in all case studies.

The target variable named *deforestation* represents yearly deforested areas, therefore, it is a temporal variable, meaning that it changes over time. We use as reference the yearly deforestation data from 2013 to 2018 from the PRODES project (INPE, 2019a). The original dataset was processed to a time series of raster data, in which pixels with a value equal to 1 represent deforestation in the current year, while 2 represents forested pixels. As the focus of the study is to identify deforestation risk, deforested areas before 2013 were removed from the ROI, as well as non-forested areas. Hereafter, each raster layer at $30\ m$ spatial resolution was resampled to $100\ m$ using the nearest neighbor method, which is more appropriate for categorical data.

Thus, the *deforestation* variable is formed by a raster time series with raster layers referring to yearly deforested areas (from 2013 to 2018). Each raster layer contains pixels representing: (i) target presence – deforested areas, and (ii) target absence – forested areas. However, classes (i) and (ii) are completely unbalanced, in general, class (i) represents less than 1% of all pixels within an ROI. Because of that, an undersampling process was carried out for the majority class. In each raster layer, twice the number of pixels of the minority class (deforested areas) was randomly selected for the majority class (forested areas). The value equal to 0 was then assigned to the remaining pixels from class (ii), representing hidden observations. Therefore, each raster layer from *deforestation* variable ends up having pixels from (i) deforested areas, (ii) forested areas, and (iii) hidden observations. From this raster time series, two datasets were created for both model training and evaluation. Approximately two-thirds of the pixels from classes (i) and (ii) were randomly selected to model training, while the remaining one-third of each class was then used to accuracy assessment.

The masks used to define the ROIs are shown in Figure 4.2. The gray-colored areas represent the ROI in each case study, while the black-colored areas represent regions of no interest. All masks have a spatial resolution of $100\text{x}100m$ and SIRGAS2000 coordinate reference system.

Figure 4.2 - Masks used to define case study regions. Amazon case study mask (a); Mato Grosso case study mask (b); and Pará case study mask (c). Black-colored areas correspond to regions of no interest.

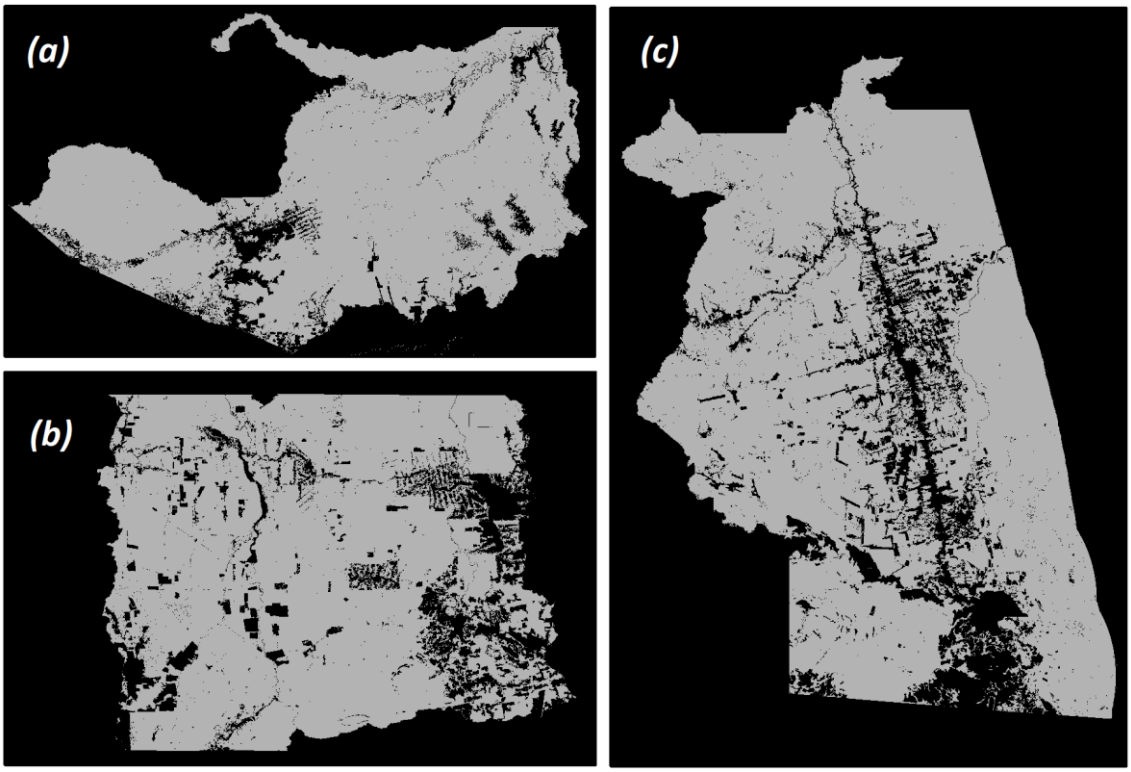

Source: author's production.

The other variables chosen to compose the modeling are from now called context variables, which are somehow related to the target variable. Their selection was supported by an expert and based on the potential relationship with the deforestation process. Table 4.1 list all selected variables.

Table 4.1 - Target and context variables with their original format and source.

Variable	Short	Variable type	Source
Deforestation	*Df*	Temporal	PRODES Project [a]
Proportion of deforested neighbors	*Ngb*	Temporal	PRODES Project [a]
Distance from degraded areas	*DDa*	Temporal	DEGRAD [b], DETER Projects [c]
Distance from hotspots fires	*DHf*	Temporal	Wildfire Project [d]
Distance from pasture areas	*DPa*	Temporal	TerraClass Project [e]
Distance from roads	*DRd*	Static	IBGE [f]
Settlement areas	*SAr*	Static	INCRA [g]
Distance from rivers	*DRv*	Static	IBGE [f]
Protected areas	*PAr*	Static	ICMBio [h], FUNAI [i], MMA [j]

[a] Brazilian Amazon Forest Monitoring by Satellite (http://terrabrasilis.dpi.inpe.br/).
[b] Brazilian Amazon Forest Degradation Mapping (http://www.obt.inpe.br/OBT/assuntos/programas/amazonia/degrad).
[c] Real-time Deforestation Detection System in Amazon Forest (http://terrabrasilis.dpi.inpe.br/).
[d] Sattelite Fire Monitoring Program (http://www.inpe.br/queimadas)
[e] TerraClass Project (https://www.terraclass.gov.br/)
[f] Brazilian Institute of Geography and Statistics (http://www.ibge.gov.br/).
[g] National Institute of Colonization and Agrarian Reform (http://acervofundiario.incra.gov.br/acervo/acv.php).
[h] Chico Mendes Institute of Conservation and Biodiversity (http://www.icmbio.gov.br/).
[i] Brazilian Indian Foundation (http://www.funai.gov.br/).
[j] Brazilian Environment Ministry (http://www.mma.gov.br/governanca-ambiental).

The *protected areas* variable refers to areas under environmental protection laws, which has a significant mitigating effect on deforestation (BARBER et al., 2014). The case studies ROIs are surrounded by many types of protected units, such as Environmental Preservation Areas, National Forests, and Indigenous Lands. Some of them are more restrictive and allow for reducing deforestation such as Indigenous Land. On the other hand, there are protected units that allow sustainable activities and do not have the same impact (AMIN et al., 2019). Hence, the original data (polygons) were rasterized to obtain one raster layer indicating unprotected, protected, and restricted areas.

Logging activities have been the most important driver of forest degradation and deforestation around the ROIs (DAVENPORT et al., 2016; PINHEIRO et al., 2016; VASCONCELOS et al., 2013a). Pinheiro et al. (2016) pointed out forest degradation as a predecessor to deforestation since degraded areas tend to be entirely cleared in subsequent years. Therefore, the *distance from degraded areas* variable is a potential indicator of deforestation. From yearly data of degraded areas (polygons), the distance

(in meters) to the nearest edge of degraded area for each pixel was calculated. The result is a raster time series with raster layers referring to the distance to yearly degraded areas.

Besides turning closed forests into degraded areas, logging activities also turn forest highly vulnerable to droughts and fires (VASCONCELOS et al., 2013a). Indeed, fires occurrence is one of the leading causes of forest degradation and deforestation (SETZER et al., 2012; TASKER; ARIMA, 2016). Thus, the *distance from hotspots fires* variable is another potential indicator of deforestation. From the hotspots fires data (points) clustered annually, the distance (in meters) to the nearest hotspot fire for each pixel was calculated. The result is a raster time series, in which each layer refers to the distance to yearly hotspots fires.

Cattle-ranching expansion is also a significant driver of deforestation (BARONA et al., 2010; SOLER; VERBURG; ALVES, 2014). As presented by Almeida et al. (2016) pasture areas occupy most of the deforested areas in the BLA, as in the case study ROIs. Thus, the *distance from pasture areas* was selected as an indicator of deforestation. LULCC annual maps from the TerraClass project (ALMEIDA et al., 2016) were processed to a raster time series with each layer representing yearly pasture and non-pasture areas. For each raster layer, the distance to the nearest pasture area for each pixel was calculated.

The construction of new roads allows access to previously inaccessible forests. Subsequently, it leads to forest fragmentation, new colonizations, and increases fire risk, as stated by Barber et al. (2014). The authors also verified more than 90% of all deforestation in the BLA occurred within $5.5\ km$ of roads. Consequently, the *distance from roads* variable should be considered as a deforestation indicator. From the road network data (lines) with the principal roads only, one raster layer was generated with the distance (in meters) to the nearest road for each pixel.

Major roads stimulate deforestation by facilitating the construction of smaller side roads as well as human settlements in remote areas (FEARNSIDE, 2015). Indeed, studies have shown that settlements with human activities (e.g., agriculture and logging) play a major role in deforestation (CHEN et al., 2015; TRITSCH; LE TOURNEAU, 2016) and fires occurrences (ALENCAR et al., 2015). Therefore, the *settlement area* variable can be considered as a deforestation indicator. The original data (polygons) were rasterized to obtain one raster layer indicating undersigned and settlement areas.

Despite roads make way for previously inaccessible areas, several locations in the BLA do not offer road accesses. The only access to roadless municipality and villages is via navigable rivers (JUSYS, 2016). According to Barber et al. (2014), navigable rivers provide another potential mode of access to untouchable forest regions and further promote logging and deforestation. The authors also show that most deforested areas in the BLA are located near to roads or navigable rivers. Consequently, the *distance from rivers* variable also should be considered as a deforestation indicator. From the river network data (lines), one raster layer was generated with the distance (in meters) to the nearest river for each pixel.

Ongoing forest fragmentation increases the changes of forest destruction in general since fragmented forests are far more susceptible to droughts, fires, logging, and any anthropogenic impact (ALENCAR et al., 2015; LAURANCE et al., 2018). Forest fragmentation creates forest areas susceptible to edge effects and, for accessibility reasons, deforestation tends to occur near to already deforested areas (BROADBEND et al., 2008). Therefore, the *proportion of deforested neighbors* variable was also selected as a deforestation indicator. To compute this variable, the original data (polygons) were processed to a raster time series with each layer containing the cumulative deforested and forested areas. The proportion of deforested neighbors for each pixel was calculated from a 5 x 5 moving window.

All the raster data collected and described above can be separated into two categories: static and temporal variables. Static variables are those features that are assumed to stay constant over time either because it is an inherent characteristic or due to the lack of information to update them (ROSA et al., 2015). Among the selected variables, *protected areas*, *distance from roads*, *settlements areas*, and *distance from rivers* are static variables. By contrast, temporal variables are those features that change over time, which were calculated for each time interval within the analysis period (ROSA et al., 2015). Hence, *deforestation*, *distance from degraded areas*, *distance from hotspots fires*, *distance from pasture areas*, and *proportion of deforested neighbors* are temporal variables. Since the data pre-processing was carried out using *R* software, all variables raster data are already as *Raster** objects, i.e., *RasterLayer* for static variables or *RasterStack* for temporal variables, as required by the *stbnR* package. Moreover, all raster data are in the SIRGAS2000 coordinate reference system.

4.3 Building the STBN models

Before building the STBN, the settings file is required in addition to the variables raster data. Both the settings file and *Raster** objects are inputs to the *BuildDataFrame* function to generate the formatted data frame. This data frame, in turn, is used as input to the *BuildSTBN* function to define STBN structure and calculate its parameters. Figure 4.3 shows the settings file formatted as required: (i) the first line is the node name, which is presented in abbreviation, (ii) second line is node states, and (ii) third line is the values from raster data to be associated to the node states. The subsequent lines follow the same pattern.

As the settings file will be employed in all case studies, variables will be equally discretized and will have the same classes. Consequently, nodes from the STBN models will also have the same name and states but different CPTs, as they are computed from the data of each case study. The interval limits chosen to discretize the continuous variables were defined from empirical and exploratory data analysis with expert support. The settings file specifications are also presented in Table 4.2 for a better understanding.

Figure 4.3 - Settings file employed in all case studies.

```
Df
deforest, forest
1, 2
PAr
unprotected, protected, restricted
0, 1, 2
DDa
500M, 1KM, MAX
-Inf, 500, 1000, Inf
DHf
500M, 1KM, MAX
-Inf, 500, 1000, Inf
DPa
1KM, 2.5KM, MAX
-Inf, 1000, 2500, Inf
DRd
1KM, 5KM, MAX
-Inf, 1000, 5000, Inf
SAr
undesignated, settlements
0, 1
DRv
500M, 1.5KM, MAX
-Inf, 500, 1500, Inf
Ngb
20%, 40%, 60%, 80%, 100%
-Inf, 0.2, 0.4, 0.6, 0.8, Inf
```

Source: author’s production.

Table 4.2 - Settings file specifications.

Df		PAr		DDa		DHf		DPa	
States	**Values**	**States**	**Values**	**States**	**Values**	**States**	**Values**	**States**	**Values**
$deforest$	1	$unprotected$	0	$500M$	$(-Inf, 500]$	$500M$	$(-Inf, 500]$	$1KM$	$(-Inf, 1000]$
$forest$	2	$protected$	1	$1KM$	$(500, 1000]$	$1KM$	$(500, 1000]$	$2.5KM$	$(1000, 2500]$
-	-	$restricted$	2	MAX	$(1000, Inf)$	MAX	$(1000, Inf)$	MAX	$(2500, Inf)$

DRd		SAr		DRv		Ngb	
States	**Values**	**States**	**Values**	**States**	**Values**	**States**	**Values**
$1KM$	$(-Inf, 1000]$	$undersigned$	0	$500M$	$(-Inf, 500]$	20%	$(-Inf, 0.2]$
$5KM$	(1000,5000]	$settlement$	1	$1.5KM$	$(500, 1500]$	40%	$(0.2, 0.4]$
MAX	$(5000, Inf)$	-	-	MAX	$(1500, Inf)$	60%	$(0.4, 0.6]$
-	-	-	-	-	-	80%	(0.6 0.8]
-	-	-	-	-	-	100%	$(0.8, Inf)$

Df – Deforestation
PAr – Protected areas
DDa – Distance from degraded areas
DHf – Distance from hotspots fires
DPa – Distance from pasture areas

DRd – Distance from roads
SAr – Settlements areas
DRv – Distance from rivers
Ngb – Proportion of deforested neighbors

Two STBN approaches were applied to each case study. The first one is a first-order Markov STBN, which assumes that an STBN slice depends only on the immediately preceding slice and not on any earlier ones. The second one refers to a second-order Markov STBN, which in turn assumes that an STBN slice depends on the immediately preceding slice as well as the slice before this one. Figures 4.4 and 4.5 show the first-order Markov STBN and the second-order Markov STBN, respectively. This STBN was employed to test whether spatio-temporal variables have some effect on deforestation beyond the one-time interval. By the way, the interval Δt between STBN time-slices is given by the raster data availability, which is one year.

Figure 4.4 - First-order Markov STBN. Blue-colored nodes represent temporal nodes, while yellow-colored nodes represent static nodes. Black fulfilled lines represent non-temporal arcs, while red dotted lines represent temporal arcs.

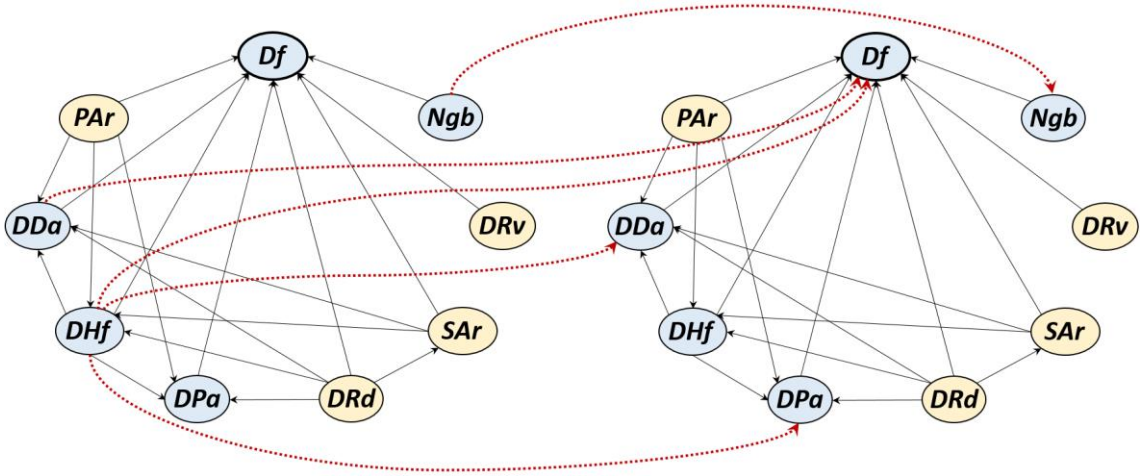

Source: author's production.

Figure 4.5 - First-order Markov STBN. Blue-colored nodes represent temporal nodes, while yellow-colored nodes represent static nodes. Black fulfilled lines represent non-temporal arcs. In turn, red dotted lines represent temporal arcs between a one-time interval, while blue dashed lines represent temporal arcs between a two-time interval.

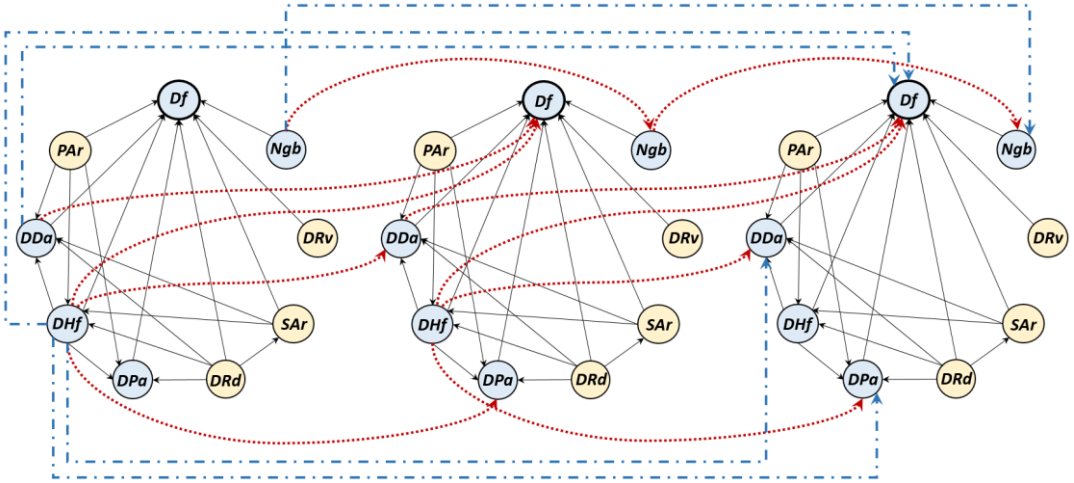

Source: author's production.

The first-order Markov STBN training, that is, the calculation of nodes' CPTs, was carried out with the training raster data from the years 2013 and 2014. While the second-order Markov STBN training was carried out with the training raster data from 2013, 2014, and 2015. This is because the second-order Markov STBN is made up of three time-slices and, therefore, three-year data is needed to compute CPTs. It is important to keep in mind that only those pixels with values other than 0 in the training raster data of the target variable (i.e., class (iii) hidden observations) are indeed observed in the raster data of other variables for parametrization of both STBN models. This means that CPTs are calculated from the observations of those sampled pixels and not from observations of all pixels within the ROIs. The values of all pixels from the ROIs are only considered when querying the STBNs. Before carrying out any query, observed values are set as evidence into the nodes.

Therefore, querying the STBN models aims to answer the following question: "what is the deforestation risk in the next year given the observed evidence in the current year?" The probability that answers that question is calculated for each pixel within the ROI. The STBN model results are probability images, one for each iteration, corresponding to deforestation risk for each year from 2014 to 2019 in the case of the first-order Markov STBN, and from 2015 to 2019 in the case of the second-order Markov STBN.

4.4 STBN models assessment

The STBN models from each case study were evaluated by comparing their predictions (i.e., the probability images) with the data selected for accuracy assessment, as detailed in section 4.2. Following, we detailed the metrics used to evaluate the models as well as variables importance.

From the confusion matrix presented below (Table 4.3), let us consider $Presence$ as deforestation occurrence while $Absence$ corresponds to forest areas. Hence, TP is true positives (i.e., deforested pixels correctly classified as deforestation), FP is false positives (i.e., deforested areas incorrectly labeled as forest areas), FN is false negatives (i.e., forest pixels incorrectly labeled as deforestation), TN is the true negatives (i.e., forest pixels correctly classified as forest area), and $N = TP + FP + FN + TN$. The metrics used to evaluate the STBN models are derived from the confusion matrix, as shown in Table 4.4.

Table 4.3 - A confusion matrix used to evaluate presence-absence models.

		$Reference$	
		$Presence$	$Absence$
$Predicted$	$Presence$	TP	FP
	$Absence$	FN	TN

Table 4.4 - Assessment metrics calculated from the confusion matrix.

Metric	**Formula**
Sensitivity	$\frac{TP}{TP + FN}$
Specificity	$\frac{TN}{TN + FP}$
Precision	$\frac{TP}{TP + FP}$
Kappa	$\frac{\left(\frac{TP + TN}{N}\right) - \frac{(TP + FP)(TP + FN) + (FN + TN)(FP + TN)}{N^2}}{1 - \frac{(TP + FP)(TP + FN) + (FN + TN)(FP + TN)}{N^2}}$

Two complementary indices are commonly used in binary classifications: sensitivity and specificity, which indicate, respectively, the true positive rate (i.e., pixels the model defined as deforestation that were truly deforestation) and the true negative rate (i.e., pixels the model defined as forests that were truly forest areas) (SWETS, 1988).

A useful graph to represent accuracy assessment in terms of these two indices is the Receiver Operating Characteristic (ROC) curve (FAWCETT, 2006). The ROC curve is constructed by using all possible thresholds (i.e., from 0 to 1) to classify the probability values into confusion matrices. Pixels with values higher then the threshold are classified as deforested areas, while pixels with values below the defined threshold are classified as forested areas. From each matrix, sensitivity and specificity are obtained. When plotting all sensitivity values against the corresponding proportion of false positives (i.e., equal to $1 - specificity$), we obtain the ROC curve (ALLOUCHE; TSOAR; KADMON, 2006).

We also evaluate the STBN models by the area under the ROC curve (AUC-ROC). It is an assessment measure of the model performance, which generally takes values ranging from 50% to 100%. Values close to 100% indicate optimal prediction. These metrics are widely used to assess the performance of probabilistic systems like BN models (DLAMINI, 2016; KRÜGER; LAKES, 2015; SEMAKULA et al., 2016).

The selected threshold is the one that produces the highest AUC-ROC. From the confusion matrix obtained with the selected threshold, the precision and Kappa statistic were also calculated. Precision is a metric that indicates how precise/accurate the model is, i.e., it reflects the percentage of model correctness concerning what it classified as deforestation. Kappa statistic is a more robust metric since it corrects the model's overall accuracy by the accuracy expected to occur by chance. (ALLOUCHE; TSOAR; KADMON, 2006; CONGALTON; GREEN, 2009).

STBN models' performance was also evaluated in terms of execution time. The STBN models of three case studies were run on an octa-core server machine with 64GB of RAM. The STBN querying and updating step is the bottleneck of all STBN modeling. Therefore, we measure the total execution time of the whole modeling as well as the time spent only on this bottleneck step.

To quantify the influence of the predictor variables on the target variable, we used Mutual Information (MI), which is defined within the information theory. MI measures how much knowing one variable reduces the uncertainty about the other. In other words, it is a measure of the amount of information that one random variable has about another variable. In this sense, MI is zero when both variables are statistically independent (VERGARA; ESTÉVEZ, 2014). The MI of two variables X and Y is given by the following equation:

$$MI(X,Y) = \sum_{x}^{n}\sum_{y}^{n} P(X = x, Y = y) * \log\frac{P(X = x, Y = y)}{P(X = x)P(Y = y)} \quad (4.1)$$

Here, $P(X = x)$ and $P(Y = Y)$ are marginal probabilities and $P(X = x, Y = Y)$ is the joint probability distribution.

5 RESULTS AND DISCUSSION

This chapter presents the deforestation risk predictions obtained with STBN models. The analyses and evaluation of results are presented by case studies. First, the Amazon case study is presented, followed by Mato Grosso case study, and last the Para case study.

Two STBNs approaches were applied in each case study. The first-order Markov STBN was trained with raster data from 2013 and 2014. Thus, predictions were made for the year 2014 onwards. As raster data were observed until 2018, the last prediction was made for 2019, so the result of the first-order Markov STBN is a six-layer raster time series, one for each year from 2014 to 2019. On the other hand, the second-order Markov STBN was trained with raster data from 2013, 2014, and 2015, as it is made up of three time-slices. Thus, predictions were made for the year 2015 until 2019, and, therefore, the result of this STNB approach is a five-layer raster time series.

Each raster layer (from both STBN models) corresponds to a probability image, in which every pixel value within the ROI represents the probability that location be deforested given observation on the context variables. From the visual analysis, it is not possible to notice significant differences among the probability images resulting from both STBN models. Regions with the highest deforestation risk are indicated by red-colored pixels in the Figures, while dark green-colored pixels indicate the contrary. White pixels within the ROIs refer to previously deforested areas (i.e., before the prediction year). These areas were removed from the probability images since there is no interest in prediction assessment in areas already deforested.

The probability images with deforestation risk over the year can be considered the main result of the STBN models developed from the *stbnR* package. The analyzes carried out from now onwards no longer concern the package implemented in this thesis. Thus, we evaluated the probability image time series in each case study by comparing them with those datasets previously selected to perform model accuracy assessment. We analyze the distribution of the probability values for the target presence and absence classes (i.e., deforested and forested areas, respectively). In general, predictions were consistent, so that the highest probability values were assigned to the majority of deforested pixels, while the lowest probability values were assigned to the majority of forest pixels.

5.1 Amazonas case study

Figure 5.1 presents the probability images time series resulting from the first-order Markov STBN, while Figure 5.2 presents the probability images time series resulting from the second-order Markov STBN. Areas with high deforestation risk can be observed around the boundaries of Boca do Acre (on the west) and Lábrea (on the east) municipalities. In this central region, there is deforestation expansion tendency towards the east, and the most vulnerable areas are predominantly neighboring already deforested areas. This central region is also under the influence of the BR-317 highway (RORIZ; YANAI; FEARNSIDE, 2017).

Figure 5.1 - Probability images time series resulting from the first-order Markov STBN in the Amazon case study.

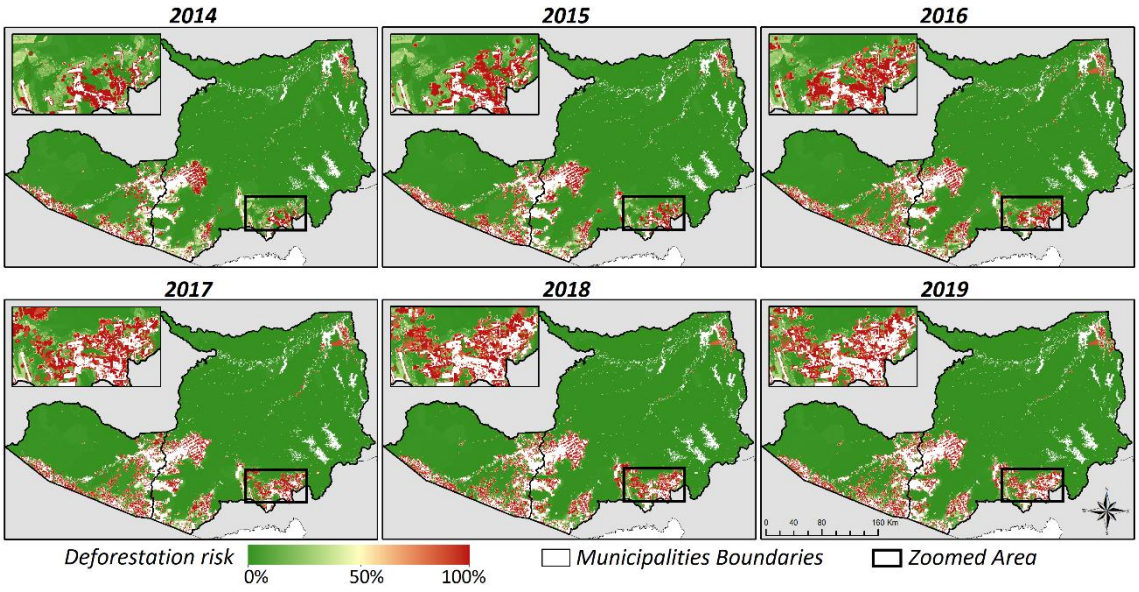

Source: author's production.

Figure 5.2 - Probability images time series resulting from the second-order Markov STBN in the Amazon case study.

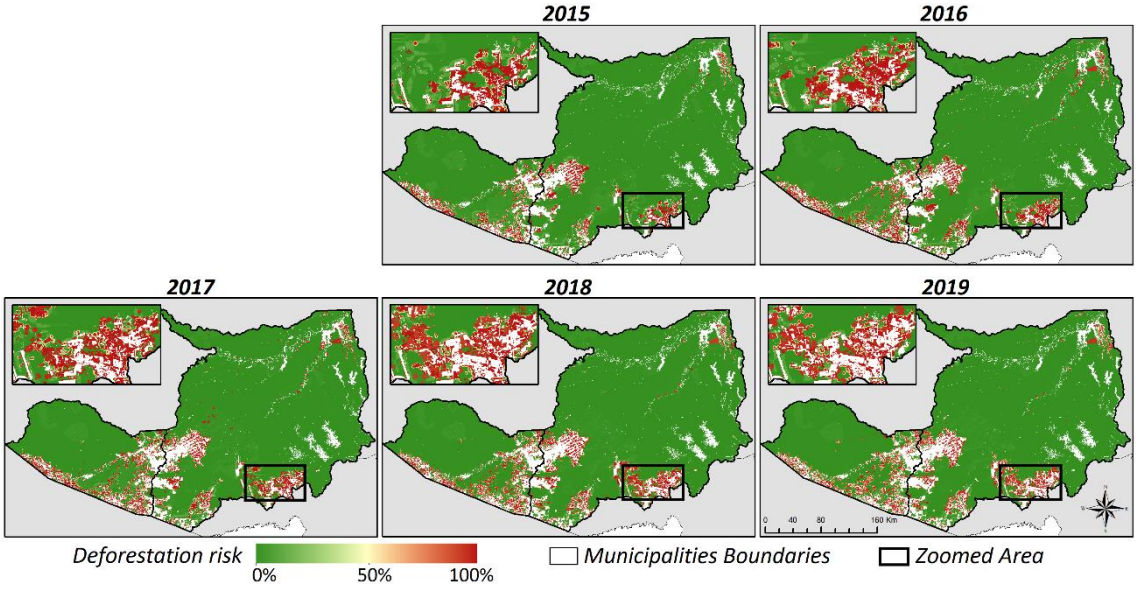

Source: author's production.

Deforestation risk areas in the ROI's southern are located at the boundaries of the Acre (on the west) and Rondônia (on the east) states. The zoomed area in Figures 5.1 and 5.2 clearly shows deforestation progress from the south towards the north over the years. One can observe that regions indicated with high deforestation risk (red-colored) were indeed deforested in the following years (previously deforested areas are shown in white in Figures 5.1 and 5.2). These regions in the south are under the influence of the BR-364 highway that connects the municipalities of Porto Velho in Rondônia state and Rio Branco in Acre state. As stated by Fearnside (2015), major roads stimulate deforestation by facilitating the construction of smaller ones.

Mutual Information (MI) was used to evaluate the importance of the context variables. Figure 5.3 shows the MI values distribution for the context variables in all scenarios. The variable *distance from hotspots fires* stands out among the others as the most important context variable. Indeed, Lábrea municipality has historically presented the highest numbers of hotspots fires in the entire Amazonas state (WHITE, 2018). The variable *distance from degraded areas* was also relevant, followed by *settlement areas*. Deforestation, forest degradation, and fires are intimately connected activities. In general, deforestation occurred in areas that presented some degradation evidence in the previous year, and the role of fires is mostly related to the conversion of forest and degraded forest into clear cut areas. Besides that, forest fires were concentrated in areas along the BR-317

and BR-364 highways and settlements on the southern and southwestern edges of Boca do Acre and Lábrea municipalities (VASCONCELOS et al., 2013a)

Figure 5.3 - Variables importance according to the MI for the first-order Markov STBN in the Amazonas case study.

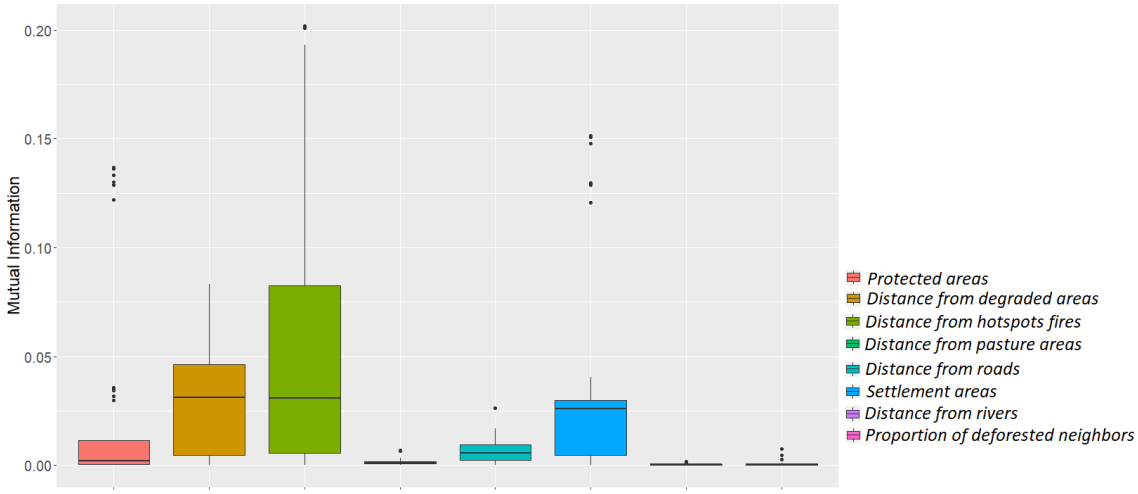

Source: author's production.

Figure 5.4 shows the distribution of the predicted probability values for deforested pixels (red boxplots) and forested pixels (green boxplots). The predicted probability values for deforestation risk decreased over the years, which can be presumed from the more sparse distributions of the red boxplots. This indicates an increase in STBNs uncertainty for long-term predictions of deforestation risk. For the first-order Markov STBN, this uncertainty gradually increases after rolling up two time-slices forward, that is, from the 2016 deforestation risk prediction (Figure 5.4 on the left). On the other hand, the second-order Markov STBN has a more pronounced increase in uncertainty right in the next time-slice forward (Figure 5.4 on the right).

Figure 5.4 - Distribution of the predicted probability values for deforestation and forest pixels selected for accuracy assessment in the Amazonas case study. On the left, for the first-order Markov STBN, and second-order Markov STBN on the right.

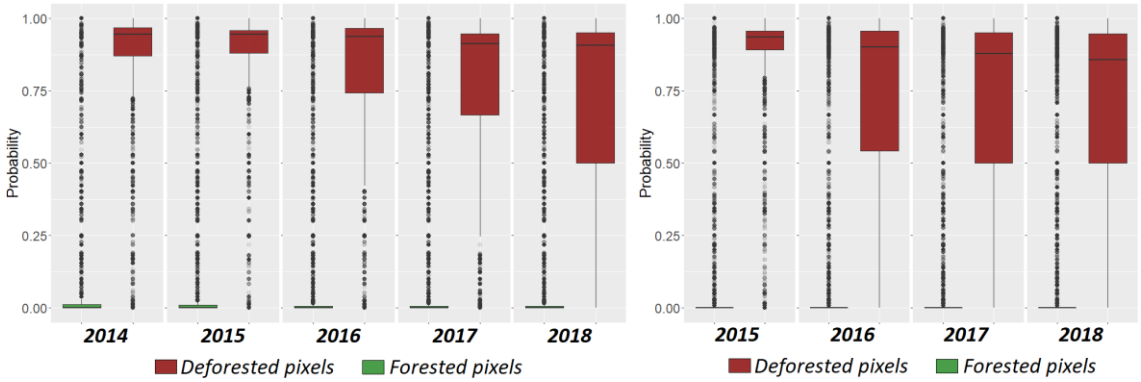

Source: author's production.

The increasing uncertainty in deforestation risk prediction can also be observed from the assessment metrics of the STBN models (see Appendix A). Figure 5.5 shows graphically the AUC-ROC, Precision, and Kappa values over the year. In general, metrics values decrease over time for both STBN approaches. This may indicate that the more long-term is the prediction, the less accurate it will be. From 2016 onwards, Precision and Kappa values were similar for both STBN models. On the other hand, the AUC-ROC metric had an opposite behavior with higher values for the first-order Markov STBN. However, the difference between the assessment metrics when compared between models is not statistically significant (see Appendix B).

Therefore, taking into account both slightly better performance (in terms of AUC-ROC values) and the distribution of the predicted probability values by the first-order Markov STBN (Figure 5.4 on the left), this approach may be the appropriate one to predict the risk of deforestation in the Amazonas case study.

Figure 5.5 - Assessment metrics of the STBNs predictions in the Amazon case study. Fulfilled lines represent assessment metrics of the First-order Markov STBN model predictions, while dashed lines represent assessment metrics of the Second-order Markov STBN model predictions. Red lines refer to AUC-ROC values, while green and blue lines refer to Kappa and Precision values, respectively.

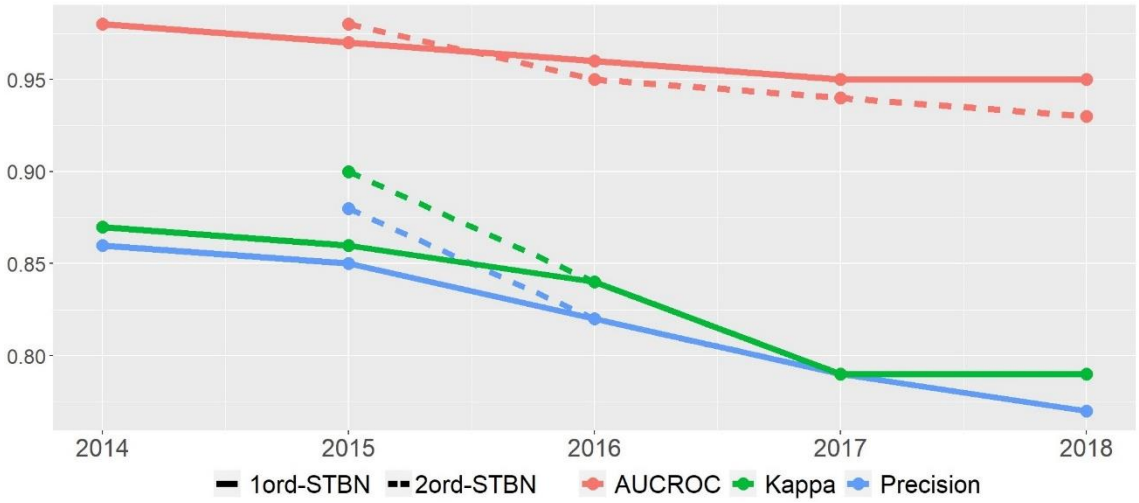

Source: author's production.

5.2 Mato Grosso case study

Figure 5.6 presents the probability images time series resulting from the first-order Markov STBN, while Figure 5.7 presents the probability images time series resulting from the second-order Markov STBN. Areas with the highest deforestation risk are mainly concentrated in the Colniza (on the north) and Aripuanã (on the southeast) municipalities. These two municipalities have had indeed the highest deforestation rates in the Mato Grosso state (INPE, 2019a). In general, areas with the highest risk are neighboring areas already deforested.

The zoomed area in Figures 5.6 and 5.7 highlights the deforestation expansion process over the years. One can observe that even though there is already a deforestation expansion tendency from the east towards the west, most of the zoomed area presented a low deforestation risk. In the following years, the STBN models' predictions indicated that new areas became vulnerable, presenting high-risk (red-colores regions). Subsequently, these high-risk areas were indeed deforested (white areas in the last year).

Figure 5.6 - Probability images time series resulting from the first-order Markov STBN in the Mato Grosso case study.

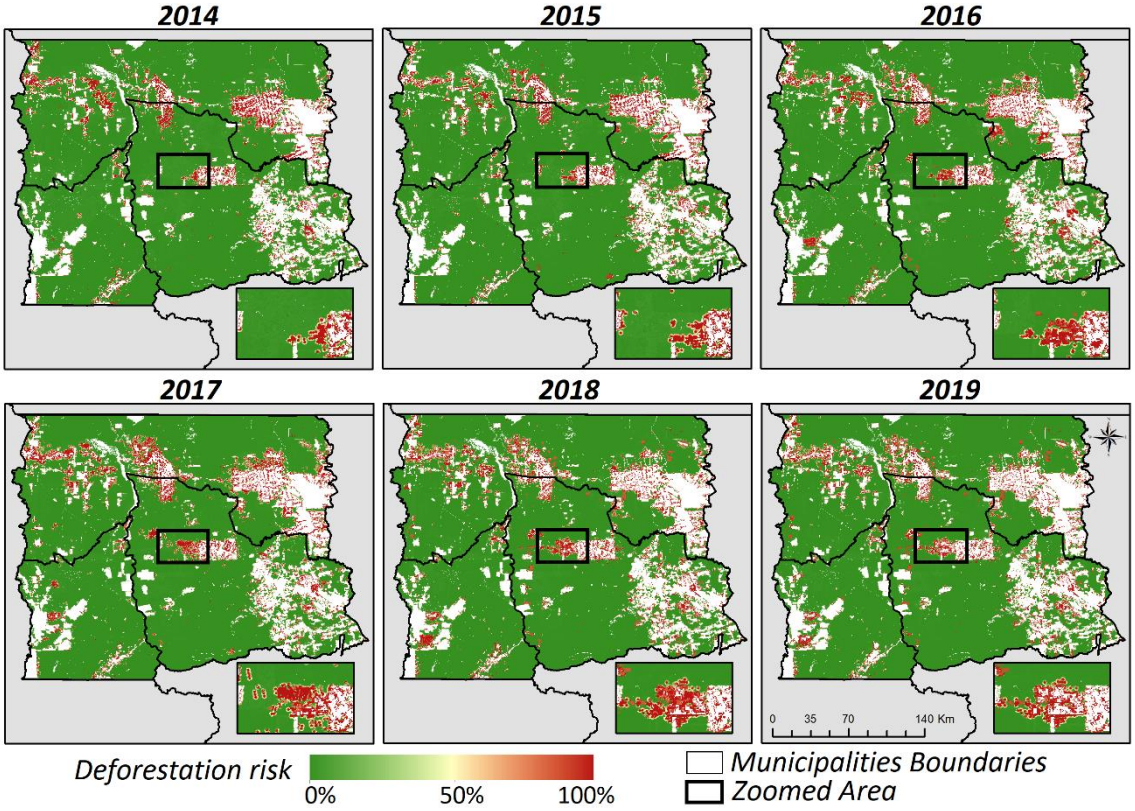

Source: author's production.

Figure 5.7 - Probability images time series resulting from the second-order Markov STBN in the Mato Grosso case study.

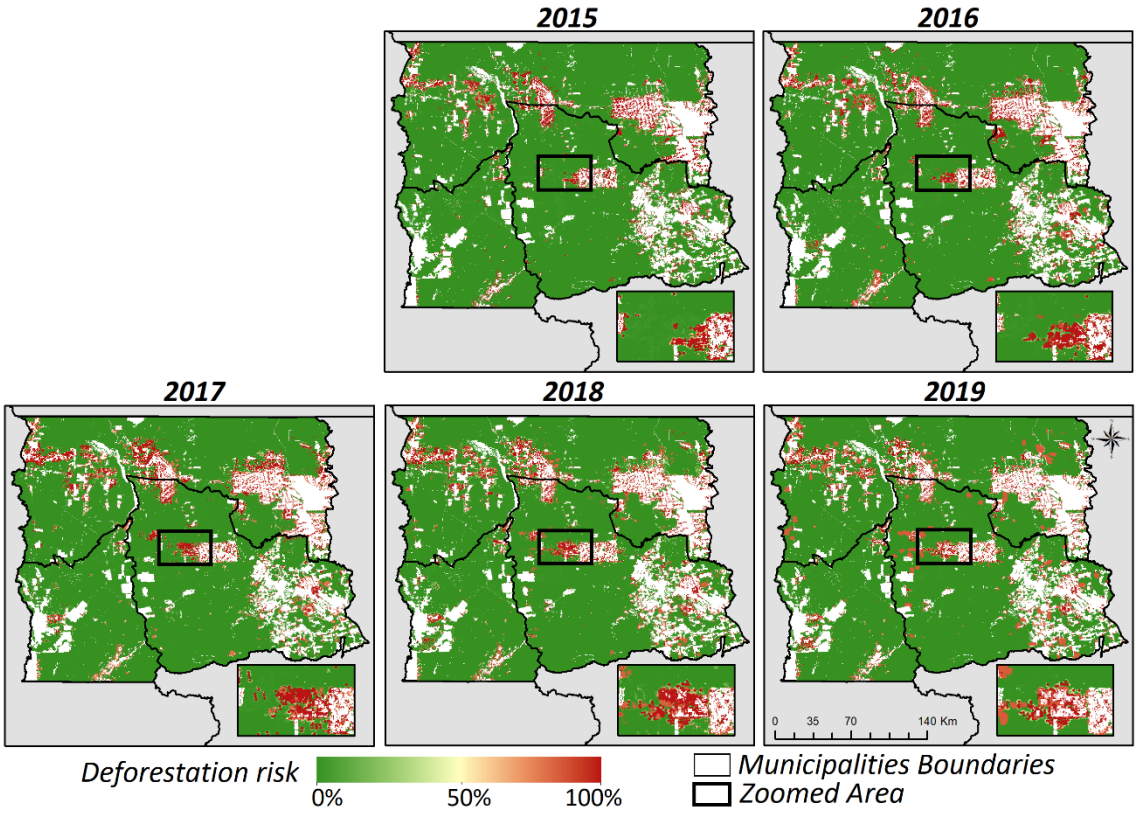

Source: author's production.

Figure 5.8 shows the distribution of the Mutual Information (MI) values for the context variables in the Mato Grosso case study. The *settlement areas* variable stands out as the most important variable. Specifically in the Mato Grosso case study, this variable is actually inversely proportional to deforestation risk. This is because the region has only a few settlements located in the northeastern, which have probably not had such an influence on deforestation. Furthermore, a large part of areas with high deforestation risk is located outside the settlement areas.

In sequence, the variables *protected areas*, *distance from degraded areas*, *distance from hotspots fires*, and *distance from pasture areas* showed similar importance. Extensive conservation units and indigenous lands located in the ROI's south-central and northern played an important role in mitigating deforestation risk. These areas presented the lowest risk. On the other hand, a huge concentration of fires has been observed clustered in the case study region over the last years (INPE, 2019b). This may be caused by the ongoing cattle-ranching expansion process, which is a deforestation driver in the region. Those already deforested areas have been predominantly converted to pasture (ALMEIDA et

al., 2016). Besides that, many forest areas are degraded because of the intense illegal logging activity in this region (SOUSA, 2016).

Figure 5.8 - Variables importance according to the MI for the first-order Markov STBN in the Mato Grosso case study.

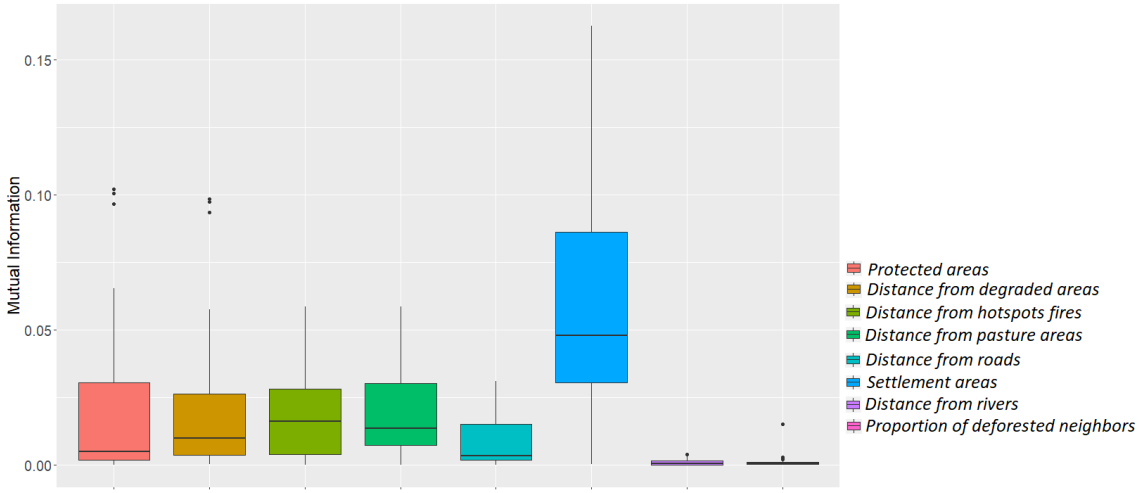

Source: author's production.

Figure 5.9 shows the distribution of the predicted probability values for deforested (red boxplots) and forested (green boxplots) pixels selected for accuracy assessment in each year. In the Mato Grosso case study, both STBN models also tend to become more uncertain over time, as one can observe from the more sparse distributions of the red boxplots for each forward prediction. The boxplots median shows that the predicted probability values decrease over the years, which can be seen as an increase in uncertainty. Here, the first-order Markov STBN uncertainty also presented a gradual increase (Figure 5.9 on the left), while the second-order Markov STBN presented a more pronounced increase in uncertainty right in the next time-slice forward (Figure 5.9 on the right).

Figure 5.9 - Distribution of the predicted probability values for deforestation and forest pixels selected for accuracy assessment in the Mato Grosso case study. On the left, for the first-order Markov STBN, and second-order Markov STBN on the right.

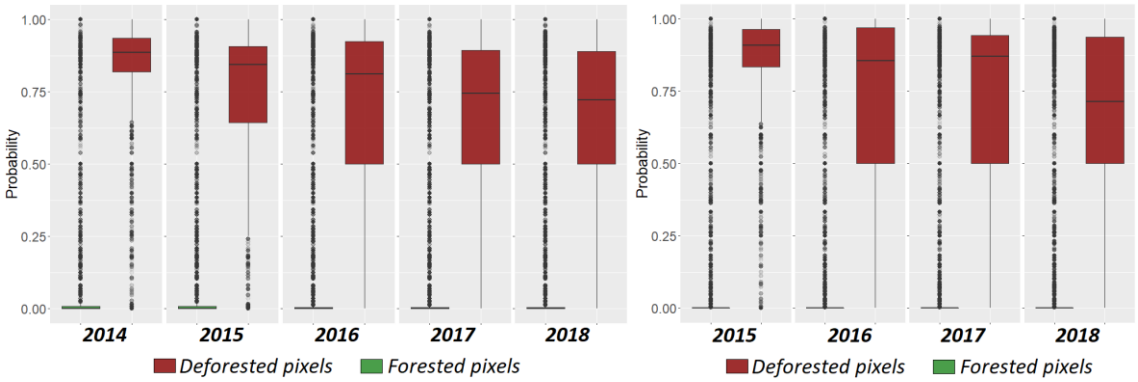

Source: author's production.

The assessment metrics of the STBN models (see Appendix A) also denote an increase in uncertainty. One can note from Figure 5.10, that AUC-ROC, Precision, and Kappa values gradually decrease over the years indicating the uncertainty increasing in deforestation risk prediction of both STBN models. Such metrics' behavior suggests that short-term predictions are more accurate. Even though the difference between the assessment metrics when compared between models is not statistically significant (see Appendix B), AUC-ROC, Precision, and Kappa metrics from the second-order Markov STBN presented slightly higher values to the metrics from the first-order Markov STBN. These results suggest that spatio-temporal variables influence deforestation risk prediction beyond the one-time interval and, therefore, the second-order Markov STBN may be the appropriate approach to predict the risk of deforestation in the Mato Grosso case study.

Figure 5.10 - Assessment metrics of the STBNs predictions in the Mato Grosso case study. Fulfilled lines represent assessment metrics of the First-order Markov STBN model predictions, while dashed lines represent assessment metrics of the Second-order Markov STBN model predictions. Red lines refer to AUC-ROC values, while green and blue lines refer to Kappa and Precision values, respectively.

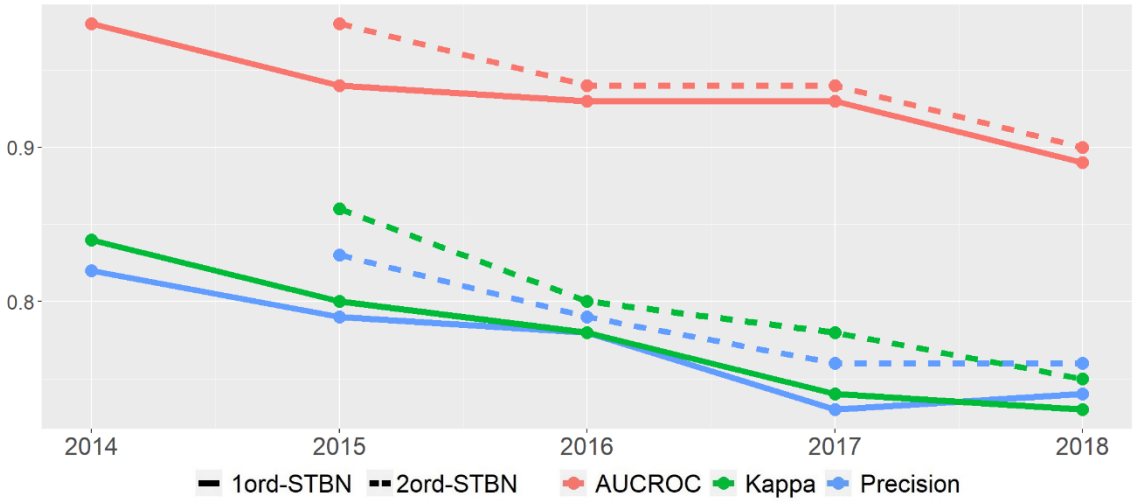

Source: author's production.

5.3 Pará case study

Figure 5.11 presents the probability images time series resulting from the first-order Markov STBN, while Figure 5.12 presents the probability images time series resulting from the second-order Markov STBN. Likewise the two previous case studies, no significant differences could be observed between the results from both STBN approaches. Regions with the highest deforestation risk are indicated by red-colored pixels, while dark green-colored pixels indicate the contrary. White pixels within the ROIs refer to previously deforested areas. These areas were removed from the probability images since there is no interest in prediction assessment in areas already deforested.

The BR-163 highway crosses the ROI from north to south. Several small roads have been branched off from the BR-163, influencing deforestation in adjacent areas. One can observe that areas with the highest deforestation risk are subject to the influence of this highway, forming a wide corridor for deforestation expansion. High-risk areas also can be seen in a second corridor, however narrower in the north of ROI. This is an area under the influence of the Transgarimpeira highway, which connects the BR-163 highway to mining areas in the west (SILVA et al., 2020).

Areas under environmental protection provided a significant mitigation effect on deforestation risk. One can observe that the Indigenous Land as well as the Military Reserve located in the ROI's eastern and southwestern, respectively, presented the lowest deforestation risk. These conservation units have more restrictive environmental laws prohibiting any exploration activities (AMIN et al., 2019). The zoomed area in Figures 5.5 and 5.6 shows that Indigenous Land in the eastern is a strong barrier against deforestation expansion.

Figure 5.11 - Probability images time series resulting from the first-order Markov STBN in the Pará case study.

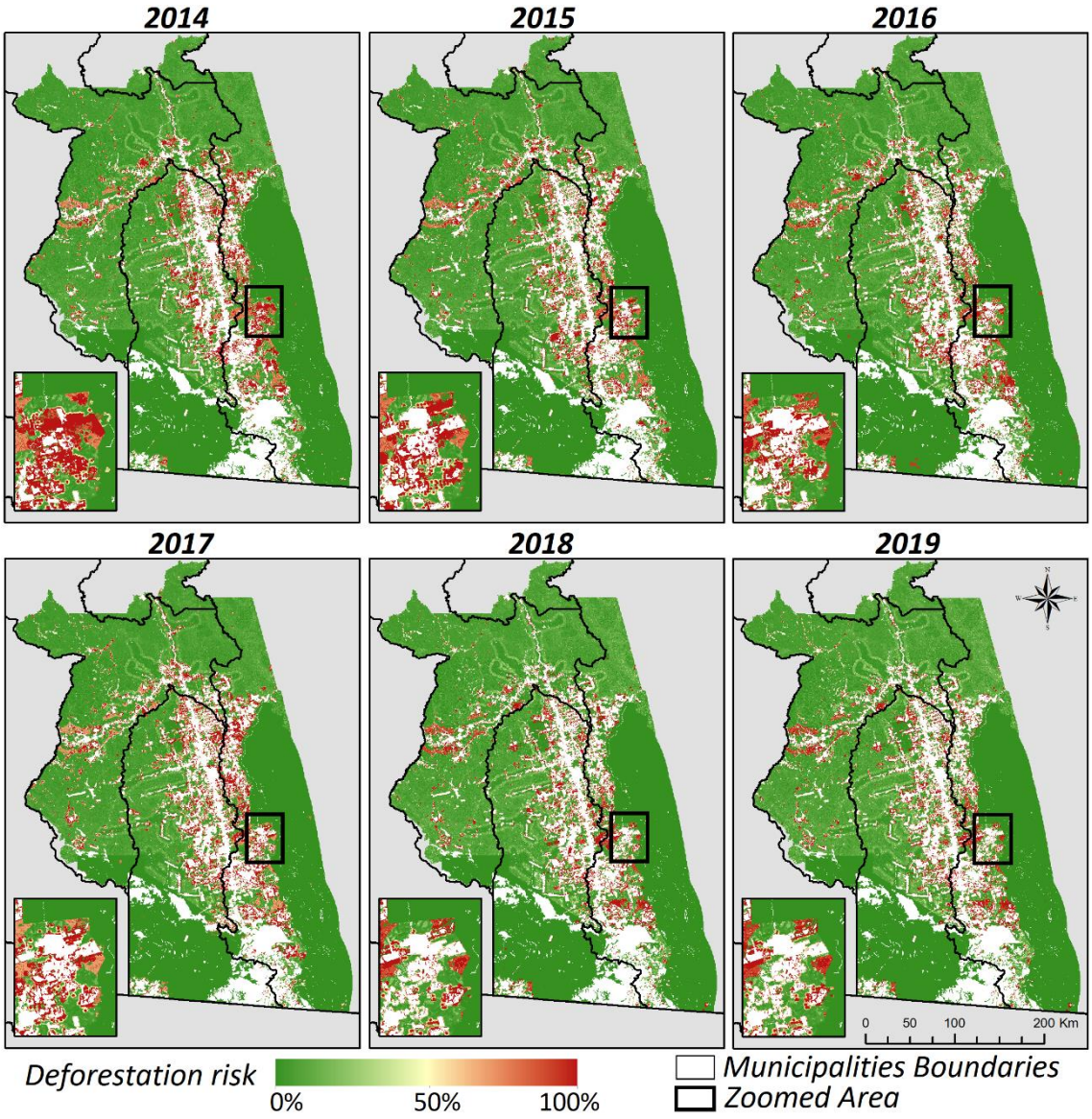

Source: author's production.

Figure 5.12 - Probability images time series resulting from the second-order Markov STBN in the Pará case study.

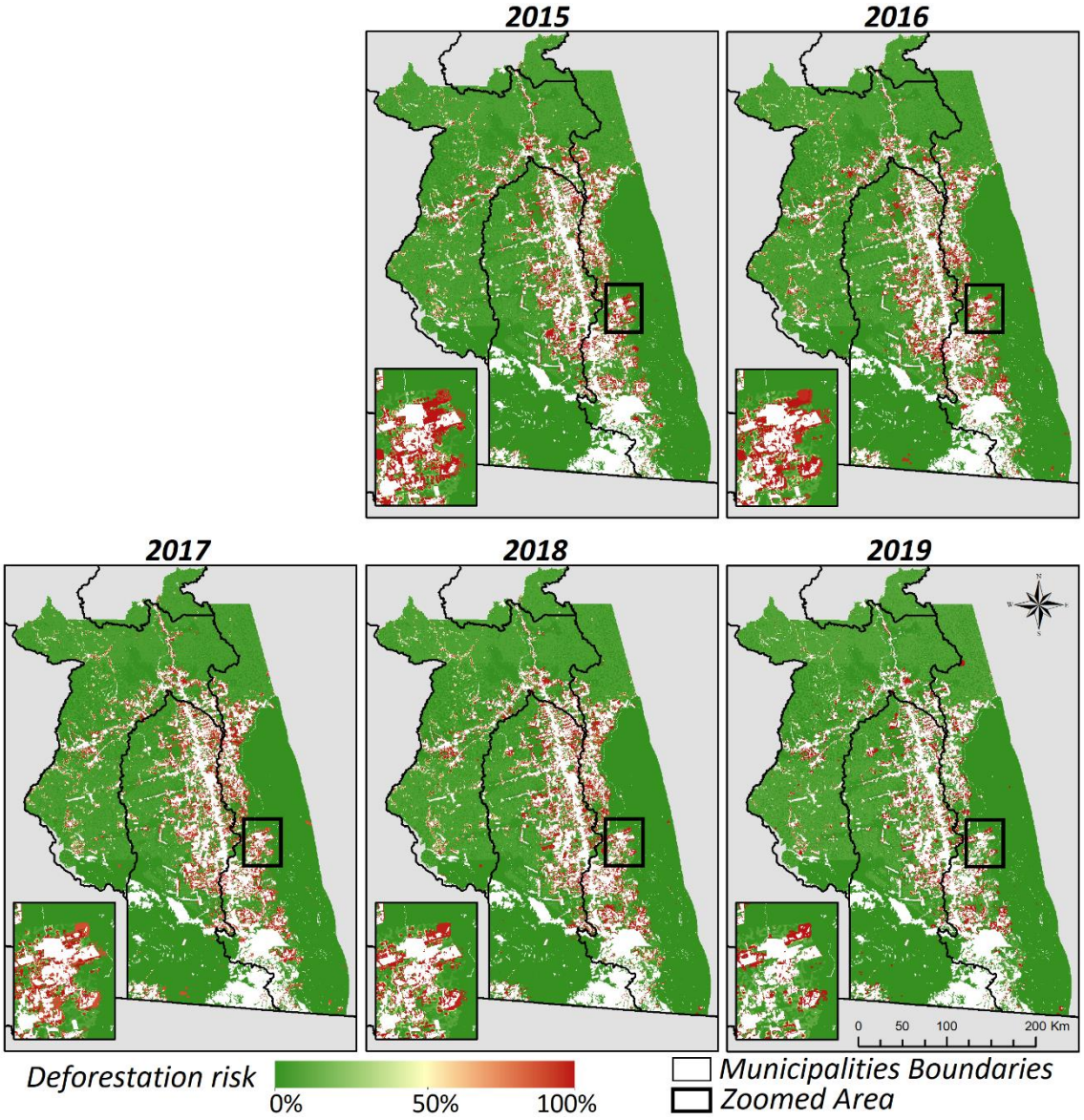

Source: author's production.

Attention should be drawn to the Jamanxim National Forest located in the ROI's midwest. The probability images show a deforestation expansion tendency from the BR-163 highway towards to west, therefore, within the Jamanxin National Forest boundaries. High deforestation risk areas in this region are mainly driven by the high frequency of hotspots fires and degraded areas (PINHEIRO et al., 2016; SILVA et al., 2020). The Jamanxim National Forest is the conservation unit with the highest deforestation rates from the BLA.

Mutual Information (MI) was used to evaluate the importance of the context variables, as shown in Figure 5.13. The variables *distance from hotspots fires* and *settlement areas* stood out as an important variable. Indeed, a huge concentration of hotspots fires has annually been observed around the BR-163 highway (INPE, 2019b). Settlements along the BR-163 highway seem to increase deforestation risk, probably due to the human activities carried out in their areas (PINHEIRO et al., 2016). In turn, the variable *protected areas* also presented great importance, due to the significative effect of deforestation risk mitigation.

Figure 5.13 - Variables importance according to the MI for the first-order Markov STBN in the Pará case study.

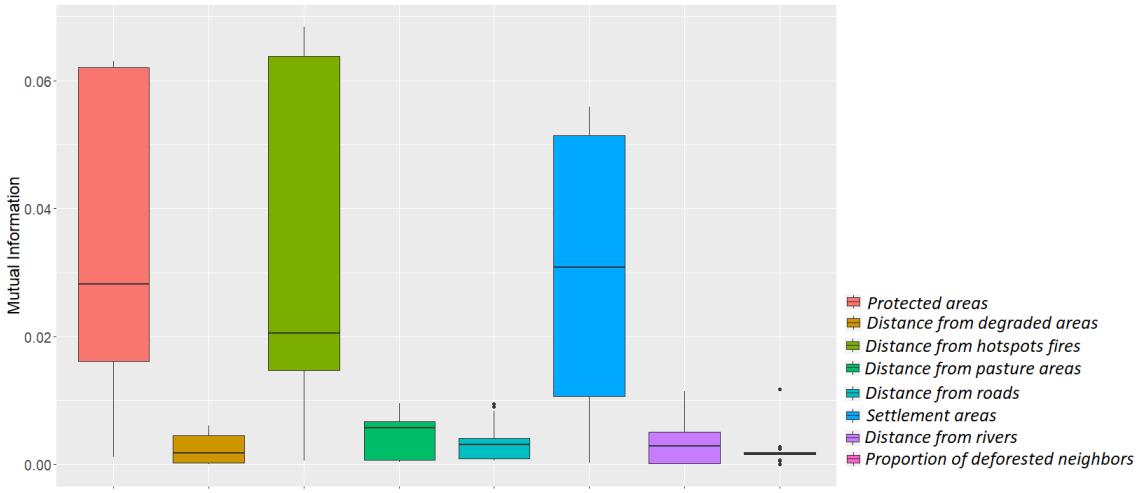

Source: author's production.

Figure 5.14 shows the distribution of the predicted probability values for deforested (red boxplots) and forested (green boxplots) pixels selected for accuracy assessment in each year. Contrary to what was observed in previous case studies, first-order Markov STBN presented a significant increase in uncertainty over time. The predicted probability values decreased drastically after forwarding prediction, as can be seen in Figure 5.14 on the left. In the 2016 prediction, probability values were more distributed in the $[0, 1]$ range. On the other hand, second-order Markov STBN seemed to have a lower level of uncertainty since the predicted probability values were concentrated in values above 0.5 (Figure 5.14 on the right).

In general, STBN models in the Pará case study were less accurate in predicting deforestation risk, when comparing the assessment metrics from the previous case studies

(see Appendix A). Even so, the metrics also showed the expected decreasing behavior over time, indicating short-term predictions as the best option. Furthermore, the higher assessment metrics of second-order Markov STBN (Figure 5.15) along with the lower level of uncertainty in this approach predictions suggest that spatio-temporal variables influence deforestation risk prediction beyond the one-time interval, being the second-order Markov STBN a more appropriate approach to predict the risk of deforestation in the Pará case study.

Figure 5.14 - Distribution of the predicted probability values for deforestation and forest pixels selected for accuracy assessment in the Pará case study. On the left, for the first-order Markov STBN, and second-order Markov STBN on the right.

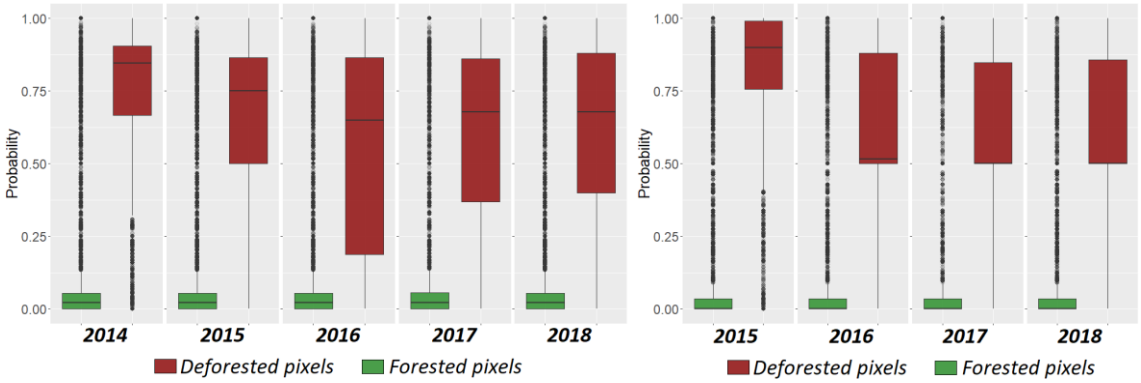

Source: author's production.

Figure 5.15 - Assessment metrics of the STBNs predictions in the Pará case study. Fulfilled lines represent assessment metrics of the First-order Markov STBN model predictions, while dashed lines represent assessment metrics of the Second-order Markov STBN model predictions. Red lines refer to AUC-ROC values, while green and blue lines refer to Kappa and Precision values, respectively.

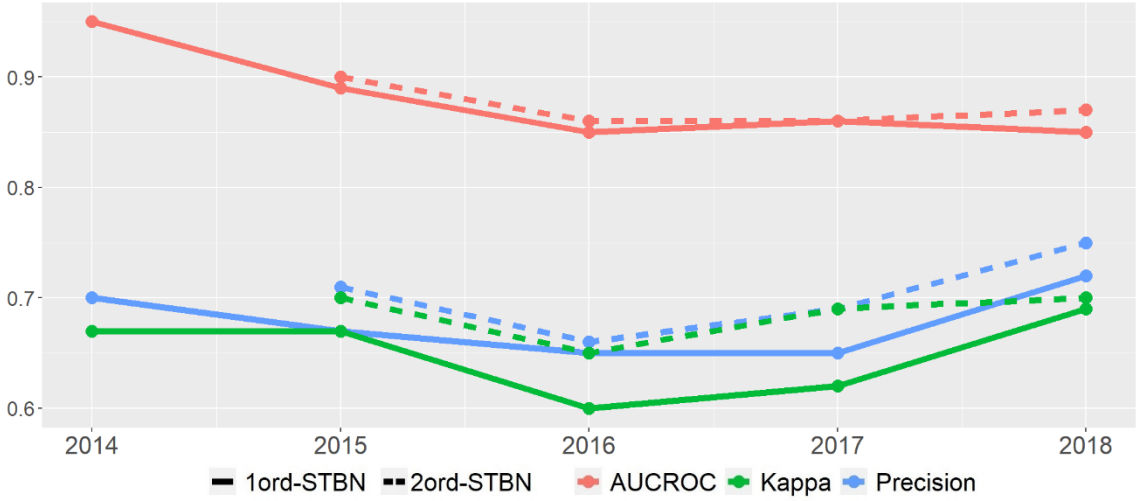

Source: author's production.

5.4 Processing time analysis

In the Amazonas case study, the first-order Markov STBN seemed to be the appropriate approach for deforestation risk prediction. On the other hand, the second-order Markov STBN showed slightly better results for both Mato Grosso and Pará case studies. However, it is up to the user to decide whether it is worth employing this approach for a better result since it requires more processing time.

The total processing time as well as the bottleneck time of both STBN models in the three case studies are shown in Table 5.1 and Figure 5.16. The bottleneck step refers to the STBN queries and updating. One can note that the bigger the network structure (second-order Markov STBN), the longer the bottleneck time (orange bars in Figure 5.16). On the contrary, the remaining steps of the entire modeling (green bars in Figure 5.16) spend relatively the same processing time for both approaches in the same case study.

It also can be noted that, in the Amazonas and Mato Grosso case studies, the total processing time of the second-order Markov STBN was approximately four times greater than the time spent by the first-order Markov STBN. In turn, the total processing time of the second-order Markov STBN in the Pará case study was approximately eight times greater than the time spent by the first-order Markov STBN. This difference can be explained by the fact that the region of interest (ROI) in the Pará case study is the largest one among all the case studies.

Table 5.1 - Processing time of the STBN approaches.

Amazonas case study		
	First-order Markov STBN	**Second-order Markov STBN**
Bottleneck	116 minutes	663 minutes
Others	63 minutes	58 minutes
Total	179 minutes	721 minutes

Mato Grosso case study		
	First-order Markov STBN	**Second-order Markov STBN**
Bottleneck	129 minutes	593 minutes
Others	30 minutes	28 minutes
Total	159 minutes	621 minutes

Pará case study		
	First-order Markov STBN	**Second-order Markov STBN**
Bottleneck	216 minutes	2527 minutes
Others	85 minutes	96 minutes
Total	301 minutes	2623 minutes

Figure 5.16 - Processing time of the STBN approaches in each case study. Orange bars refer to the bottleneck step processing time, while the green bars refer to the remaining steps of the entire modeling.

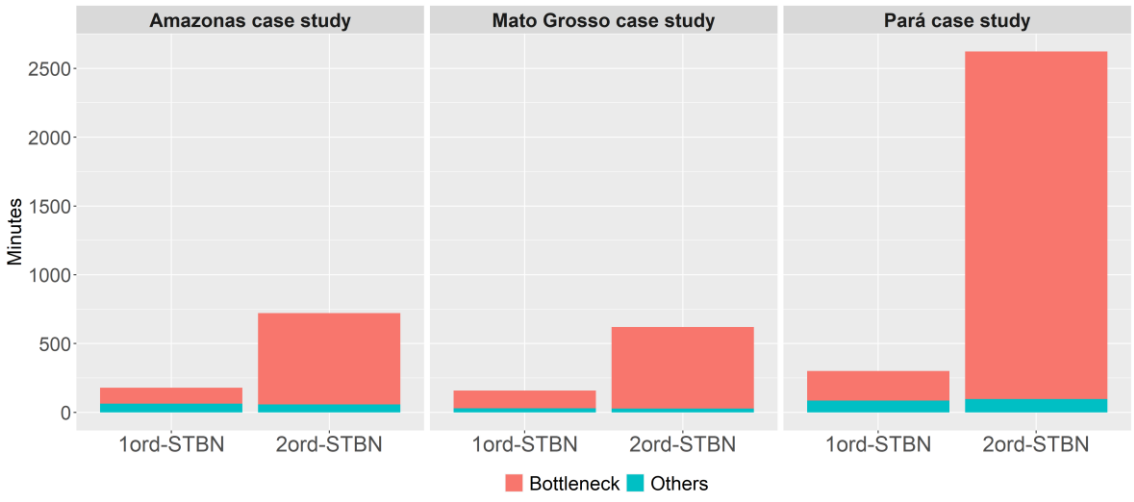

Source: author's production.

6 CONCLUSION

The main goal of this doctoral thesis was to build a Spatio-Temporal Bayesian Network (STBN) model to predict deforestation risk. To accomplish the objective of this work, we implemented an *R* package called *stbnR* (**S**patio-**T**emporal **B**ayesian **N**etwork for **R**), which allows the development of STBN-based LULCC models within a single integrated environment, thus avoiding challenges such as data conversion and transfer from different software tools. The *stbnR* package was developed in *R* because this is an open-source programing language, which allows the proposed package to be thoroughly tested in several applications. The *stbnR* package documentation is being finalized and will soon be available on the GitHub website https://github.com/alexsandrocandido/stbnR and maybe in the CRAN repository (Comprehensive R Archive Network).

We presented in the main functions of the *stbnR* package and how to use them to carry out a complete workflow of LULCC modeling based on an STBN. Although employing BNs to predict deforestation risk has been proposed before (DLAMINI, 2016; KRÜGER; LAKES, 2015; MAYFIELD et al., 2017), the temporal domain has not been taken into account, and deforestation has been considered as a static process when modeled by BN approaches. Therefore, the STBN models developed in this work aimed to meet such demand, by incorporating both spatial and temporal information into the modeling.

Three deforestation frontier regions in the Amazon Forest were selected to apply the STBN models to evaluate them and demonstrate their potential in predicting deforestation risk over time. For each case study region, two STBN approaches were applied: a first-order Markov STBN and a second-order Markov STBN. Through the application of both models, we were able to confirm the work's hypothesis that STBN-based LULCC models are able to capture and represent the variables' spatio-temporal relationships to appropriately predict deforestation risk.

The probability images time series are the main STBN models outputs. In each probability image, each pixel value represents the probability of that location being deforested given the values observed in the context variables. According to the accuracy assessment indexes, the STBN models presented a strong performance with a great agreement between deforestation events and predictions. Furthermore, the second-order Markov STBN overperformed the first-order Markov STBN in two case study regions. This

indicates that deforestation risk prediction is influenced not only by variables in the previous time-slice but also by variables from earlier time-slices.

However, we could note that there was an increase in uncertainty for both STBN models in deforestation risk prediction over time, indicating that the more long-term is the prediction, the less accurate it will be. Thus, we can state that STNB-based LULCC models are suitable for short-term predictions. Besides the uncertainty increasing, the second-order Markov STBN application can bring another concern about the execution time. In the three case study regions, this model spent much more time than the first-order Markov STBN. Therefore, even though computer systems currently offer sufficient resources to perform robust tasks, the user may consider weighting between a better result or a faster result.

Among the variables selected to compose the STBN models, the *distance from hotspots fires* stood out as one of the most important variables for predicting deforestation risk. This variable is directly related to human activities such as illegal logging and cattle-ranching expansion, which are the main deforestation drivers in the Amazon forest. In addition to that, the *protected areas* variable was also extremely important but not as a driver but as a mitigator of deforestation risk. Indeed, the lowest values of risk were found in conservation units such as indigenous land.

The probability images obtained from the STBN models can be used as indicators of the areas most vulnerable to deforestation and support for decision-makers to implement directed preventive action plans, for instance, focused on priority areas. As future work, we suggest testing the application of STBN models with higher-order Markov for predicting deforestation risk. These models may obtain more accurate results. Furthermore, a thorough sensitivity analysis should be conducted to measure the impact in the STBN models' predictions from changes in the discretization thresholds of the context variables as well as in the variables' relationship. It is also important to test the robustness of the stbnR package with available benchmarking to ensure its quality. In addition to that, we also suggest the development of STBN-based LULCC models from the *stbnR* package for other Earth observation applications besides the deforestation process.

REFERENCES

ABEBE, Y.; KABIR, G.; TESFAMARIAM, S. Assessing urban areas vulnerability to pluvial flooding using GIS applications and Bayesian Belief Network model. **Journal of Cleaner Production**, v. 174, p. 1629–1641, Feb. 2018.

ABIDEN, M. Z. Z. et al. **Comparative study on stochastic and deterministic approaches in urban growth model**. In: IEEE INTERNATIONAL COLLOQUIUM ON SIGNAL PROCESSING AND ITS APPLICATIONS, 9., 2013. **Anais**...IEEE, 2013. Available from: <http://ieeexplore.ieee.org/document/6530064/>.

ABURAS, M. M.; AHAMAD, M. S. S.; OMAR, N. Q. Spatio-temporal simulation and prediction of land-use change using conventional and machine learning models: a review. **Environmental Monitoring and Assessment**, v. 191, n. 4, p. 205, 5 Apr. 2019.

AGUILERA, P. A. et al. Bayesian networks in environmental modelling. **Environmental Modelling & Software**, v. 26, n. 12, p. 1376–1388, Dec. 2011.

AITKENHEAD, M. J.; AALDERS, I. H. Predicting land cover using GIS, Bayesian and evolutionary algorithm methods. **Journal of Environmental Management**, v. 90, n. 1, p. 236–250, 2009.

AL-SHARIF, A. A. A.; PRADHAN, B. Spatio-temporal prediction of urban expansion using bivariate statistical models: assessment of the efficacy of evidential belief functions and frequency ratio models. **Applied Spatial Analysis and Policy**, v. 9, n. 2, p. 213–231, 8 June. 2016.

ALENCAR, A. A. et al. Landscape fragmentation, severe drought, and the new Amazon forest fire regime. **Ecological Applications**, v. 25, n. 6, p. 1493–1505, Sept. 2015.

ALLOUCHE, O.; TSOAR, A.; KADMON, R. Assessing the accuracy of species distribution models: prevalence, kappa and the True Skill Statistic (TSS). **Journal of Applied Ecology**, v. 43, n. 6, p. 1223–1232, 12 Sept. 2006.

ALMEIDA, C. A. DE et al. High spatial resolution land use and land cover mapping of the Brazilian Legal Amazon in 2008 using Landsat-5/TM and MODIS data. **Acta Amazonica**, v. 46, n. 3, p. 291–302, Sept. 2016.

ALVES, L. M. et al. Sensitivity of Amazon regional climate to deforestation. **American Journal of Climate Change**, v. 06, n. 01, p. 75–98, 2017.

AMIN, A. et al. Neighborhood effects in the Brazilian Amazônia: protected areas and deforestation. **Journal of Environmental Economics and Management**, v. 93, p. 272–288, Jan. 2019.

ARIMA, E. Y. et al. Public policies can reduce tropical deforestation: lessons and challenges from Brazil. **Land Use Policy**, v. 41, p. 465–473, Nov. 2014.

ARTAXO, P. Working together for Amazonia. **Science**, v. 363, n. 6425, p. 323–323, 25 Jan. 2019.

BALBI, S. et al. A spatial Bayesian network model to assess the benefits of early warning for urban flood risk to people. **Natural Hazards and Earth System Sciences**, v. 16, p. 1323–1337, 2016.

BARBER, C. P. et al. Roads, deforestation, and the mitigating effect of protected areas in the Amazon. **Biological Conservation**, v. 177, p. 203–209, Sept. 2014.

BARBER, D.; CEMGIL, A. Graphical models for time-series. **IEEE Signal Processing Magazine**, v. 27, n. 6, p. 18–28, Nov. 2010.

BARONA, E. et al. The role of pasture and soybean in deforestation of the Brazilian Amazon. **Environmental Research Letters**, v. 5, n. 2, e 024002, Apr. 2010.

BASSE, R. M. et al. Land use changes modelling using advanced methods: cellular automata and artificial neural networks: the spatial and explicit representation of land cover dynamics at the cross-border region scale. **Applied Geography**, v. 53, p. 160–171, Sept. 2014.

BAYESFUSION. **BayesFusion|GeNIe**. Available from: <https://www.bayesfusion.com/genie/>. Access in: July 3, 2019.

BRADLEY, A. V. et al. An ensemble of spatially explicit land-cover model projections: prospects and challenges to retrospectively evaluate deforestation policy. **Modeling Earth Systems and Environment**, v. 3, n. 4, p. 1215–1228, 5 Dec. 2017.

BRASIL. MINISTÉRIO DO MEIO AMBIENTE. **Action plan to prevent and control deforestation in Amazon**. Available from: <https://www.mma.gov.br/informma/item/616-prevenção-e-controle-do-desmatamento-na-amazônia>.

BRASIL. MINSTÉRIO DO MEIO AMBIENTE **Action plan to prevent and control deforestation in Amazon - 2nd phase**. Available from: <https://www.mma.gov.br/informma/item/616-prevenção-e-controle-do-desmatamento-na-amazônia>.

BRASIL. PRESIDÊNCIA DA REPÚBLICA. **Lei complementar nº124, de 03 de janeiro de 2007:** institui a Superintendência do Desenvolvimento da Amazônia: SUDAM. Available from: <http://www.planalto.gov.br/ccivil_03/leis/lcp/Lcp124.htm>. Access in: Jjune 22, 2019.

BRASIL. PRESIDÊNCIA DA REPÚBLICA. **Lei nº 12.727, de 17 de outubro de 2012:** altera a Lei nº 12.651, de 25 de maio de 2012, que dispõe sobre a proteção da vegetação nativa. Available from: <http://www.planalto.gov.br/ccivil_03/_Ato2011-2014/2012/Lei/L12727.htm>. Access in: June 22, 2019.

BROADBEND, E. et al. Forest fragmentation and edge effects from deforestation and selective logging in the Brazilian Amazon. **Biological Conservation**, v. 141, n. 7, p. 1745–1757, July 2008.

BROWN, D. G. et al. Modeling land use and land cover change. In: GUTMAN, G. et al. (Ed.). **Land change science:** remote sensing and digital image processing. Dordrecht: Springer Netherlands, 2012. v. 6, p. 395–409.

BROWN, D. G. et al. Opportunities to improve impact, integration, and evaluation of land change models. **Current Opinion in Environmental Sustainability**, v. 5, n. 5, p. 452–457, Oct. 2013.

BROWN, D. G. et al. **Advancing land change modeling: opportunities and research requirements**. Washington: National Academies Press, 2014.

CAI, B.; LIU, Y.; XIE, M. A dynamic-bayesian-network-based fault diagnosis methodology considering. **IEEE Transactions on Automation Science and Engineering**, v. 14, n. 1, p. 276–285, 2016.

CÂMARA, G. et al. **Metodologia para o cálculo da taxa anual de desmatamento na Amazônia Legal**. São José dos Campos, Brazil: INPE. Available from: <http://www.obt.inpe.br/prodes/metodologia_TaxaProdes.pdf>.

CAO, C.; DRAGIĆEVIĆ, S.; LI, S. Land-use change detection with convolutional neural network methods. **Environments**, v. 6, n. 2, p. 25, 2019.

CARMONA, C.; CASTILLO, G.; MILLÁN, E. Designing a dynamic Bayesian network for modeling students' learning styles. In: IEEE INTERNATIONAL CONFERENCE ON ADVANCED LEARNING TECHNOLOGIES, 8., 2008. **Proceedings**... IEEE, 2008. Available from: <http://ieeexplore.ieee.org/document/4561705/>.

CARVALHO, W. D. et al. Deforestation control in the Brazilian Amazon: a conservation struggle being lost as agreements and regulations are subverted and bypassed. **Perspectives in Ecology and Conservation**, v. 17, n. 3, p. 122–130, July 2019.

CELIO, E.; KOELLNER, T.; GRÊT-REGAMEY, A. Modeling land use decisions with Bayesian networks: Spatially explicit analysis of driving forces on land use change. **Environmental Modelling & Software**, v. 52, p. 222–233, Feb. 2014

CHANDRASHEKAR, G.; SAHIN, F. A survey on feature selection methods. **Computers & Electrical Engineering**, v. 40, n. 1, p. 16–28, Jan. 2014.

CHANG-MARTÍNEZ, L. et al. Modeling historical land cover and land use: a review from contemporary modeling. **ISPRS International Journal of Geo-Information**, v. 4, n. 4, p. 1791–1812, 2015.

CHEE, Y. E. et al. Modelling spatial and temporal changes with GIS and Spatial and Dynamic Bayesian Networks. **Environmental Modelling & Software**, v. 82, p. 108–120, 2016.

CHEN, G. et al. Spatiotemporal patterns of tropical deforestation and forest degradation in response to the operation of the Tucuruí hydroelectric dam in the Amazon basin. **Applied Geography**, v. 63, p. 1–8, Sept. 2015.

CHEN, J. et al. Risk analysis for real-time flood control operation of a multi-reservoir system using a dynamic Bayesian network. **Environmental Modelling & Software**, v. 111, p. 409–420, Jan. 2019.

CHEN, S. H.; POLLINO, C. A. Good practice in Bayesian network modelling. **Environmental Modelling and Software**, v. 37, p. 134–145, 2012.

CHHABRA, R.; KRISHNA, C. R.; VERMA, S. Smartphone based context-aware driver behavior classification using dynamic bayesian network. **Journal of Intelligent & Fuzzy Systems**, v. 36, n. 5, p. 4399–4412, 2019.

CONGALTON, R. G.; GREEN, K. **Assessing the accuracy of remotely sensed dData**: principles and practices. 2.ed. [S.l.]: CRC Press/Taylor & Francis, 2009.

CUAYA, G. et al. A dynamic Bayesian network for estimating the risk of falls from real gait data. **Medical and Biological Engineering and Computing**, v. 51, n. 1–2, p. 29–37, 2013.

DALLA-NORA, E. L. et al. Why have land use change models for the Amazon failed to capture the amount of deforestation over the last decade? **Land Use Policy**, v. 39, p. 403–411, 2014.

DANG, A. N.; KAWASAKI, A. A review of methodological integration in land-use change models. **International Journal of Agricultural and Environmental Information Systems**, v. 7, n. 2, p. 1–25, Apr. 2016.

DAS, M. et al. FORWARD: a model for forecasting reservoir water dynamics using Spatial Bayesian Network (SpaBN). **IEEE Transactions on Knowledge and Data Engineering**, v. 29, n. 4, p. 842–855, 2017.

DAS, M.; GHOSH, S. K. Space-time prediction of high resolution raster data: an approach based on Spatio-temporal Bayesian Network (STBN). In: ACM INDIA JOINT INTERNATIONAL CONFERENCE ON DATA SCIENCE AND MANAGEMENT OF DATA, 2019. **Proceedings…** New York, USA: ACM Press, 2019. Available from: <http://dl.acm.org/citation.cfm?doid=3297001.3297017>.

DAVENPORT, R. B. et al. A policy mix to prevent a non-commons tragedy for collective forest reserves in agrarian settlements in northwest Mato Grosso. **Revista de Economia Contemporânea**, v. 20, n. 3, p. 405–429, 2016.

DE SANTANA, Á. L. et al. Strategies for improving the modeling and interpretability of Bayesian networks. **Data & Knowledge Engineering**, v. 63, n. 1, p. 91–107, Oct. 2007.

DING, Q.; CHEN, W.; HONG, H. Application of frequency ratio, weights of evidence and evidential belief function models in landslide susceptibility mapping. **Geocarto International**, v. 32, n. 6, p. 1–21, 2016.

DINIZ, C. G. et al. DETER-B: The new Amazon near real-time deforestation detection system. **IEEE Journal of Selected Topics in Applied Earth Observations and Remote Sensing**, v. 8, n. 7, p. 3619–3628, 2015.

DLAMINI, W. M. Analysis of deforestation patterns and drivers in Swaziland using efficient Bayesian multivariate classifiers. **Modeling Earth Systems and Environment**, v. 2, n. 4, p. 1–14, 2016.

FAWCETT, T. An introduction to ROC analysis. **Pattern Recognition Letters**, v. 27, n. 8, p. 861–874, June 2006.

FEARNSIDE, P. M. Brazil's Cuiabá- Santarém (BR-163) highway: the environmental cost of paving a soybean corridor through the Amazon. **Environmental Management**, v. 39, n. 5, p. 601–614, 2007.

FEARNSIDE, P. M. Highway construction as a force in the destruction of the Amazon Forest. In: VAN DER REE, R.; SMITH, D. J.; GRILO, C. (Ed.). **Handbook of road ecology**. Chichester, UK: John Wiley & Sons, 2015. p. 414–424.

FENG, Y.; TONG, X. Calibrating nonparametric cellular automata with a generalized additive model to simulate dynamic urban growth. **Environmental Earth Sciences**, v. 76, n. 14, p. 496, 2017.

FERREIRA, J. et al. Brazil's environmental leadership at risk. **Science**, v. 346, n. 6210, p. 706–707, 2014.

GHANMI, N.; AWAL, A.-M.; KOOLI, N. Dynamic Bayesian networks for handwritten Arabic word recognition. In: INTERNATIONAL WORKSHOP ON ARABIC SCRIPT ANALYSIS AND RECOGNITION (ASAR), 1., 2017. **Proceedings…** IEEE, 2017. Available from: <http://ieeexplore.ieee.org/document/8067769/>.

GIBBS, H. K. et al. Brazil's soy moratorium. **Science**, v. 347, n. 6220, p. 377–378, 2015.

GIRETTI, A.; CARBONARI, A.; NATICCHI, B. A spatio-temporal Bayesian network for adaptive risk management in territorial emergency response operations. In: PREMCHAISWADI, W. (Ed.). . **Bayesian networks**. [S.l.]: InTech, 2012. p. 114.

GONZALEZ-REDIN, J. et al. Spatial Bayesian belief networks as a planning decision tool for mapping ecosystem services trade-offs on forested landscapes. **Environmental Research**, v. 144, p. 15–26, 2016.

GRÊT-REGAMEY, A.; STRAUB, D. Spatially explicit avalanche risk assessment linking Bayesian networks to a GIS. **Natural Hazards and Earth System Science**, v. 6, n. 6, p. 911–926, 2006.

GRINAND, C. et al. Estimating deforestation in tropical humid and dry forests in Madagascar from 2000 to 2010 using multi-date Landsat satellite images and the random forests classifier. **Remote Sensing of Environment**, v. 139, p. 68–80, Dec. 2013.

GROENEVELD, J. et al. Theoretical foundations of human decision-making in agent-based land use models: a review. **Environmental Modelling & Software**, v. 87, p. 39–48, Jan. 2017.

HADDAWY, P. et al. Spatiotemporal Bayesian networks for malaria prediction. **Artificial Intelligence in Medicine**, v. 84, p. 127–138, Jan. 2018.

HAMMER, D. et al. Inequalities for Shannon entropy and Kolmogorov complexity. **Journal of Computer and System Sciences**, v. 60, p. 442–464, 2000.

HASAN, A. H. M. I.; HADDAWY, P. Integrating ARIMA and spatiotemporal Bayesian networks for high resolution malaria prediction. **Frontiers in Artificial Intelligence and Applications**, v. 285, p. 1783–1790, 2016.

HEISTERMANN, M.; MÜLLER, C.; RONNEBERGER, K. Land in sight? achievements, deficits and potentials of continental to global scale land-use modeling. **Agriculture, Ecosystems & Environment**, v. 114, n. 2–4, p. 141–158, June 2006.

HELBER, P. et al. Introducing Eurosat: a novel dataset and deep learning benchmark for land use and land cover classification. In: IEEE INTERNATIONAL GEOSCIENCE AND REMOTE SENSING SYMPOSIUM (IGARSS), 2018. **Proceedings…** IEEE, jul. 2018. Disponível em: <https://ieeexplore.ieee.org/document/8519248/>.

HIJMANS, R. J. et al. **raster: Geographic Data Analysis and Modeling**CRAN, , 2019. Disponível em: <https://cran.r-project.org/web/packages/raster/index.html>

HØJSGAARD, S. Graphical Independence Networks with the gRain Package for R. **Journal of Statistical Software**, v. 46, n. 10, p. 1–26, 2012.

HØJSGAARD, S. **gRain: graphical independence networks.** CRAN, , 2019. Available from: <https://cran.r-project.org/web/packages/gRain/index.html>.

HU, J. et al. Fault propagation behavior study and root cause reasoning with dynamic Bayesian network based framework. **Process Safety and Environmental Protection**, v. 97, p. 25–36, 2015.

HUGINEXPERT. **Hugin expert**. Available from: <http://www.hugin.com/>. Access in: July 3, 2019.

INSTITUTO BRASILEIRO DE GEOGRAFIA E ESTATÍSTICA - IBGE. **Amazônia Legal**. Available from: <https://www.ibge.gov.br/geociencias/organizacao-do-territorio/estrutura-territorial/15819-amazonia-legal.html?=&t=sobre>. Access in: Aug. 22, 2019.

INSTITUTO NACIONAL DE PESQUISAS ESPACIAIS - INPE. **Monitoramento da cobertura florestal da Amazônia por satélites:** sistemas PRODES, DETER, DEGRAD e QUEIMADAS 2007-2008. São José dos Campos: INPE. Available from: <http://www.obt.inpe.br/prodes/Relatorio_Prodes2008.pdf>.

INSTITUTO NACIONAL DE PESQUISAS ESPACIAIS - INPE. **PRODES (Deforestation)**. Available from: <http://terrabrasilis.dpi.inpe.br/app/dashboard/deforestation/biomes/legal_amazon/rates>. Access in: June 22, 2019a.

INSTITUTO NACIONAL DE PESQUISAS ESPACIAIS - INPE **Programa QUEIMADAS**. Available from: <http://queimadas.dgi.inpe.br/queimadas/bdqueimadas>. Access in: Aug. 23, 2019b.

INSTITUTO NACIONAL DE PESQUISAS ESPACIAIS - INPE. **Brazilian Amazon deforestation monitoring by satellite**. Available from: <http://www.obt.inpe.br/OBT/assuntos/programas/amazonia/prodes>. Access in: 23 ago. 2019c.

JOHNSON, S.; LOW-CHOY, S.; MENGERSEN, K. Integrating Bayesian networks and geographic information systems: good practice examples. **Integrated Environmental Assessment and Management**, v. 8, n. 3, p. 473–479, July 2012.

JUSYS, T. Fundamental causes and spatial heterogeneity of deforestation in Legal Amazon. **Applied Geography**, v. 75, p. 188–199, Oct. 2016.

KAMLUN, K. U.; BÜRGER ARNDT, R.; PHUA, M.-H. Monitoring deforestation in Malaysia between 1985 and 2013: insight from South-Western Sabah and its protected peat swamp area. **Land Use Policy**, v. 57, p. 418–430, Nov. 2016.

KAMUSOKO, C.; GAMBA, J. Simulating urban growth using a Random Forest-Cellular Automata (RF-CA) model. **ISPRS International Journal of Geo-Information**, v. 4, n. 2, p. 447–470, 2015.

KHAKZAD, N. Modeling wildfire spread in wildland-industrial interfaces using dynamic Bayesian network. **Reliability Engineering and System Safety**, v. 189, p. 165–176, 2019.

KHAKZAD, N.; KHAN, F.; AMYOTTE, P. Risk-based design of process systems using discrete-time Bayesian networks. **Reliability Engineering & System Safety**, v. 109, p. 5–17, 2013.

KOOMEN, E.; BEURDEN, J. B. **Land-use modelling in planning practice**. Dordrecht: Springer Netherlands, 2011. v. 101

KOOMEN, E.; RIETVELD, P.; DE NIJS, T. Modelling land-use change for spatial planning support. **The Annals of Regional Science**, v. 42, n. 1, p. 1–10, 2008.

KORB, K. B.; NICHOLSON, A. E. **Bayesian artificial intelligence**. 2.ed. [s.l.] CRC Press, 2010.

KOUROU, K. et al. Cancer classification from time series microarray data through regulatory Dynamic Bayesian Networks. **Computers in Biology and Medicine**, v. 116, p. 103577, Jan. 2020.

KOZLOW, P.; ABID, N.; YANUSHKEVICH, S. Gait type analysis using dynamic bayesian networks. **Sensors (Switzerland)**, v. 18, n. 10, 2018.

KRÜGER, C.; LAKES, T. Bayesian belief networks as a versatile method for assessing uncertainty in land-change modeling. **International Journal of Geographical Information Science**, v. 29, n. 1, p. 111–131, 2 jan. 2015.

KUMAR, S.; RADHAKRISHNAN, N.; MATHEW, S. Land use change modelling using a Markov model and remote sensing. **Geomatics, Natural Hazards and Risk**, v. 5, n. 2, p. 145–156, 2014.

LANDUYT, D. et al. A review of Bayesian belief networks in ecosystem service modelling. **Environmental Modelling & Software**, v. 46, p. 1–11, Aug. 2013.

LANDUYT, D. et al. A GIS plug-in for Bayesian belief networks: towards a transparent software framework to assess and visualise uncertainties in ecosystem service mapping. **Environmental Modelling & Software**, v. 71, p. 30–38, 2015.

LANDUYT, D.; BROEKX, S.; GOETHALS, P. L. M. Bayesian belief networks to analyse trade-offs among ecosystem services at the regional scale. **Ecological Indicators**, v. 71, p. 327–335, 2016.

LAURANCE, W. F. et al. An Amazonian rainforest and its fragments as a laboratory of global change. **Biological Reviews**, v. 93, n. 1, p. 223–247, 2018.

LOSIRI, C. et al. Modeling urban expansion in Bangkok metropolitan region using demographic – economic data through cellular automata-Markov chain and multi-layer perceptron-Markov chain models. **Sustainability**, v.8, n.7, 686, 2016.

MALDONADO, A. D. et al. Prediction of a complex system with few data: evaluation of the effect of model structure and amount of data with dynamic bayesian network models. **Environmental Modelling & Software**, v. 118, p. 281–297, Aug. 2019.

MARCOT, B. G.; PENMAN, T. D. Advances in Bayesian network modelling: integration of modelling technologies. **Environmental Modelling & Software**, v. 111, p. 386–393, Jan. 2019.

MAS, J.-F. et al. Inductive pattern-based land use/cover change models: a comparison of four software packages. **Environmental Modelling & Software**, v. 51, p. 94–111, Jan. 2014.

MASANTE, D. **bnspatial: spatial implementation of Bayesian networks and mapping.** CRAN, , 2019. Available from: <https://cran.r-project.org/web/packages/bnspatial/index.html>.

MAYFIELD, H. et al. Use of freely available datasets and machine learning methods in predicting deforestation. **Environmental Modelling & Software**, v. 87, p. 17–28, Jan. 2017.

MCNAUGHT, K. R.; ZAGORECKI, A. Using Dynamic Bayesian Networks for prognostic modelling to inform maintenance decision making. In: IEEE INTERNATIONAL CONFERENCE ON INDUSTRIAL ENGINEERING AND ENGINEERING MANAGEMENT, 2009. **Proceedings...** IEEE, 2009.

MELLO, N. G. R.; ARTAXO, P. Evolução do plano de ação para prevenção e controle do desmatamento na Amazônia Legal. **Revista do Instituto de Estudos Brasileiros**, n. 66, p. 108, 2017.

MELLO, M. et al. Bayesian Networks for Raster Data (BayNeRD): plausible reasoning from observations. **Remote Sensing**, v. 5, n. 11, p. 5999–6025, 2013.

MICHETTI, M.; ZAMPIERI, M. Climate–human–land interactions: a review of major modelling approaches. **Land**, v. 3, n. 3, p. 793–833, 2014.

MOLINA, J. et al. Dynamic Bayesian Networks as a decision support tool for assessing climate change impacts on highly stressed groundwater systems. **Journal of Hydrology**, v. 479, p. 113–129, Feb. 2013.

MÜLLER, H. et al. Beyond deforestation: differences in long-term regrowth dynamics across land use regimes in southern Amazonia. **Remote Sensing of Environment**, v. 186, p. 652–662, Dec. 2016.

MURPHY, K. P. **Dynamic Bayesian Networks:** representation, inference and learning. Berkeley: University of California, 2002.

MUSTAFA, A. et al. Coupling agent-based, cellular automata and logistic regression into a hybrid urban expansion model (HUEM). **Land Use Policy**, v. 69, p. 529–540, Dec. 2017.

MUSTAFA, A. et al. Comparing support vector machines with logistic regression for calibrating cellular automata land use change models. **European Journal of Remote Sensing**, v. 51, n. 1, p. 391–401, 2018.

NASIRI, V. et al. Land use change modeling through an integrated multi-layer perceptron neural network and Markov Chain analysis (case study: Arasbaran region , Iran). **Journal of Forestry Research**, v. 30, 2018.

NEAPOLITAN, R. E. **Learning bayesian networks**. 2.ed. New Jersey: Person Prentice Hall, 2004.

NEPSTAD, D. et al. Slowing Amazon deforestation through public policy and interventions in beef and soy supply chains**. Science**, v. 344, n. 6188, p. 1118-1123, 2014.

NOBRE, C. A.; BORMA, L. D. S. 'Tipping points' for the Amazon forest. **Current Opinion in Environmental Sustainability**, v. 1, n. 1, p. 28–36, Oct. 2009.

NOSZCZYK, T. A review of approaches to land use changes modeling. **Human and Ecological Risk Assessment: An International Journal**, p. 1–29, May 2018.

NOWOSAD, J.; STEPINSKI, T. F.; NETZEL, P. Global assessment and mapping of changes in mesoscale landscapes: 1992–2015. **International Journal of Applied Earth Observation and Geoinformation**, v. 78, p. 332–340, June 2019.

OGC, O. G. C. **OGC GeoTIFF standard**. Available from: <http://www.opengis.net/doc/IS/GeoTIFF/1.1>. Accesso in: Dec. 3, 2019.

OMRANI, H. et al. Multi-label class assignment in land-use modelling. **International Journal of Geographical Information Science**, v. 29, n. 6, p. 1023–1041, 2015.

PÉREZ-MIÑANA, E. Improving ecosystem services modelling: insights from a Bayesian network tools review. **Environmental Modelling & Software**, v. 85, p. 184–201, Nov. 2016.

PETOUSIS, P. et al. Prediction of lung cancer incidence on the low-dose computed tomography arm of the National Lung Screening Trial: a dynamic Bayesian network. **Artificial Intelligence in Medicine**, v. 72, p. 42–55, Sept. 2016.

PINHEIRO, T. F. et al. Forest degradation associated with logging frontier expansion in the Amazon: the BR-163 Region in Southwestern Pará, Brazil. **Earth Interactions**, v. 20, n. 17, p. 1–26, July 2016.

POLLINO, C. A.; HENDERSON, C. **Bayesian networks :** a guide for their application in natural resource management and policy landscape logic technical report. Available from: <www.landscapelogic.org.au>.

POPESCU, V. et al. A Lane assessment method using visual information based on a Dynamic Bayesian Network. **Journal of Intelligent Transportation Systems**, v. 19, n. 3, p. 225–239, 2015.

PUGA, J. L.; KRZYWINSKI, M.; ALTMAN, N. Points of significance: Bayesian statistics. **Nature Methods**, v. 12, n. 5, p. 377–378, 2015.

QU, Y.; ZHANG, Y.; WANG, J. A dynamic Bayesian network data fusion algorithm for estimating leaf area index using time-series data from in situ measurement to remote sensing observations. **International Journal of Remote Sensing**, v. 33, n. 24, p. 1106–1125, 2012.

R CORE TEAM. **R: a language and environment for statistical computing.** Vienna, Austria, 2019. Available from: <https://www.r-project.org/>.

REICHE, J. et al. Fusing Landsat and SAR time series to detect deforestation in the tropics. **Remote Sensing of Environment**, v. 156, p. 276–293, Jan. 2015.

REN, Y. et al. Spatially explicit simulation of land use/land cover changes: current coverage and future prospects. **Earth-Science Reviews**, v. 190, p. 398–415, Mar. 2019.

RIMAL, B. et al. Land use/land cover dynamics and modeling of urban land expansion by the integration of cellular automata and Markov Chain. **ISPRS International Journal of Geo-Information**, v. 7, n. 4, p. 154, 2018.

ROCHEDO, P. R. R. et al. The threat of political bargaining to climate mitigation in Brazil. **Nature Climate Change**, v. 8, n. 8, p. 695–698, 2018.

RORIZ, P. A. C.; YANAI, A. M.; FEARNSIDE, P. M. Deforestation and carbon loss in southwest Amazonia: impact of Brazil's revised forest code. **Environmental Management**, v. 60, n. 3, p. 367–382, 2017.

ROSA, I. M. D. et al. Modelling land cover change in the Brazilian Amazon: temporal changes in drivers and calibration issues. **Regional Environmental Change**, v. 15, n. 1, p. 123–137, 2015.

ROSA, I. M. D.; AHMED, S. E.; EWERS, R. M. The transparency, reliability and utility of tropical rainforest land-use and land-cover change models. **Global Change Biology**, v. 20, n. 6, p. 1707–1722, June 2014.

RUSSELL, S. J.; NORVING, P. **Artificial intelligence:** a modern approach. 3.ed. Egnlewood Cliffs - New Jersey: [s.n.], 2009.

SAHIN, O. et al. Spatial Bayesian Network for predicting sea level rise induced coastal erosion in a small Pacific Island. **Journal of Environmental Management**, v. 238, p. 341–351, May 2019.

SALES, M. et al. A spatiotemporal geostatistical hurdle model approach for short-term deforestation prediction. **Spatial Statistics**, v. 21, p. 304–318, Aug. 2017.

SAMARDŽIĆ-PETROVIĆ, M. et al. Machine learning techniques for modelling short term land-use change. **ISPRS International Journal of Geo-Information**, v. 6, n. 12, p. 387, 2017.

SCUTARI, M. Learning Bayesian Networks with the bnlearn R package. **Journal of Statistical Software**, v. 35, n. 3, p. 22, 2009.

SCUTARI, M. **bnlearn: Bayesian Network structure learning, parameter learning and inference.** 2019. Available from: <http://cran.r-project.org/web/packages/bnlearn/index.html>.

SEMAKULA, H. M. et al. A Bayesian belief network modelling of household factors influencing the risk of malaria: a study of parasitemia in children under five years of age in sub-Saharan Africa. **Environmental Modelling and Software**, v. 75, p. 59–67, 2016.

SETZER, A. W. et al. A case of illegal clearing in Amazonia antecipated by the detection of fires and forest degradation. In: SEMINÁRIO DE ATUALIZAÇÃO EM SENSORIAMENTO REMOTO E SISTEMAS DE INFORMAÇÕES GEOGRÁFICAS APLICADOS À ENGENHARIA FLORESTAL, 10., 2012. **Anais**...Curitiba, PR, 2012. Available from: <http://queimadas.cptec.inpe.br/~rqueimadas/documentos/201210_Setzer_etal_DesmateIlegal_XSengef.pdf>.

SHIHAB, K. Dynamic modeling of groundwater pollutants with Bayesian Networks. **Applied Artificial Intelligence**, v. 22, n. 4, p. 352–376, 2008.

SHIMABUKURO, Y. E. et al. The Brazilian Amazon Monitoring Program: PRODES and DETER projects. In: ACHARD, F.; HANSEN, M. C. (Ed.). **Global forest monitoring from Earth observation**. [S.l.]: CRC Press/Taylor & Francis, 2012. p. 354.

SILVA, A. C. O.; FONSECA, L. M. G.; KÖRTING, T. S. Bayesian network model to predict areas for sugarcane expansion in Brazilian Cerrado. **Brazilian Journal of Cartography**, v. 69, n.5, p. 857–467, 2017.

SILVA, A. C. O. et al. A spatio-temporal Bayesian Network approach for deforestation prediction in an Amazon rainforest expansion frontier. **Spatial Statistics**, v. 35, e 100393, Mar. 2020.

SIMMONS, C. S. The local articulation of policy conflict: land use, environment, and Amerindian rights in eastern Amazonia. **The Professional Geographer**, v. 54, n. 3, p. 241–258, Aug. 2002.

SOARES-FILHO, B. et al. Cracking Brazil's forest code. **Science**, v. 344, n. 6182, p. 363–364, 2014.

SOARES-FILHO, B.; RODRIGUES, H.; FOLLADOR, M. A hybrid analytical-heuristic method for calibrating land-use change models. **Environmental Modelling & Software**, v. 43, p. 80–87, May 2013.

SOLER, L.; VERBURG, P.; ALVES, D. Evolution of land use in the Brazilian Amazon: from frontier expansion to market chain dynamics. **Land**, v. 3, n. 3, p. 981–1014, 2014.

SOMA, A. S.; KUBOTA, T.; ADITIAN, A. Comparative study of land use change and landslide susceptibility using frequency ratio, certainty factor, and logistic regression in upper area of Ujung-Loe watersheds South Sulawesi Indonesia. **International Journal of Erosion Control Engineering**, v. 11, n. 4, p. 103–115, 2019.

SONG, X.-P. et al. Global land change from 1982 to 2016. **Nature**, v. 560, n. 7720, p. 639–643, 2018.

SOUSA, P. Decreasing deforestation in the southern Brazilian Amazon: the role of administrative sanctions in Mato Grosso State. **Forests**, v. 7, n. 12, p. 66, 2016.

SOUZA, JR, C. et al. Ten-year Landsat classification of deforestation and forest degradation in the Brazilian Amazon. **Remote Sensing**, v. 5, n. 11, p. 5493–5513, 2013.

SPEROTTO, A. et al. Reviewing Bayesian Networks potentials for climate change impacts assessment and management: a multi-risk perspective. **Journal of Environmental Management**, v. 202, p. 320–331, Nov. 2017.

STEINIGER, S.; HAY, G. J. Free and open source geographic information tools for landscape ecology. **Ecological Informatics**, v. 4, n. 4, p. 183–195, Sept. 2009.

STELZENMÜLLER, V. et al. Assessment of a Bayesian Belief Network-GIS framework as a practical tool to support marine planning. **Marine Pollution Bulletin**, v. 60, n. 10, p. 1743–1754, 2010.

SUN, B.; ROBINSON, D. Comparisons of statistical approaches for modelling land-use change. **Land**, v. 7, n. 4, p. 144, 2018.

SWETS, J. Measuring the accuracy of diagnostic systems. **Science**, v. 240, n. 4857, p. 1285–1293, 1988.

TASKER, K. A.; ARIMA, E. Y. Fire regimes in Amazonia: the relative roles of policy and precipitation. **Anthropocene**, v. 14, p. 46–57, June 2016.

TEGEGNE, Y. T. et al. Evolution of drivers of deforestation and forest degradation in the Congo Basin forests: exploring possible policy options to address forest loss. **Land Use Policy**, v. 51, p. 312–324, Feb. 2016.

TRIFONOVA, N. et al. Spatio-temporal Bayesian network models with latent variables for revealing trophic dynamics and functional networks in fisheries ecology. **Ecological Informatics**, v. 30, p. 142–158, 2015.

TRIFONOVA, N. et al. Predicting ecosystem responses to changes in fisheries catch, temperature, and primary productivity with a dynamic Bayesian network model. **ICES Journal of Marine Science**, v. 74, n. 5, p. 1334–1343, 1 maio 2017.

TRITSCH, I.; LE TOURNEAU, F.-M. Population densities and deforestation in the Brazilian Amazon: New insights on the current human settlement patterns. **Applied Geography**, v. 76, p. 163–172, Nov. 2016.

UUSITALO, L. Advantages and challenges of Bayesian networks in environmental modelling. **Ecological Modelling**, v. 203, n. 3/4, p. 312–318, 2007.

UUSITALO, L. et al. An overview of methods to evaluate uncertainty of deterministic models in decision support. **Environmental Modelling & Software**, v. 63, p. 24–31, Jan. 2015.

UUSITALO, L. et al. Hidden variables in a Dynamic Bayesian Network identify ecosystem level change. **Ecological Informatics**, v. 45, p. 9–15, May 2018.

VASCONCELOS, S. S. et al. Forest fires in southwestern Brazilian Amazonia: estimates of area and potential carbon emissions. **Forest Ecology and Management**, v. 291, p. 199–208, Mar. 2013a.

VASCONCELOS, S. S. et al. Variability of vegetation fires with rain and deforestation in Brazil's state of Amazonas. **Remote Sensing of Environment**, v. 136, p. 199–209, Sept. 2013b.

VERBURG, P. H. et al. Land use change modelling: current practice and research priorities. **GeoJournal**, v. 61, n. 4, p. 309–324, Dec. 2004.

VERGARA, J. R.; ESTÉVEZ, P. A. A review of feature selection methods based on mutual information. **Neural Computing and Applications**, v. 24, n. 1, p. 175–186, Jan. 2014.

WAGNER, P. D. et al. Comparing the effects of dynamic versus static representations of land use change in hydrologic impact assessments. **Environmental Modelling & Software**, v. 122, e103987, Dec. 2019.

WHITE, B. L. A. Spatiotemporal variation in fire occurrence in the state of Amazonas, Brazil, between 2003 and 2016. **Acta Amazonica**, v. 48, n. 4, p. 358–367, Dec. 2018.

WIJESIRI, B. et al. Use of surrogate indicators for the evaluation of potential health risks due to poor urban water quality: a Bayesian Network approach. **Environmental Pollution**, v. 233, p. 655–661, Feb. 2018.

WILKINSON, L. et al. An object-oriented spatial and temporal bayesian network for managing willows in an american heritage river catchment. **CEUR Workshop Proceedings**, v. 1024, p. 77–86, 2013.

WORLDWIDE FOUND - WWF. **Inside the Amazon**. Available from: <https://wwf.panda.org/knowledge_hub/where_we_work/amazon/about_the_amazon/>. Access in: Aug. 22, 2019.

ZHANG, C. et al. Joint deep learning for land cover and land use classification. **Remote Sensing of Environment**, v. 221, p. 173–187, Feb. 2019.

ZHANG, Y. et al. Estimating leaf area index from MODIS and surface meteorological data using a dynamic Bayesian network. **Remote Sensing of Environment**, v. 127, p. 30–43, 2012.

APPENDIX A: ASSESSMENT METRICS OF THE STBN MODELS PREDICTIONS.

Table A.1 - Assessment metrics of the STBNs predictions in the Amazon case study.

	First-order Markov STBN					Second-order Markov STBN			
	2014	**2015**	**2016**	**2017**	**2018**	**2015**	**2016**	**2017**	**2018**
Threshold	0.32	0.44	0.44	0.25	0.18	0.35	0.30	0.16	0.27
Sensitivity	0.96	0.95	0.94	0.91	0.94	0.97	0.94	0.90	0.93
Specificity	0.95	0.94	0.93	0.92	0.91	0.95	0.93	0.91	0.90
AUC-ROC	0.98	0.97	0.96	0.95	0.95	0.98	0.95	0.94	0.93
Precision	0.86	0.85	0.82	0.79	0.77	0.88	0.82	0.79	0.79
Kappa	0.87	0.86	0.84	0.79	0.79	0.90	0.84	0.79	0.79

Table A.2 - Assessment metrics of the STBNs predictions in the Mato Grosso case study.

	First-order Markov STBN					Second-order Markov STBN			
	2014	**2015**	**2016**	**2017**	**2018**	**2015**	**2016**	**2017**	**2018**
Threshold	0.32	0.25	0.33	0.23	0.23	0.36	0.32	0.33	0.31
Sensitivity	0.97	0.93	0.91	0.92	0.86	0.97	0.92	0.94	0.88
Specificity	0.94	0.92	0.92	0.89	0.90	0.94	0.92	0.90	0.91
AUC-ROC	0.98	0.94	0.93	0.93	0.89	0.98	0.94	0.94	0.90
Precision	0.82	0.79	0.78	0.73	0.74	0.83	0.79	0.76	0.76
Kappa	0.84	0.80	0.78	0.74	0.73	0.86	0.80	0.78	0.75

Table A.3 - Assessment metrics of the STBNs predictions in the Pará case study.

	First-order Markov STBN					Second-order Markov STBN			
	2014	**2015**	**2016**	**2017**	**2018**	**2015**	**2016**	**2017**	**2018**
Threshold	0.22	0.16	0.09	0.16	0.16	0.21	0.19	0.21	0.20
Sensitivity	0.90	0.88	0.79	0.81	0.81	0.89	0.81	0.81	0.81
Specificity	0.89	0.88	0.86	0.86	0.90	0.88	0.86	0.86	0.90
AUC-ROC	0.95	0.89	0.85	0.86	0.85	0.90	0.86	0.86	0.87
Precision	0.70	0.67	0.65	0.65	0.72	0.71	0.66	0.69	0.75
Kappa	0.67	0.67	0.60	0.62	0.69	0.70	0.65	0.69	0.70

APPENDIX B: HYPOTHESIS TESTING FOR THE ASSESSMENT METRICS.

AUC-ROC, Precision, and Kappa metrics values for the first-order Markov STBN were compared with the values of the same metrics for the second-order Markov STBN. To test the hypothesis that there is a significant difference between the metrics of both models, an independent t-test was performed for each one of those three metrics in each case study. Considering μ_1 as the mean of the first-order Markov STBN assessment metric, and μ_2 as the mean of the same assessment metric but for the second-order Markov STBN, all independent t-tests performed had the null and alternative hypotheses as follows:

H_0: $\mu_1 - \mu_2 = 0$, i.e., the difference between the means equals to zero,

H_a: $\mu_1 - \mu_2 \neq 0$, i.e., the difference between the means differs from zero.

Table B.1 shows the mean and standard deviation of each metric for both models as well as the p-value obtained from the independent t-test with a significance level of 5%. One can note that the p-value is greater than 0.05 in all t-tests performed, this states that the difference found between the means is not statistically significant.

Table B.1 - AUC-ROC, Precision, and Kappa metrics mean and standard deviation for the STBN models. The p-value obtained from the independent t-test is also shown.

Amazon case study					
	First-order Markov STBN		**Second-order Markov STBN**		
	Mean	**Std. Deviation**	**Mean**	**Std. Deviation**	**p-value**
AUC-ROC	0.962	0.013	0.95	0.0216	0.3758
Precision	0.818	0.0383	0.82	0.0424	0.9439
Kappa	0.83	0.038	0.83	0.0523	0.9999

Mato Grosso case study					
	First-order Markov STBN		**Second-order Markov STBN**		
	Mean	**Std. Deviation**	**Mean**	**Std. Deviation**	**p-value**
AUC-ROC	0.934	0.0321	0.94	0.0326	0.7911
Precision	0.772	0.037	0.785	0.0332	0.5966
Kappa	0.7975	0.045	0.7975	0.0464	0.9999

Pará case study					
	First-order Markov STBN		**Second-order Markov STBN**		
	Mean	**Std. Deviation**	**Mean**	**Std. Deviation**	**p-value**
AUC-ROC	0.88	0.0424	0.8725	0.0189	0.7361
Precision	0.678	0.0311	0.7025	0.0377	0.9439
Kappa	0.685	0.038	0.685	0.0238	0.9999

The values from Table B.1 are graphically presented in Figure B.1. The mean value of each metric is plotted along with the standard deviation error bar. Assessment metrics are shown by rows while study cases are shown by columns. One can note that, for the three metrics in all case studies, there is an overlap between the error bars when comparing them between models. This overlap is another indication that the difference between metrics by models is not statistically significant.

Figure B.1 - Mean of the AUCROC, Precision, and Kappa metrics by STBN models and by case studies with standard deviation error bars.

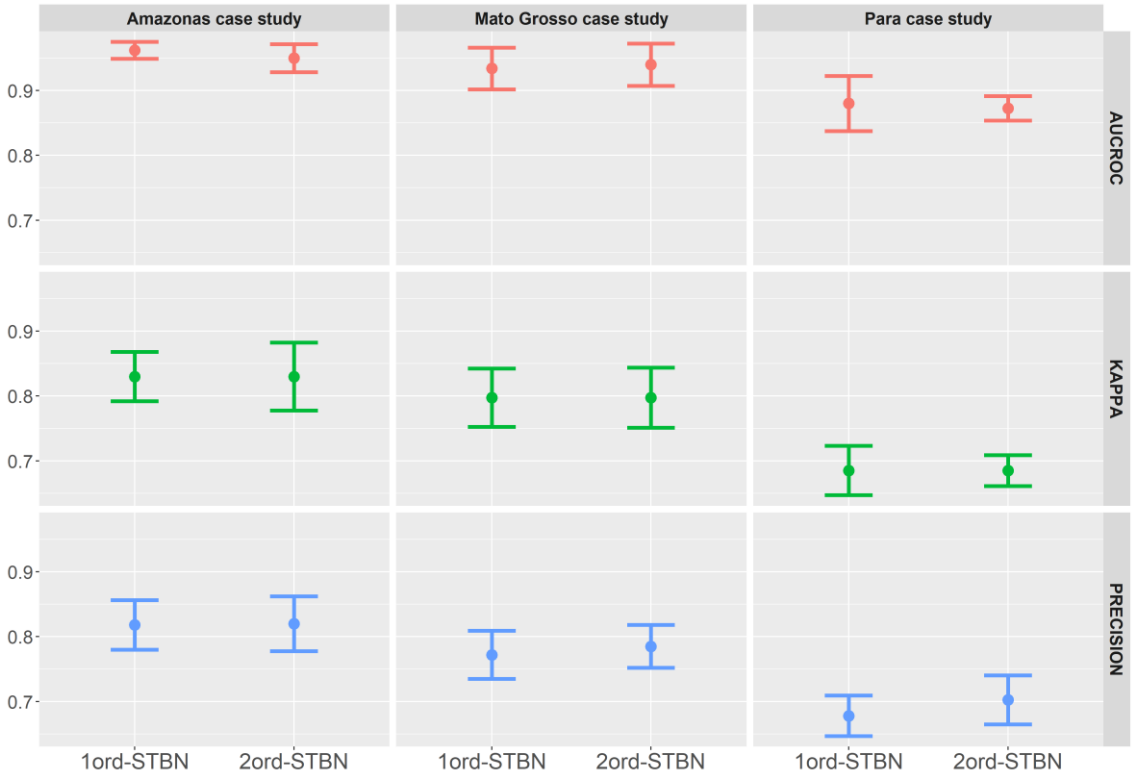

Source: author's production.